FIELD DEMONSTRATION OF THE KRAUKLIS SEISMIC WAVE IN A NOVEL MVA METHOD FOR GEOLOGIC CO_2 STORAGE

Final Report

(for the period of October 1, 2016 – December 31, 2018)

Prepared for:

AAD Document Control

National Energy Technology Laboratory
U.S. Department of Energy
626 Cochrans Mill Road
PO Box 10940, MS 921-107
Pittsburgh, PA 15236-0940

Cooperative Agreement No. DE-FE0028659
DOE Technical Monitor: William Aljoe

Prepared by:

Shaughn A. Burnison
Amanda J. Livers-Douglas
Lu Jin
Neil W. Dotzenrod
John A. Hamling
Charlie D. Gorecki

Energy & Environmental Research Center
University of North Dakota
15 North 23rd Street, Stop 9018
Grand Forks, ND 58202-9018

2018-EERC-12-06 December 2018

EERC DISCLAIMER

LEGAL NOTICE This research report was prepared by the Energy & Environmental Research Center (EERC), an agency of the University of North Dakota, as an account of work sponsored by the U.S. Department of Energy (DOE) National Energy Technology Laboratory. Because of the research nature of the work performed, neither the EERC nor any of its employees makes any warranty, express or implied, or assumes any legal liability or responsibility for the accuracy, completeness, or usefulness of any information, apparatus, product, or process disclosed or represents that its use would not infringe privately owned rights. Reference herein to any specific commercial product, process, or service by trade name, trademark, manufacturer, or otherwise does not necessarily constitute or imply its endorsement or recommendation by the EERC.

ACKNOWLEDGMENT

This project was cofunded through the EERC–DOE Joint Program on Research and Development for Fossil Energy-Related Resources Cooperative Agreement No. DE-FE0028659. Nonfederal funding was provided by Seismos, Inc., and Computer Modelling Group, Ltd.

DOE DISCLAIMER

This report was prepared as an account of work sponsored by an agency of the United States Government. Neither the United States Government, nor any agency thereof, nor any of their employees, makes any warranty, express or implied, or assumes any legal liability or responsibility for the accuracy, completeness, or usefulness of any information, apparatus, product, or process disclosed, or represents that its use would not infringe privately owned rights. Reference herein to any specific commercial product, process, or service by trade name, trademark, manufacturer, or otherwise does not necessarily constitute or imply its endorsement, recommendation, or favoring by the United States Government or any agency thereof. The views and opinions of authors expressed herein do not necessarily state or reflect those of the United States Government or any agency thereof.

TABLE OF CONTENTS

LIST OF FIGURES

Continued . . .

LIST OF FIGURES

FIELD DEMONSTRATION OF THE KRAUKLIS SEISMIC WAVE IN A NOVEL MVA METHOD FOR GEOLOGIC CO2 STORAGE

EXECUTIVE SUMMARY

The Energy & Environmental Research Center (EERC) conducted a feasibility study of a new, low-impact geophysics monitoring method designed to incrementally track the saturation front of CO_2 injected into a reservoir. The method leverages a new way of transmitting energy from the surface to the reservoir and employs a new subsurface signal called the Krauklis wave (K-wave) and other guided waves for seismic monitoring that may be applicable in carbon capture, utilization, and storage (CCUS) applications. The EERC partnered with Seismos, Inc., the company that holds the exclusive technology license for this method, to advance the development of K-wave technology, and Denbury Onshore, LLC (Denbury), to field-test the system. The system was field-tested at Denbury's Bell Creek oil field, currently undergoing CO_2-based enhanced oil recovery (EOR) in southeastern Montana, the site of the EERC's Plains CO_2 Reduction (PCOR) Partnership Program large-scale CO_2 storage demonstration project.

The K-wave system uses a wellhead-mounted source to propagate energy down the wellbore in the form of a tube wave and through the well perforations into the reservoir. Part of the energy transmitted through the perforations into the reservoir converts to compressional and shear body waves that disperse, but some of the energy propagates as slower waves in the form of K-waves and/or other guided waves that are expected to propagate through the formation to intersect neighboring wells (Figure ES-1). The propagated signal would induce tube waves in the neighboring wells that return to the surface to be recorded with a wellhead-mounted receiver. The propagation time of the signal is directly affected by the presence of CO_2 between the wells, so the difference in the recorded transit time of the returning signal between pre- and postinjection data sets could be used to help define the lateral extent of a CO_2 saturation front.

The objectives of the feasibility study were to demonstrate, validate, and evaluate the K-wave method's ability to monitor the morphology of the injected CO_2 and estimate the saturation distribution over a study area incorporating up to 30 wells. Results from the demonstration were to be compared to carefully timed conventional 4-D surface seismic methods, dynamic reservoir simulations, and CO_2 breakthrough data to validate the technology and provide useful information that may result in improvements.

Prior to mobilizing for the full scale K-wave baseline survey, three initial steps were required: a reconnaissance survey and hardware field test at Bell Creek, numerical modeling of the K-wave method, and design and procurement of the 3-D surface seismic survey over the study area. The field test occurred in late November and early December 2016 and incorporated three wells. The purpose was to better understand the wellhead hardware configurations and test the response from the Bell Creek reservoir. Useful operational information resulted, but signal from the first-generation gas release/gas injection source was not recorded in neighboring wells. As a result, development of a stronger, hydraulically driven "displacement" source that had been planned was accelerated.

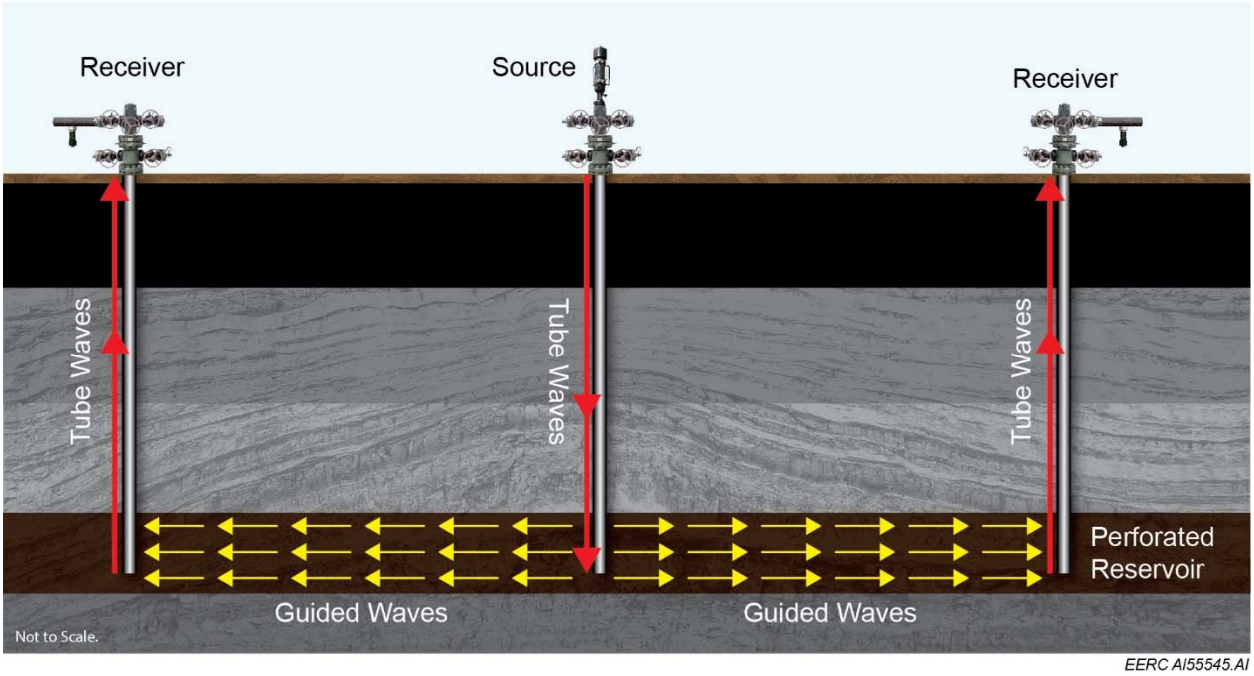

Figure ES-1. Simplified K-wave system illustration showing two well pairs (one "source" well and two "receiver" wells).

After the initial field test, numerical modeling of the K-wave method using parameters specific to the Bell Creek Field was initiated and completed over a period of 7 months from April through mid-November 2017. Modeling results indicated that even with the new source design the fundamental concepts behind the K-wave method exhibited problems. The modeling revealed a significantly greater attenuation of the signal at the wellbore perforations than expected, totaling on the order of 10^{-8} from source well to receiver well over a 400-m well spacing. Modeling also showed that greater source frequency bandwidth was needed to produce guided waves that would propagate within a 30-foot-thick reservoir layer's such as that at Bell Creek. And to keep guided waves contained in the reservoir, the modeling showed that the reservoir layer seismic velocity would need to be slower than the velocities of the bounding layers. This geologic velocity relationship exists in some fields but is opposite to what exists at Bell Creek.

The modeling results prompted the second field test with the stronger, second-generation "displacement" source that had been developed in the interim to determine if a stronger source could transmit a signal that could be detected at the neighboring wells. The displacement source was tested on a four-well geometry and, after analysis, was shown to have also failed to produce a detectable signal at neighboring wells. Concurrent with the field test, a 3-D seismic survey intended to serve as a baseline for project validation was acquired. The 3-D seismic survey also served as a monitor data set for the portion of the project area where CO_2 injection had already commenced in case well-spacing considerations forced a replan of the project location to an area with closer well spacing. This was a concern at the time as the project area was developed with twice the well spacing than what was expected in the original plan (160-acre 5-spot well spacing instead of 40-acre well spacing).

The new source failed to produce a detectable signal which appeared to confirm the modeling results and indicated that the Bell Creek Field is not an ideal site for the K-wave test. It was concluded that a source with sufficient strength and bandwidth could not be built to overcome these factors as discovered by the modeling within a reasonable amount of time. Several other sites undergoing CO_2-based EOR were also evaluated; however, none of these sites was amenable because of geology, limitations in the source and receiver hardware, or the advanced state of the CO_2 flood, which would preclude the acquisition of baseline measurements. In addition, two other configurations of the source and receiver layout were also considered; however, these design modifications either changed the scope of the project or did not meet the goals of the Carbon Storage Program. In consultation with the U.S. Department of Energy Project Manager and Technology Manager, a no-go decision was invoked to forego additional expenditures as the technology would not meet the current project objectives. Project activities to date have moved the technology forward by developing modeling equations that can be applied elsewhere, advanced the state of wellhead sensors and sources, and spurred improvements to field operations. The 3-D seismic survey in the project area and the dynamic reservoir simulations done as part of this study have provided value for ongoing and future synergistic activities at Bell Creek related to U.S. Department of Energy carbon storage goals.

FIELD DEMONSTRATION OF THE KRAUKLIS SEISMIC WAVE IN A NOVEL MVA METHOD FOR GEOLOGIC CO_2 STORAGE

INTRODUCTION

The Energy & Environmental Research Center (EERC) conducted a feasibility study of a new, low-impact geophysics monitoring method designed to incrementally track the saturation front of CO_2 injected into a reservoir. The method leverages a new way of transmitting energy from the surface to the reservoir and employs a new subsurface signal called the Krauklis wave (K-wave) and/or other guided waves for seismic monitoring that may be applicable in carbon capture, utilization, and storage (CCUS) applications. The EERC partnered with Seismos, Inc., (Seismos) the company that holds the exclusive technology license for this method, to advance the development of K-wave technology, and Denbury Onshore, LLC (Denbury), to field-test the system in their CO_2 enhanced oil recovery (EOR) development at Bell Creek Field in southeastern Montana, the site of the EERC's Plains CO_2 Reduction (PCOR) Partnership Program large-scale CO_2 storage demonstration project (Figure 1) (Hamling and others, 2016).

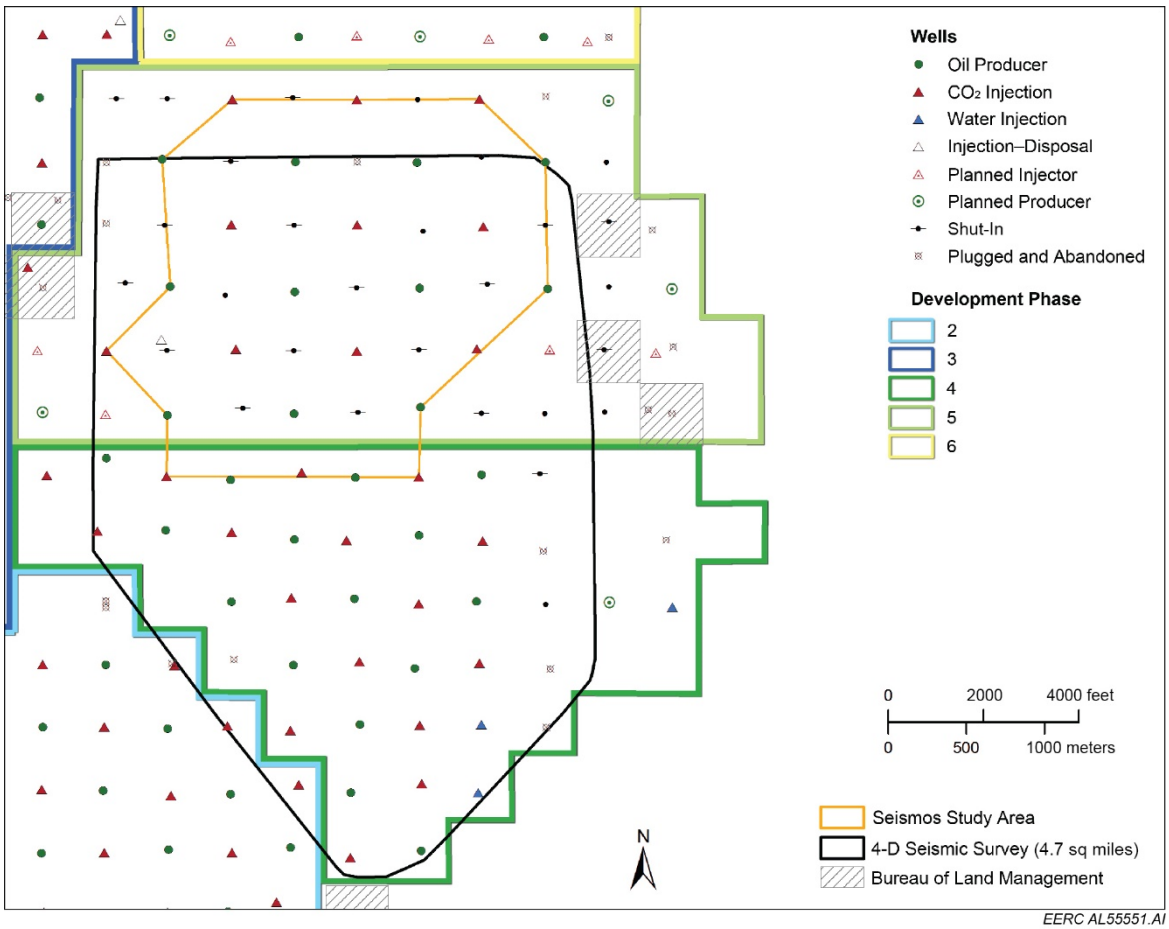

Figure 1. Map of the proposed study area showing the notional extent of the 3-D seismic survey. Phases are CO_2 EOR infrastructure development areas.

The K-wave system uses a wellhead-mounted source to propagate energy down the wellbore in the form of a tube wave and through the well perforations into the reservoir. Part of the energy would consist of compressional and shear body waves that would disperse, but slower guided energy in the form of K-waves or other guided waves was expected to propagate through the formation to intersect neighboring wells (Figure 2). The propagated signal would induce a tube wave in the neighboring well that returns to the surface to be recorded with a wellhead-mounted receiver. The propagation speed of the signal is directly affected by the presence of CO_2 between the wells, so the difference in the recorded transit time of the returning signal between pre- and postinjection data sets could be used to help define the lateral extent of a CO_2 saturation front between monitored wells. With wellhead-mounted equipment and a way to track the incremental progress of injected CO_2 through the reservoir, the K-wave method presented a potential means to mitigate several shortcomings of traditional seismic monitoring methods, such as high cost, disruptive surface impacts, and long intervals between surveys, while providing timely actionable information to the field operator in the form of periodically updated CO_2 saturation front maps. The CO_2 saturation distribution maps produced using the K-wave method could be used to improve CO_2 sweep efficiency and CO_2 storage efficiency, meet regulatory compliance, and realize economic value by improving pattern management and increasing oil recovery.

The objectives of this feasibility study were to demonstrate, validate, and evaluate the K-wave method's ability to monitor the morphology of CO_2 saturation distribution over a study area incorporating up to 30 wells in a portion of the Bell Creek oil field. The Bell Creek oil field appeared to be an ideal test location as the geology is comparatively simple (Appendix A). Structurally, the field is a monocline dipping 1°–2° to the northwest with a 30-foot-thick sandstone reservoir with high porosity (15%–35%) and high permeability (150–1175 mD) between bounding shales. Results from the demonstration were to be compared to carefully timed conventional 4-D surface seismic methods, dynamic reservoir simulations, and CO_2 breakthrough data to validate the technology and provide useful information to guide improvements.

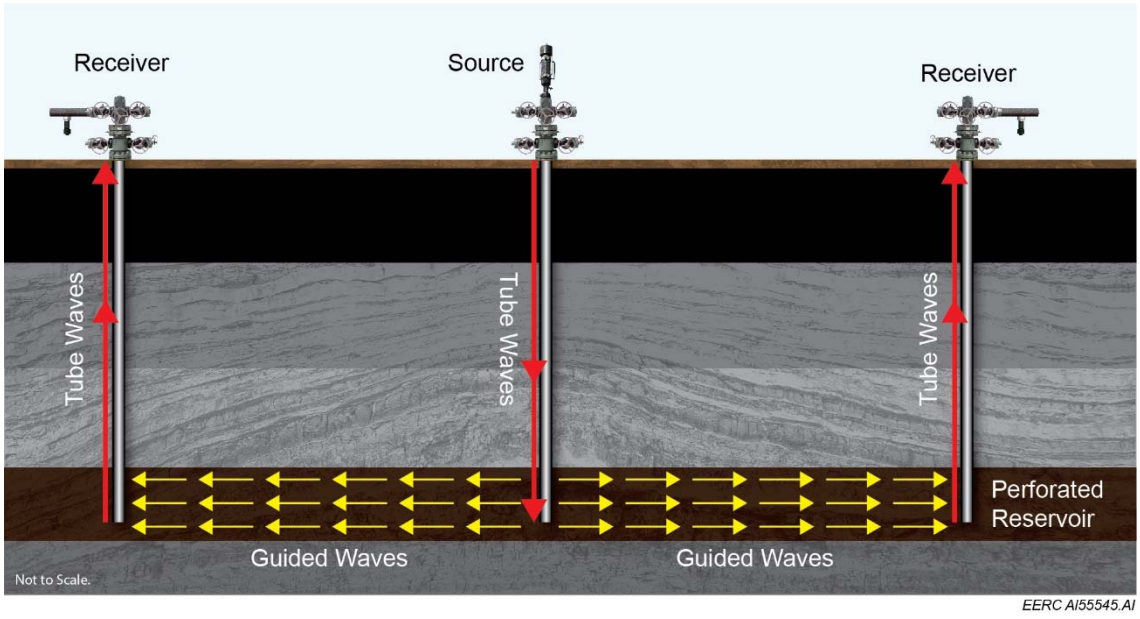

Figure 2. Simplified K-wave system illustration showing two well pairs (one "source" well and two "receiver" wells).

The proposed project was divided by a go/no-go decision point. The objectives prior to the decision point were to install Seismos's K-wave system and acquire a baseline K-wave data set together with a concurrent 3-D surface seismic survey to be used later for validation (Appendix B). Three or four months after the baseline survey, a K-wave monitor data set was to be acquired. The processed baseline and monitor data would be compared to evaluate whether time-lapse differences were discernible. This constituted the go/no go assessment. If time-lapse differences were discernible, the K-wave system would be considered viable, and the project would proceed to the next budget period and access funding to acquire two or three more monitor data sets and a second 3-D surface seismic survey to conclude data acquisition. Project activities would conclude with analysis and validation efforts to evaluate the method as a monitoring, verification, and accounting (MVA) method for CCUS applications as a fully integrated prototype technology tested at a field site, thus advancing the technology from technology readiness level (TRL) 4 to TRL7 (system prototype validated in an operational system).

Prior to a large-scale deployment of equipment to the field, initial steps included a reconnaissance survey and field test at Bell Creek and numerical modeling of the K-wave method using parameters specific to the Bell Creek Field. A 3-D survey design was also needed to get acquisition contractor bids and a seismic acquisition permit. An initial three-well field test was done to better understand the wellhead hardware configurations and test the response from the Bell Creek reservoir. Although useful operational information resulted, signal from the first-generation valve-actuated gas release and gas injection source was not recorded in neighboring wells. As a result, development of a stronger, hydraulically driven "displacement" wellhead-mounted source that had been planned was accelerated.

After the initial field test, numerical modeling efforts conforming to the Bell Creek geology and well characteristics progressed over a period of months from April through November 2017, with preliminary reports in the interim (Appendix C). Modeling results indicated that even with the new source design, the fundamental concepts behind the K-wave method exhibited problems. The modeling revealed a significantly greater attenuation of the signal at the wellbore perforations than expected, totaling on the order of 10^{-8} from source well to receiver well over a 400-m well spacing. Modeling also showed that greater source frequency bandwidth was needed to produce guided waves that would propagate within a 30-foot-thick reservoir layer such as that at Bell Creek. In addition, to keep guided waves contained in the reservoir, the modeling showed that the reservoir layer seismic velocity would need to be slower than the velocities of the bounding layers. This geologic velocity relationship exists in some fields but is opposite to what exists at Bell Creek.

The modeling results prompted the second field test with the stronger second-generation "displacement" source that had been developed in the interim, on the possibility that the modeling result was incorrect. The displacement source was tested on a four-well geometry and, after analysis, was shown to have also failed to produce a detectable signal at neighboring wells (Appendix D). Concurrent with the field test, a 3-D seismic survey intended to serve as a baseline for project validation was acquired. The 3-D seismic survey also served as a monitor data set for the portion of the project area where CO_2 injection had already commenced in case well-spacing considerations forced a replan of the project location to an area with closer well spacing. This was a concern at the time as the project area was developed with twice the well spacing than what was expected in the original plan (160-acre 5-spot well spacing instead of 40-acre well spacing).

This report details the findings from the two field tests and the modeling effort as it relates to this no-go decision. Although no baseline and monitor data were collected as part of this study using the K-wave method, the 3-D seismic survey initially intended to serve as a baseline survey for method validation purposes was successfully acquired (Appendix B). This 3-D seismic survey serves as a monitor data set for the portion of the project area where CO_2 injection had commenced prior to the start of this project (Appendix B). The 3-D and 4-D seismic interpretations of the reservoir in the project area as well as the geologic modeling and dynamic reservoir simulations done as part of this study have provided value for ongoing and future synergistic activities at Bell Creek related to the U.S. Department of Energy (DOE) carbon storage goals (Appendix E).

KRAUKLIS WAVE TECHNOLOGY

In 1962, Dr. Pavel V. Krauklis, a Polish–Russian mathematician, predicted the existence of a slow-moving wave in a fluid layer bounded by two elastic halfspaces (Krauklis, 1962). This slow fluid wave has been referred to as the K-wave since 2012. At low frequencies, it is dispersive, with a phase velocity approaching zero as frequency approaches zero and an amplitude that is frequency-independent (Korneev and others, 2012). Wave energy is predominantly within the fluid, as displacement within the bounding layers rapidly falls to zero. Korneev and others (2012) note that at the high-frequency limit, the slow fluid wave becomes a nondispersive Scholte wave, a guided wave that propagates along a solid–fluid interface (Scholte, 1942).

Similar to the guided waves such as Stoneley and Scholte waves, the K-wave is less susceptible to attenuation than P- and S-waves (Krauklis and others, 1992) as the energy does not disperse geometrically as a body wave and appears as a late-arriving, high-amplitude event in seismic data (Figure 3)(Shigapov and Kashtan, 2011). Although rarely detected, slow-moving waves thought to be K-waves have been observed in field and laboratory data (Tang and Cheng, 1988; Nakagawa and others, 2016; Ferrazzini and Aki, 1987; Hassan and Nagy, 1997; Goloshubin and others, 1994). Numerical modeling has been done in order to better understand the properties and potential applications of the K-wave (Frehner and Schmalholz, 2010; Korneev, 2008; Krylova and Goloshubin, 2016; Liang and others, 2017). Proposed applications for this wave include hydraulic fracture monitoring and reservoir monitoring.

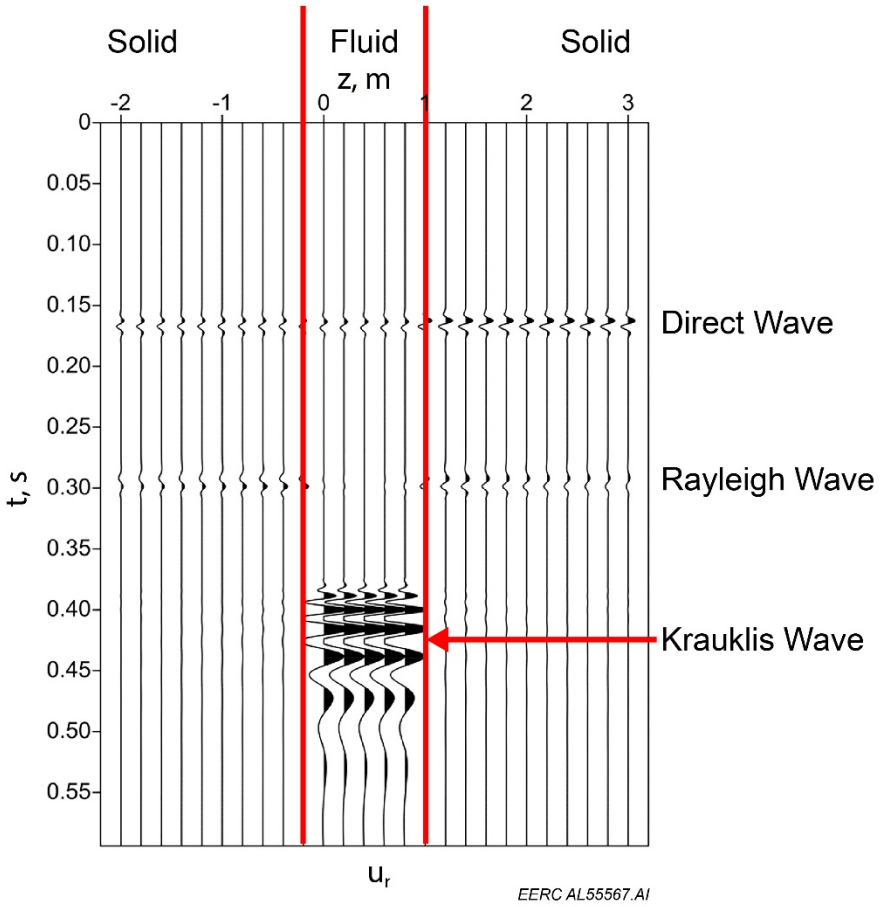

Figure 3. Simulation data showing synthetic seismic records generated from propagating signal through a model containing a fluid-filled fracture (modified from Shigapov and Kashtan, 2011).

Prior to this study, the development of K-wave technology for reservoir monitoring had reached TRL4, where basic technology components had been integrated and validated in a laboratory environment by Seismos. The K-wave technology builds on studies done by Korneev and others (2006) and Lawrence Berkeley National Laboratory (Korneev and Bakulin, 2009). Korneev and others (2006) conducted numerical simulations to demonstrate how guided waves can be used for time-lapse monitoring of fluid-saturated reservoirs where an injected fluid displaces in situ fluids. The K-wave method proposed the use of a wellhead-mounted source to generate tube waves to propagate energy down the wellbore, which would convert into guided waves at the reservoir layer, propagate horizontally in the reservoir, convert back to tube waves at neighboring wells, and propagate up to wellhead-mounted receivers (Figure 2). For real-world conditions that conform to the attenuation and wave conversion assumptions used by Korneev and others (2006), guided waves showed promise for time-lapse monitoring of reservoirs undergoing CO_2 injection.

Seismos has developed hardware sources and receivers that can be mounted to wellheads. By outfitting multiple wells with sources and receivers, in theory, a mesh of crosswell ray path coverage within the reservoir would be created (Figure 4). Data recorded at receiver wells during a preinjection baseline survey would be analyzed to identify the source energy wave train and establish the well-to-well velocities and travel times, signal attenuation, frequency characteristics and, possibly, other useful attributes. In a reservoir not dominated by fractures that propagate K-waves, the method may still work by monitoring other guided waves that propagate laterally through the reservoir, including Stoneley, Scholte, and Lamb waves. The Bell Creek reservoir is not known to have fractures, so for this study, K-waves were unlikely to be a factor; it would be a test using other guided waves. After collecting a preinjection baseline survey, as incremental injection proceeded, additional time-lapse surveys would evaluate changes in the well-to-well attributes to infer the presence and extent of CO_2 saturations between source and receiver wells. After the initial challenge of baseline data analysis, it was anticipated that subsequent surveys would require incremental processing that would be completed in a matter of days and updated CO_2 saturation front map images would be created for the field operator (Figure 5). In a future evolution of the method, Wi-Fi-enabled recording devices paired with semipermanent installation of the sources and receivers would upload the data to an Internet cloud-based system for processing and subsequent delivery of interpretable output.

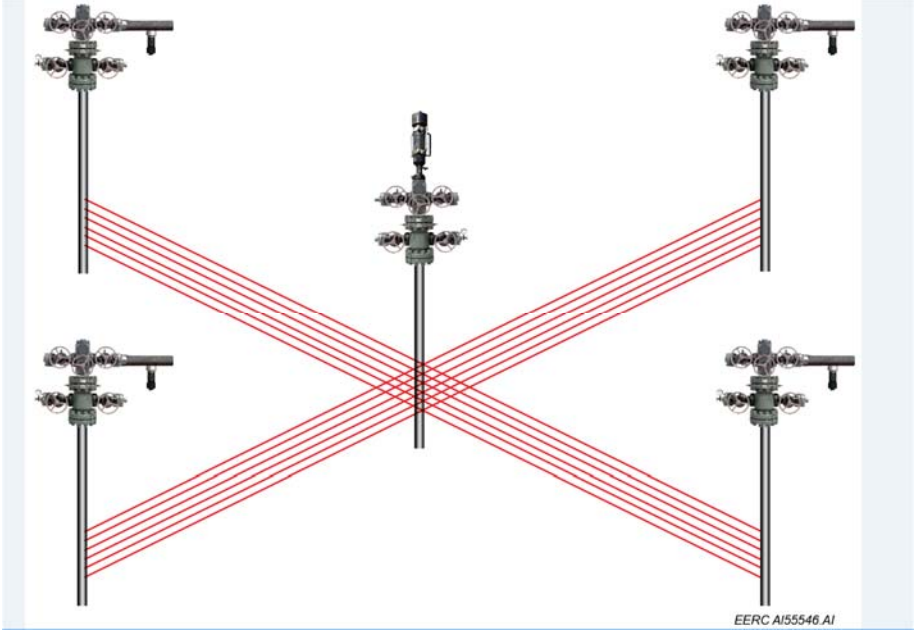

Figure 4. Illustration of K-wave ray paths monitored in a hypothetical “five-spot” injection pattern. The injector well fitted with source is in the middle. Outer wells are fitted with receivers.

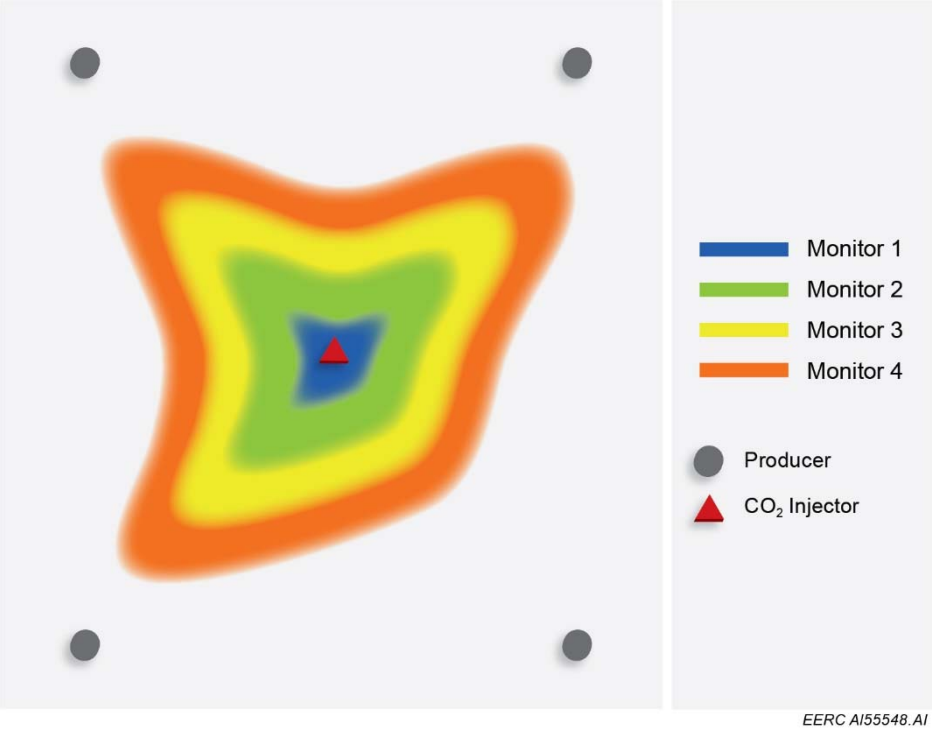

Figure 5. Plan view illustration of a hypothetical CO_2 saturation front evolution within a five-spot pattern as inferred from successive monitor surveys using the K-wave system.

The commercial implementation of the K-wave system components is at an early stage of TRL4. The field instrumentation hardware and energy sources have been demonstrated in semiautomated mode, which means on-site personnel are required for data acquisition. It was anticipated that semiautomated operation would continue for the foreseeable future. The concept of field Wi-Fi data transfer was tested in the lab and used in the field over a local portable network to collect data on a laptop for on-site evaluation and quality control (QC). Power to field data acquisition stations was supplied by batteries. Solar panels and a control system to maintain power in the field for a semipermanent installation are a future evolution.

FIELD TESTING AND MODELING

The project plan included outfitting up to 30 wells in the project area with equipment and acquiring a baseline survey and multiple monitor data sets (Figure 6). Prior to committing to a large deployment of equipment to the field for the baseline survey, a reconnaissance trip and initial field test took place in November 2016 to test the response of the Bell Creek reservoir and gather information about the wellhead hardware configuration for connecting the source and receivers to the wellheads. In-depth numerical modeling efforts conforming to the Bell Creek geology and well characteristics progressed from April through November 2017 following the initial test. In October 2017, a second field test was done to test a newly developed source that was designed to generate a much stronger signal than the first-generation source.

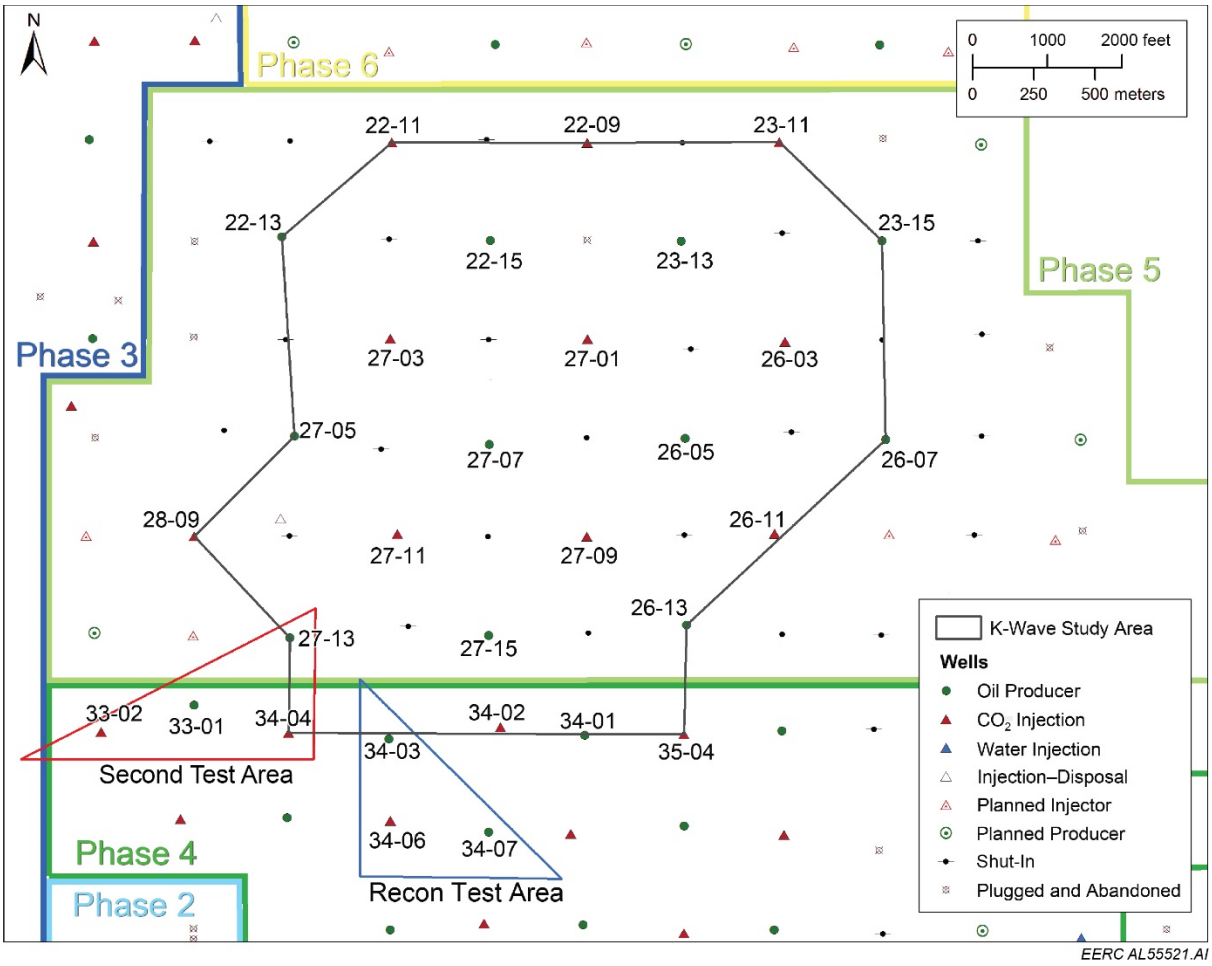

Figure 6. Map of the planned project area and the wells used during the two field tests.

Reconnaissance and Initial Field Test

The first field test occurred November 30 – December 1, 2016, and deployed equipment that included a first-generation wellhead source, wellhead receivers, continuous recorders, source control electronics, and a local Wi-Fi network (Figure 7). The first-generation source was a valve-actuated device designed to either briefly vent CO_2 gas from an injection well or inject a pulse of nitrogen into a production well fluid column to create a displacement pulse that travels down the well as a tube wave. Wellhead receivers are a specially configured hydrophone that uses a piezoelectric sensor to generate an electrical signal in response to a change in pressure in the fluid column (Figure 8). The cable attached to the receiver has an amplifier with a fixed gain to adjust the amplitude of the signal, which is recorded by and stored on the continuous recorder. A portable Wi-Fi network is used to enable a laptop computer to wirelessly access data on the continuous recorder and operate the source in the field.

Figure 7. Field equipment used in the first field test.

Figure 8. Wellhead hydrophone receiver.

Data acquisition equipment was temporarily installed on three wells: two producers, 34-03 and 34-07, and one injector, 34-06 (Figure 6). The source and receiver were installed on Wells 34-06 and 34-07 in turn using two temporary flange mounts (Figures 9 and 10), and a receiver was mounted directly on Well 34-03 (Figure 10). A tank of compressed nitrogen was used to actuate the mounted source. Depending on the wellhead pressure, the source is operated in one of two ways. For injection wells under high pressure, an exhaust valve vents a small jet of CO_2 for one-tenth of a second (Figure 11). The pressure release induces a pulse in the well. For producing wells operating under lower pressure, compressed nitrogen is connected to the valve and injected into the well to induce a pulse (Figure 11). The injector 34-06 was operating at ~1400 psi, and producer 34-07 was operating at a lower pressure of ~400 psi. Operation at the producing well required two nitrogen bottles, one to operate the valve and the other to provide high-pressure gas injection.

Figure 9. Left: two fabricated flange mounts. Right: a flange mount connected to the top of the CO_2 injection well with source and receiver attached to the horizontal arms.

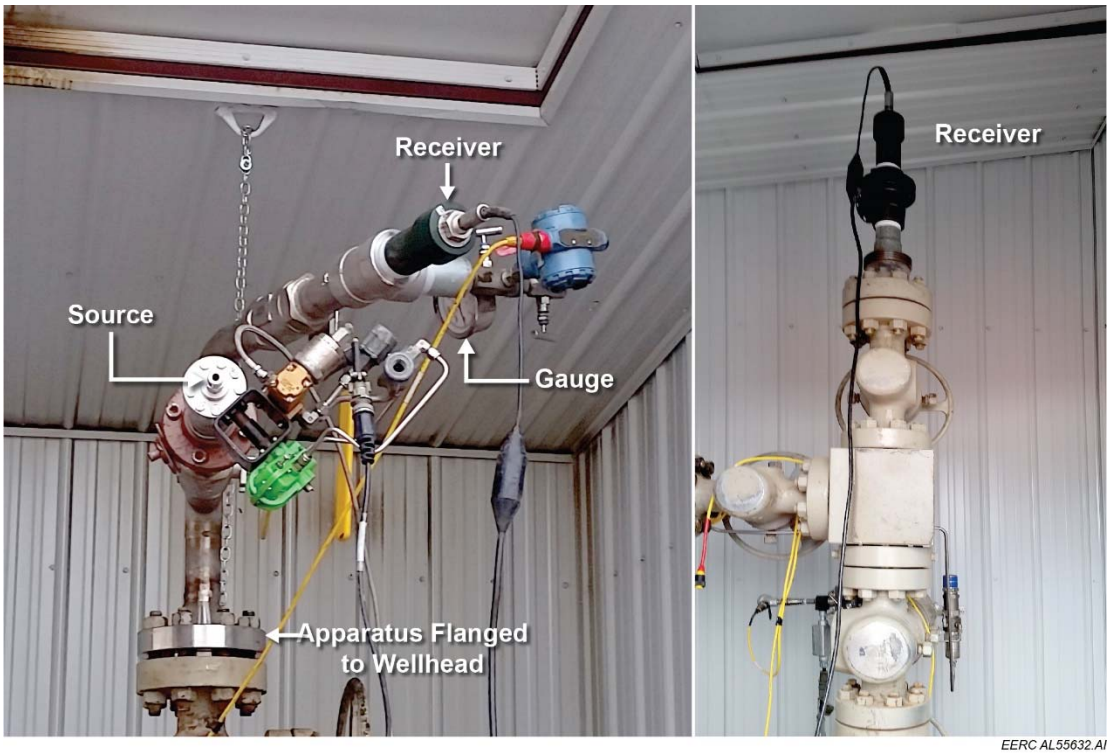

Figure 10. Left: wellhead equipment set up for injector Well 34-06. Right: receiver attached directly to the production Well 34-03.

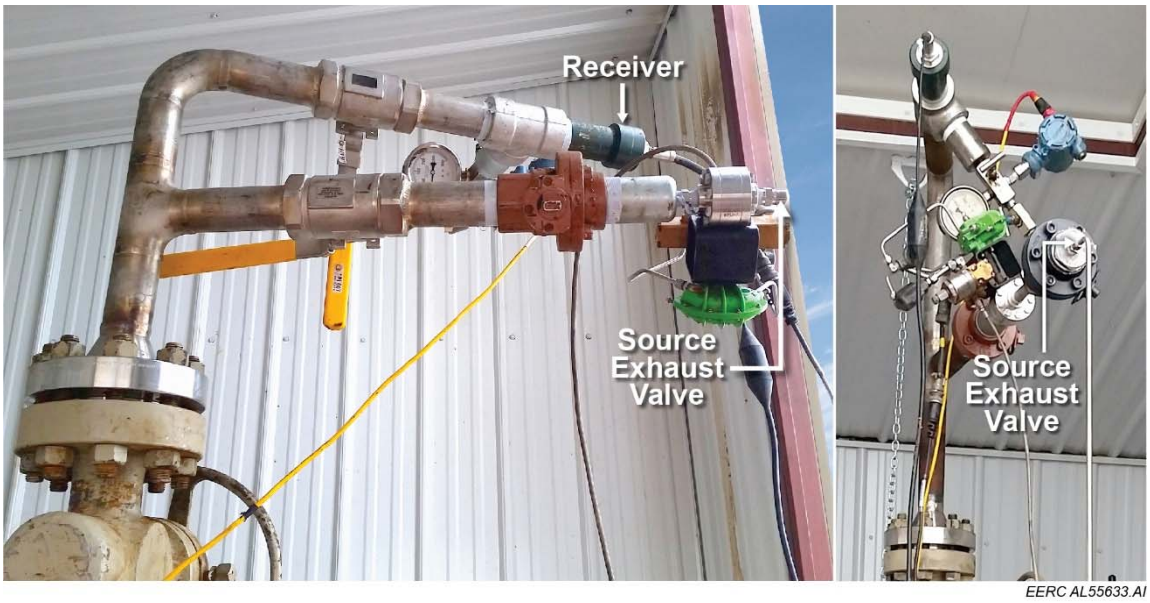

Figure 11. Left: the wellhead mounted source indicating the source exhaust valve. Right: mounted on the 34-07 production well, tubing carrying highly compressed nitrogen is attached to the source valve.

Data were acquired by firing the source in a programmed sequence controlled by a laptop computer via the portable Wi-Fi network. Approximately 150 shots were fired at 45-second intervals at Well 34-06. Data records were downloaded wirelessly to the laptop from the data recorder to QC test shots in the field. Test shots on Well 34-06 as recorded with the mounted receiver showed a strong initial pulse from the source and a series of good tube wave reflections off the well bottom with round trip times of about 6 seconds (Figure 12). As the source fired at 34-06, data were also being recorded by the receivers on Wells 34-07 and 34-03. However, as the timing and character of the received signals, if any, was unknown and expected to be highly attenuated, field inspection of data recorded at the nearby wells would not be useful. These data were later processed in the office by Seismos for interpretation, but no discernible received signal was identified on the data from the nearby wells.

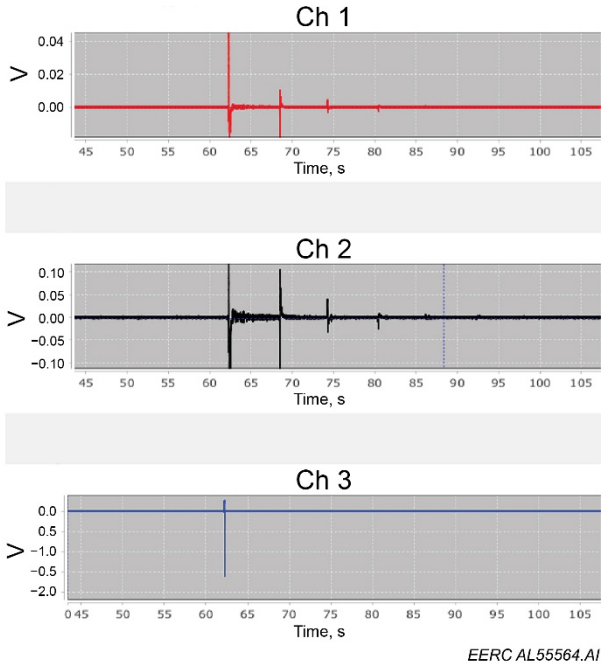

Figure 12. Test shot data from the source and receiver mounted on Well 34-06. Channels 1 and 2 have different gain settings, but both show the initial shot pulse followed by echoes off the well bottom. Channel 3 is the source time break. Note the tube wave returns have alternating opposite polarity with each echo off the bottom and attenuate to the noise level after 5 or 6 reflections.

Test shots acquired with the source at Well 34-07 did not show good tube wave returns. The waveform had some apparent consistency of character but not in a manner similar to those at the injector well, and echoes from the well bottom were not recognizable or occurred at unexpected time intervals (Figure 13). Several troubleshooting tests were performed in various combinations, although none resolved the problem. Tests included increasing source nitrogen pressure to 1500 psi to boost amplitude, fashioning an accumulator volume from a valve to increase the volume of nitrogen at the injection point, shutting off production flow to test a nonflowing well,

bleeding gas from the top of the apparatus and tree until liquid appeared in an attempt to eliminate bubbles of either produced CO_2 or induced N_2 from the source injection bottle, and powering down the chemical pump to test if noise was being induced in the line. The configuration of the receiver on Well 34-07 is physically at the highest point on the wellhead tree. Gas that had collected there was bled off several times during the test. It was noted by the field operator that CO_2 breakthrough was occurring at this well, and it was thought that the CO_2 gas was coming out of solution in the tubing as it flowed from the higher-pressure reservoir to the surface. The gas appeared to be impacting both the transmitted signal and its reflection. Gas that collected under the receiver was also probably impacting the measured initial pulse and any received signal. As with shots from Well 34-06, no received signal was identified on data recorded at the neighboring wells.

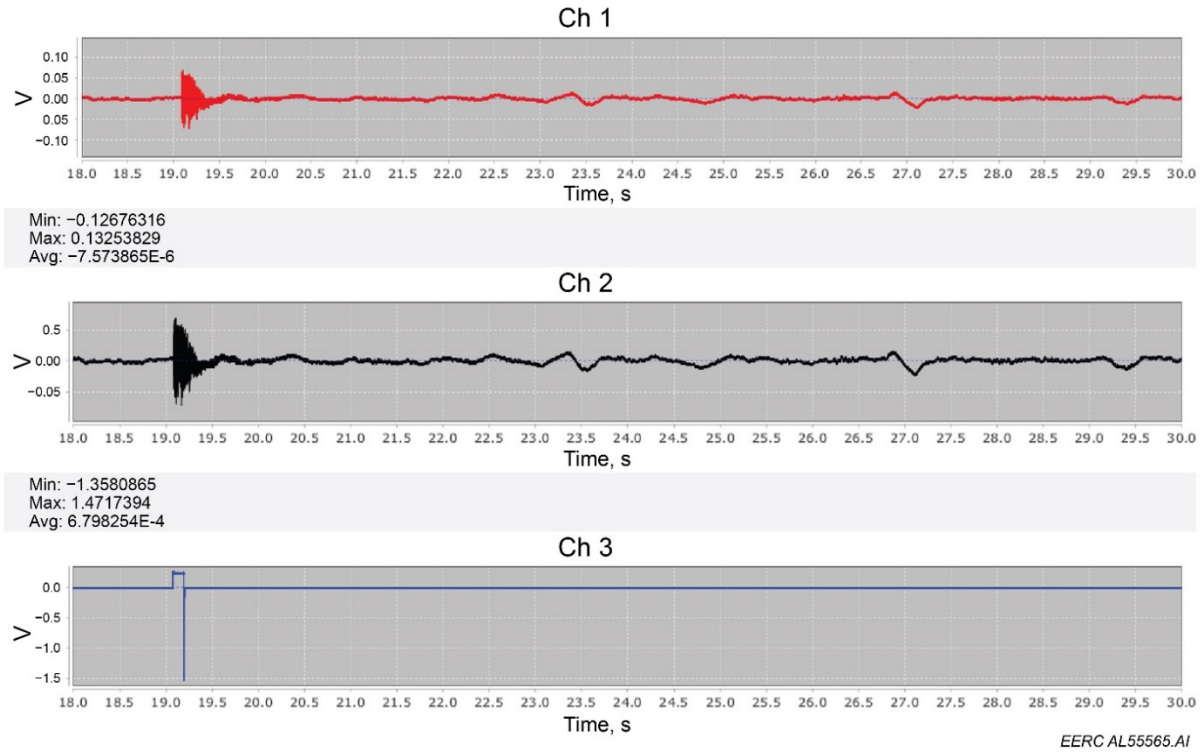

Figure 13. Test shot data from the source and receiver mounted on well 34-07. Channels 1 and 2 show a test shot displayed with different gains. Channel 3 is the source impulse. Note the impulse character on Channels 1 and 2 is not sharp, and there are no identifiable tube wave returns at the expected 6-second return times. Damped event arrivals with polarity consistent to that of the source are visible ~4 and ~8 seconds after firing, but their origin is unknown. Free gas within the well and collecting in front of the receiver is thought to be part of the cause.

Numerical Modeling

Numerical modeling was conducted by the Seismos technical team to better understand the physics of the conversion from tube waves generated in the well to seismic waves in the formation and back again at a nearby well. The modeling objective was to determine numerical solution(s) to the equations that control conversion from tube waves to seismic waves, code the solution, apply

material properties relevant to Bell Creek, and quantify signal amplitudes for conditions relevant to Bell Creek.

A simple model was built to study the effect of energy conversion on the amplitude of returning signal at neighboring wells. It was expected that only 0.1%–1% of the energy from the tube wave at the source well gets converted into seismic waves that propagate through the formation. Similarly, only 0.1%–1% of the seismic wave energy that arrives at a nearby well is converted through the perforations to tube waves at the receiver well. Two types of coupling were examined in order to quantify this conversion of energy. Coupling 1 occurs at the well bottom where the pressure changes carried by the tube wave generate a downward force on the reservoir producing seismic waves. The mathematics of Coupling 1 is represented in the geophysical literature. Coupling 2 occurs at the perforations where the tube wave pressure change pushes fluid through the perforation generating seismic waves. No representation of Coupling 2 existed in the literature, and the mathematics of the energy conversion were derived as part of the current research (Appendix C). Energy conversion from coupling along the borehole wall, a third coupling mode, was assumed to be negligible for cased wells and was not considered for this study. The coupling schemes were integrated into a simple model that consisted of two wells 400 m (~1300 ft) apart: one filled with water and the other with CO_2 (Figure 14). The model did not incorporate geologic variables initially, as the intent was to understand the coupling mechanisms. Once the coupling mechanisms were understood, a layered structural model based on Bell Creek geology was included in the analysis, along with a homogeneous model using average values from the layered model.

Two versions of the initial model were used for simulation: one with a homogeneous medium and another that incorporated a low-velocity layer near the bottom of the wells with a thickness of 84 m (~275 ft) and a seismic velocity 20% lower than surrounding layers. The source was positioned on the well filled with water, and the receiver was on the well with CO_2. The source incorporated amplitude, duration, and frequency values consistent with the second-generation displacement source. Open-source code, AWP-ODC-OS, was used to solve the 3-D elastic wave equation using the staggered grid finite difference method in order to simulate seismic wave propagation in the model. No tube wave attenuation was accounted for in the simulations.

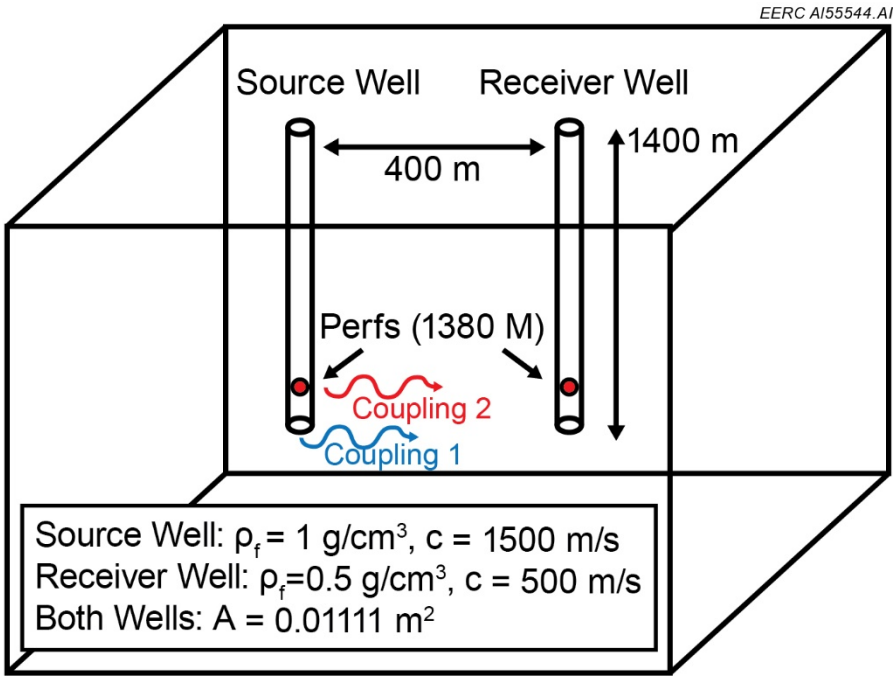

Figure 14. 3-D model used for numerical modeling containing two wells. Coupling from tube waves to seismic waves (and vice versa) occurs at both the well bottom (Coupling 1) and at the perfs (Coupling 2) (image modified from Seismos [2017]).

A Gaussian pulse with a 10-Hz frequency and amplitude of 1 MPa was used to represent the tube wave source. A maximum amplitude of 2 MPa occurs at the source well bottom as the source pulse constructively interferes as it reflects. The simulated signal recorded at the wellhead receiver was of very low amplitude with a computed pressure change of ~0.02 and ~0.04 Pa (Figure 15), which is an attenuation of 10^{-8}. The dominant arrivals at the receiver well are associated with the seismic body waves (P- and S-waves). At the modeled well spacing, recorded signal showed little to no separation between P- and S-wave arrivals. Guided wave arrivals appear soon after body wave arrivals but have significantly lower amplitudes. It was concluded that low-frequency guided waves were not efficiently trapped in the low-velocity layer. The simulation results show that the coupling at the perforations, Coupling 2, was two orders of magnitude higher than coupling at the bottom of the well, Coupling 1. The simulations confirmed that the signal amplitude is inversely proportional to the well separation distance, as expected of body waves.

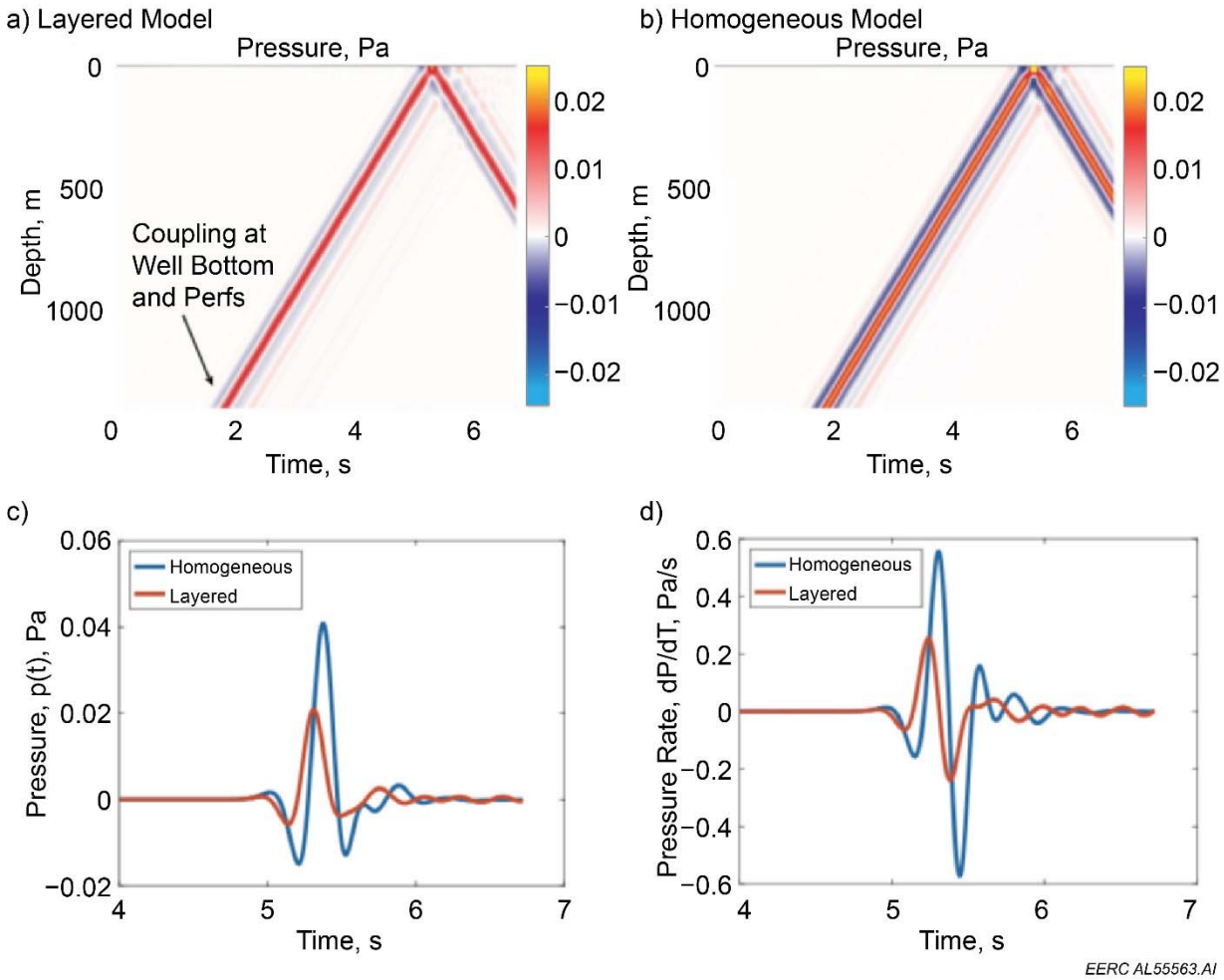

Figure 15. Simulation results for the receiver well. a) Space-time plot showing excitation of tube waves by seismic wave coupling at the well bottom (Coupling 1) and perfs (Coupling 2) for the layered structural model and b) for the homogeneous half-space structural model. c) time series of pressure, p(t), at receiver wellhead. d) Same as "c" but plotting pressure rate, dP/dt, as would be recorded by a hydrophone. Waveforms from the layered structural model are similar in amplitude and waveform shape to those from a homogeneous model. There are no obvious guided wave arrivals (Seismos, 2017 Appendix C) (image courtesy of Seismos).

Bell Creek well log data were integrated into the model, and simulations were rerun. Material properties were assigned using log values. The perforated interval length, a parameter, was set at 5 m. Simulation results led to three main observations about challenges associated with successful application of the K-wave technology at Bell Creek (Appendix C):

1. The Bell Creek sand reservoir is not conducive to guided wave propagation. The reservoir sand has a higher velocity than the surrounding shale layers. A lower reservoir velocity than surrounding layers is a condition for the layer to act as a wave guide. Stoneley waves may exist at the boundary between the reservoir and surrounding rock; however, no evidence of Stoneley waves was found in simulations. Guided waves are

more likely to be seen when the source energy bandwidth includes wavelengths comparable to or smaller than the reservoir thickness. For the 10 -m thickness of the Bell Creek sand reservoir, a source bandwidth that includes frequencies of 100 Hz or greater are needed.

2. Coupling at the perforations between the well and formation has a low conversion efficiency at both the source and receiver wells, which results in very low amplitude signal at the receiver well; an amplitude reduction by a factor of 10^{-8}. Coupling would be more efficient at higher frequencies as demonstrated by several crosswell imaging studies such as Korneev and others (2005) that used high-frequency sources to test tube wave to seismic wave to tube wave conversions.

3. Lack of distinct P- and S-wave arrivals at the receiver well makes identification of related arrivals in the tube wave time series difficult. A source with higher bandwidth frequency output would help by making the separation between P- and S-wave arrivals more distinct and provide more detail to thinner structural layers.

Displacement Source Test

Contemporaneous with the modeling, a stronger second-generation displacement source was developed and constructed. Although the modeling results were not encouraging, the technical teams at the EERC and at Seismos, in consultation with the project manager at DOE, concluded that a second field test employing the new source would be the appropriate next action on the possibility that the modeling result was incorrect. Lessons learned during the first field test would be applied by avoiding wells known to have CO_2 breakthrough, if possible, and placing receiver hardware lower on the wellhead assemblies using hardware developed specifically for the Bell Creek wellheads.

Another technical concern had manifested itself during the modeling as the field operator had chosen to develop the project test area using one-quarter of the wells and at double the well-spacing as previous development phases (160-acre spacing compared to 40-acre spacing). This meant that signal entering the reservoir at a well would need to propagate twice as far to reach neighboring wells (up to 800 meters). Propagating measurable signal over such a distance was expected to require a wellhead source with significant energy, and it was unknown if the new source would provide sufficient energy. To test how far a signal from the displacement source could propagate, the field test was designed using a four-well geometry so that four different distances would be tested: single well spacing, double well spacing, and the diagonals between both. If the source could propagate a measurable signal between single-spaced wells, but not double-spaced wells, a contingency plan was expected to involve collecting project data in Phase 4, which had single-spaced wells, although care would need to be taken to avoid areas where significant CO_2 had already been injected.

Shortly after the second field test, the 3-D seismic survey intended to serve as a baseline for project validation was acquired during the last days of October 2017. The survey, when time-lapse differenced from the existing 2015 baseline survey, also served as a monitor data set for the portion of the project area where CO_2 injection had already commenced in case signal quality problems in

the expanded well-spacing area in Phase 5 forced a replan of the project location to Phase 4 with a 40-acre well spacing.

The displacement source uses a hydraulic power pack to operate a piston system connected directly to the wellhead that generates a pulse by displacing fluid in the wellhead fluid column (Figure 16). Unlike the first-generation source, the new source does not have an exhaust valve and was designed to inject a pulse into the well, regardless of the wellhead pressure. A new and more robust source-well receiver designed to accommodate the higher-pressure pulse of the displacement source was deployed to capture the source signature (Figure 17).

Figure 16. Left: the second-generation hydraulic “displacement” source. Right: source hydraulic power pack.

Figure 17. Second-generation hydrophone receiver for use on the source well. High-pressure pulses produced by the hydraulic displacement source required a more robust receiver design.

Four wells were outfitted for testing with the source and receivers: two injectors 33-02 and 34-04 and two producers 33-01 and 27-13 (Figure 6). Equipment was deployed in similar configurations at each well. The source was mounted vertically at the top of the wellhead, with the new receiver mounted directly below. The first-generation receiver for measuring smaller return signals was attached on all four wells, but on the bottom side of the bridle to reduce the impact of gas bubbles directly interfering with its response (Figure 18).

The source was deployed at each well in turn. Data acquisition at the first well, 27-13, proceeded without incident with over 6 hours of pulsing, although it was noted that the hydraulic hose to the source was beginning to wear from constant rubbing against the wellhead. At the second well, 33-02, a valve within the hydraulic power pack needed replacement after 2 hours of pulsing, and Viton o-ring seals failed within the source 30 minutes after the valve was repaired. Seal damage was severe and was attributed to exposure to the small amount of H_2S in the wells, which is known to damage Viton. Seal problems at Bell Creek would likely be remedied with a different choice of seal material that is resistant to H_2S, such as Nitrile. The hydraulic line from the power pack was noted to have become twisted during acquisition on the third well, 33-01, on which pulsing proceeded for more than 6 hours. There were also indications that CO_2 breakthrough was occurring and may have severely impacted the strength of the source signal; the source is at the highest point on the wellhead, so free gas could collect below the source and interfere with the displacement pulse. Acquisition on the fourth well, 34-04, was concluded early because of seal failure after about 100 pulses. Other acquisition challenges that affected the source operations

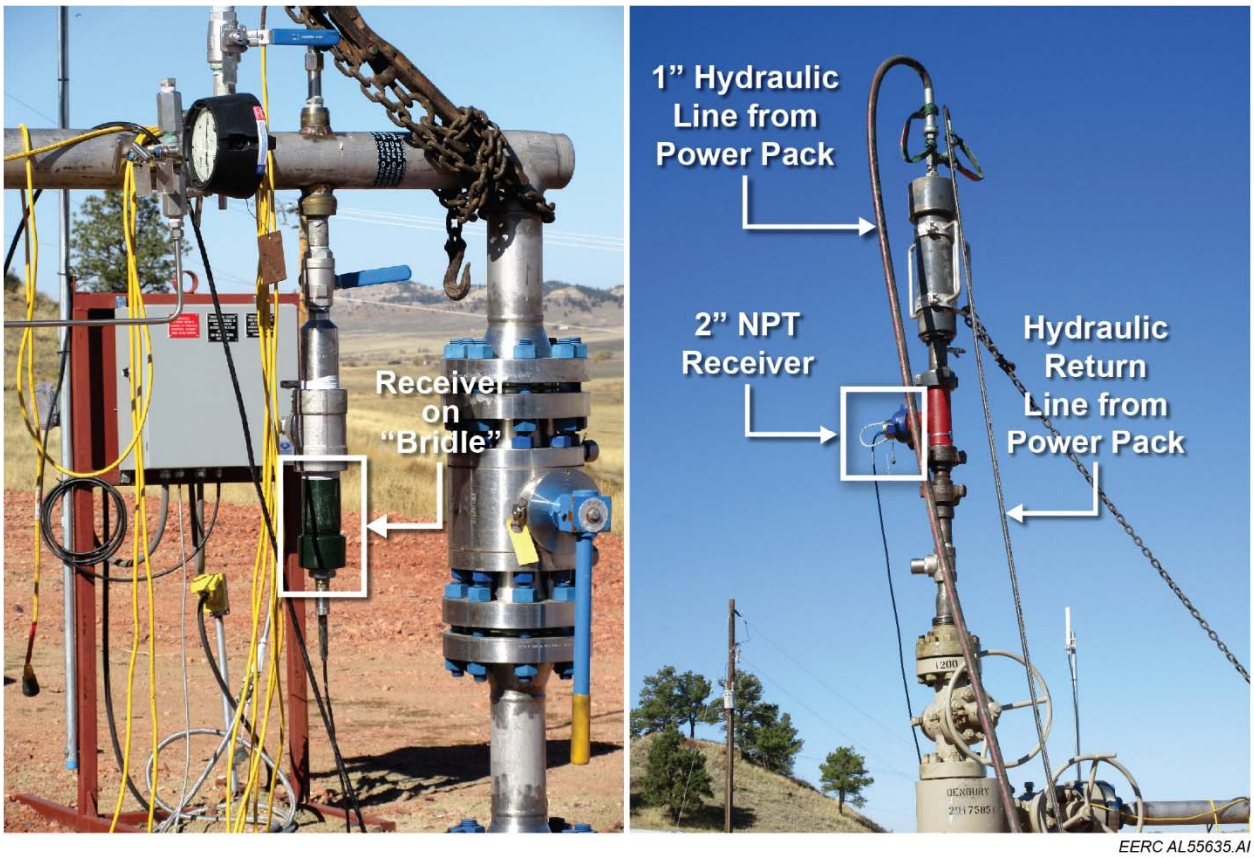

Figure 18. Left: a first-generation receiver mounted on the wellhead bridle. Right: second-generation source and monitor receiver mounted on the wellhead.

included the pressure differences between injection and producing wells; pulsing on injectors with high back pressure induced stress on the source, and low-pressure producers might have free gas coming out of solution or insufficient back pressure to move the source back to the starting position. More details of the field test can be found in the Seismic field report in Appendix D.

Successful tube wave returns were recorded at each well except producer 33-01, which indicated CO_2 breakthrough as noted earlier (Figure 19). Data were analyzed and interpreted by Seismos to determine if any recorded signals at neighboring wells could be attributed to the source. Results showed that no signal was recorded between the two producers (33-01 and 27-13), and no signals were recorded between injectors and producers. A signal that correlated with the source appears to have been recorded between the two injectors (Figure 20). The correlated signal recorded between the two injectors has a time lag of 12.2 seconds, which is anomalously long. Analysis was done to see if a pathway could be determined that would exhibit such a long travel time, but one could not be found. The pathway was not interpreted to be through the formation and may be signal that travels through CO_2 flowlines that connect the two wells through the distribution manifold more than 2 miles from the well pads (Figure 21).

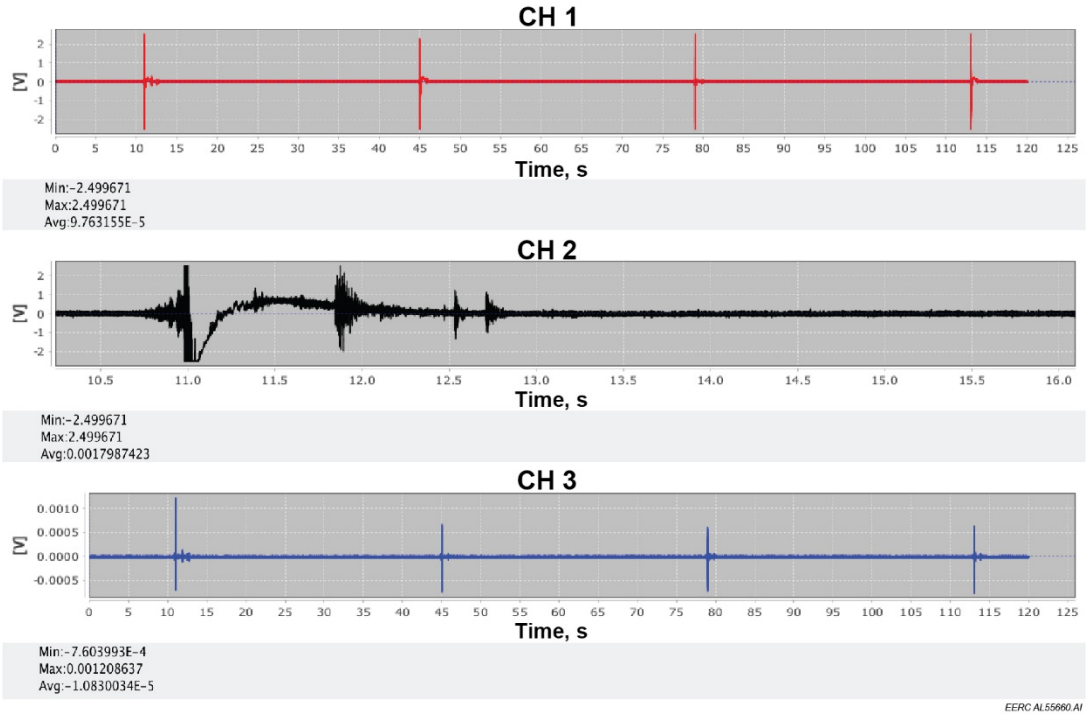

Figure 19. Test shot data from the source and receiver mounted on Well 33-01. Channels 1 and 2 show test shots with source signal but no well bottom tube wave echoes. Channel 2 is a zoom of the initial pulse possibly showing effects of free gas. Channel 3 is the source impulse. This well is a producer, and breakthrough is thought to be occurring. Refer to Figure 12 for a conventional waveform.

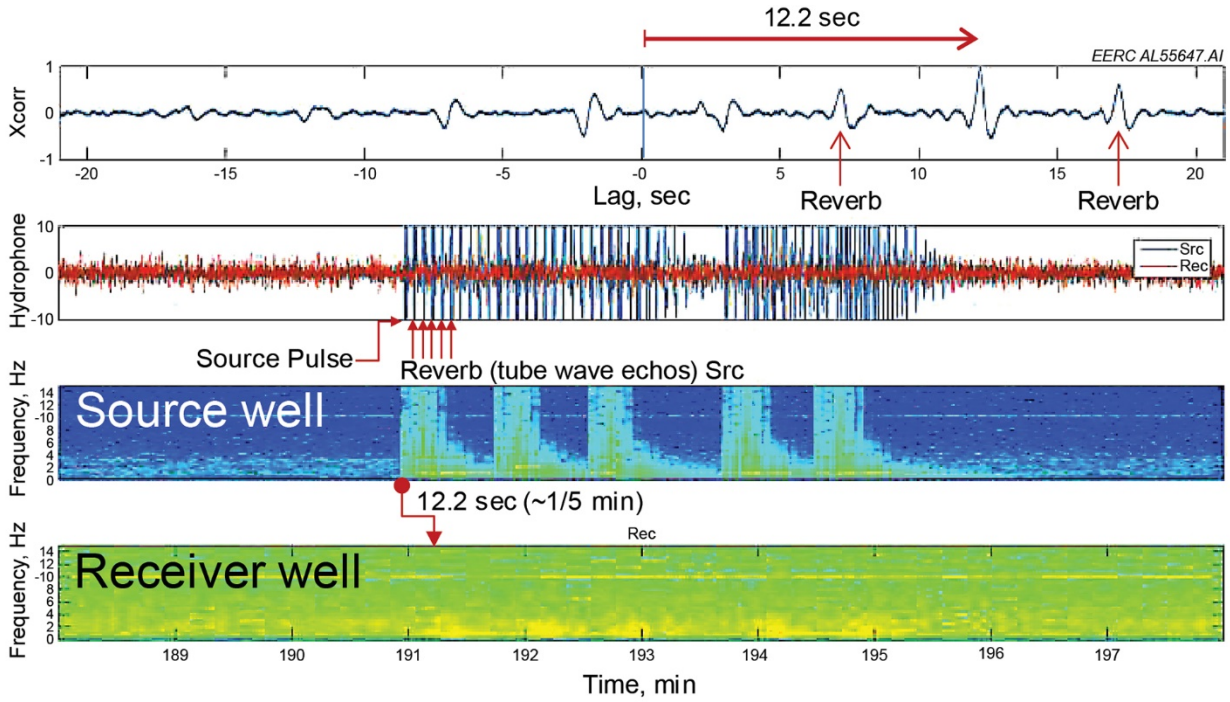

Figure 20. Anomalous result from the second field test with the source at injector 33-02 and receiver at injector 34-04. Top panel: cross correlation between the source signature and the recorded signal at the neighboring well, with the strongest correlation at 12.2 seconds lag. Reverberations at ~5-second intervals are source well tube wave echos. Second panel: source well (blue) and receiver well (orange) recorded traces are overlain. Spikes on the source well trace are pulses and tube wave echoes. Panels 3 and 4 are spectral displays of the source well and receiver well data. Panels 2 and 3 share the time axis (in minutes) on Panel 4. Source energy in Panel 3 is visible on Panel 4 after a lag of ~ 1/5 of a minute (~12 seconds).

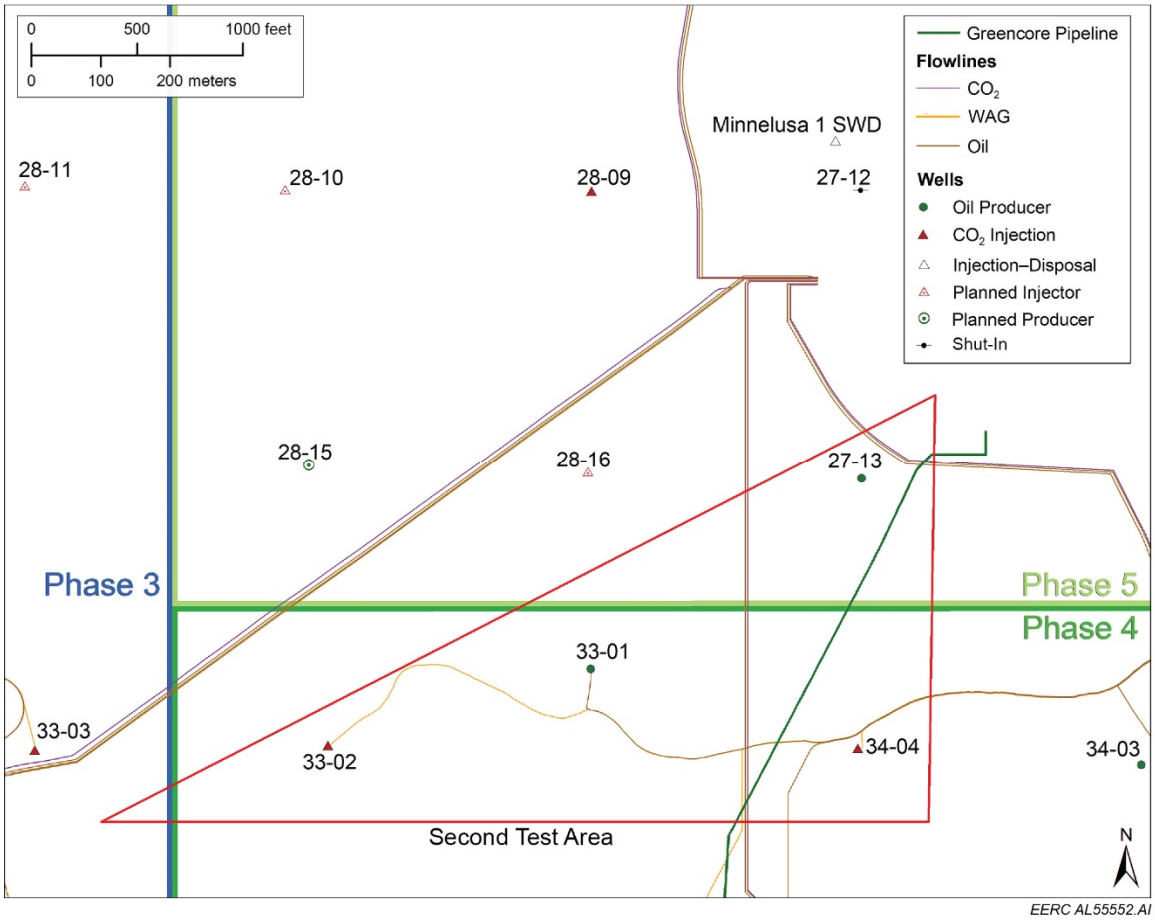

Figure 21. Map of the pipelines in the vicinity of the field test area. Red triangle encompasses the four wells used in the test.

The new hydraulic displacement source failed to produce a detectable signal in neighboring wells, a result which was supported by the modeling results. It was concluded that a source with sufficient strength and bandwidth could not be built to overcome these factors at Bell Creek or other fields within a reasonable amount of time. Five other fields, also undergoing CO_2 injection, were evaluated as possible alternative test locations. However, it was determined that it was highly unlikely that the existing source and receiver system would have sufficient strength to be successful. In consultation with the DOE project manager and technology manager, a no-go decision was invoked to forego additional expenditures as the technology would not meet the current project objectives as defined.

POTENTIAL APPLICATIONS FOR THE K-WAVE TECHNOLOGY

The K-wave test was unsuccessful in meeting the original project objectives of using a new method for tracking the saturation front of injected CO_2 in a CCUS application, although there may be other applications to use guided waves, such as K-waves to better understand the subsurface. The K-wave project design was constructed using wellhead-mounted sources and

receivers in a time-lapse manner to track the evolving saturation front through a sedimentary reservoir over time. Because of the strength of the sources and the attenuation of the signal, this configuration was unsuccessful. Two other configurations were also discussed, which did not meet the project goals, but could have applicability for better characterizing the subsurface.

One potential alteration to the design was to lower the seismic source into the wellbore, which may be able to reduce the attenuation of the signal and provide a higher-frequency range. The thought behind this design was that, with the seismic source closer to the perforated interval, a stronger guided wave package might be able to be produced that could be detected at neighboring wellhead receivers. Although this method has some merit, it is a completely different project design and is very similar in design to crosswell seismic surveys. It may be possible to utilize existing crosswell seismic equipment to track CO_2 saturation fronts through the reservoir over time using guided waves. However, this method is quite invasive, which was counter to the original design.

Another potential application for K-waves and other guided waves is for characterizing hydraulic fracturing operations. In this application, a wellhead source and receiver pair is placed on the well undergoing hydraulic fracturing. In this design, the wellhead source is fired prior to hydraulic fracturing on a single stage and the signal is transmitted down the well in the form of a tube wave. The energy is then transmitted into any existing fractures at the perforations in the form of guided waves; the guided waves travel to the end of the fractures and return via the fractures to the perforations. The energy is then converted back into tube waves and travel back up the well to the wellhead-mounted receivers. After this baseline is acquired, a single-stage hydraulic fracture job is completed, and then the wellhead source is fired again. After the hydraulic fracturing operations, the formation has a lot more fractures, and the repeat signal will be substantially different, such that differencing the baseline and repeat survey can give the operator an idea of the extent of the hydraulic fracturing operations. This process can then be repeated for each stage of the hydraulic fracturing operation and could be used as a tool to better stimulate conventional and unconventional wells. Again, this method was significantly different than the original design and does not meet the project or Carbon Storage Program Goals.

CONCLUSIONS

The EERC and its project partners deployed and field-tested a prototype MVA technology, the K-wave method, in the Bell Creek Field, an operational CCUS field environment. The K-wave method leverages a new way of transmitting energy from the surface to the reservoir targeting guided wave propagation within the reservoir. Guided waves of interest include a new type of wave: the K-wave, a slow-moving, high-amplitude wave that propagates within a fluid-filled fracture.

Prior to full-scale deployment of the K-wave test, two field tests were conducted to better understand wellhead configurations and test equipment. The first trip resulted in several acquisition lessons learned, including the need for a stronger and more robust source and receivers which were applied during the second field test. The first test was unsuccessful in obtaining measurable signal returns at the neighboring wells. Newly developed second-generation source

and receivers were tested during the second field trip. Despite the increased source strength of the second-generation source, returning signals were not successfully recorded at neighboring wells similar to the first field test. Numerical modeling solutions revealed technical challenges of the methodology, including a high degree of signal attenuation on the order of 10^{-8} for a 400-m well spacing and the need for a source capable of producing frequencies of 100 Hz or more to produce guided waves in reservoirs with layer dimensions similar to Bell Creek. The current source has negligible power above 10 to 20 Hz. Additionally, the reservoir at Bell Creek does not have the ideal low-velocity conditions conducive to guided wave propagation. Given the finding from the two field tests and the modeling effort, a no-go decision was made to not pursue the acquisition of additional data in the Bell Creek Field using the K-wave method. It was deemed unlikely that a source with the necessary frequency characteristics could be developed in the project time frame if at all. In addition, secondary sites undergoing CO_2 injection were also investigated. However, it was determined that there was a low likelihood of success at any site using the existing sources and receivers in the proposed design configuration. As a result of these findings, it was determined, in consultation with the DOE project manager and technology manager, to halt the project and invoke the no-go decision.

As part of this study, dynamic reservoir simulations were conducted, and a 3-D seismic baseline data set was acquired and processed. A planned 3-D monitor survey was not conducted as this was meant as a method for validation after the successful acquisition of a baseline and repeat K-wave survey. The original intent was to use these data sets as method validation to determine if CO_2 saturation front extents produced using the K-wave method matched those of conventional methods. Although these data sets were not able to be used for this project, they provide tremendous value for other DOE-funded carbon management research projects and potential future projects conducted at the Bell Creek Field. One example is the Colorado School of Mines project, Charged Wellbore Casing–Controlled Source Electromagnetics (CWC–CSEM) on Reservoir Imaging and Monitoring. This project is located in the same development phase of the Bell Creek Field as the intended K-wave project area. The 3-D seismic data and simulation results provide useful reservoir characterization information for this project. Additionally, the 3-D seismic survey acts as a monitor survey for areas of the field where CO_2 injection had been initiated prior to the acquisition of the survey, which can help validate the CWC–CSEM method. Potential exists for future joint inversion projects using the 3-D seismic surface data and CSEM data.

REFERENCES

Ferrazzini, V., and K. Aki, 1987, Slow waves trapped in a fluid-filled infinite crack—implication for volcanic tremor: Journal of Geophysical Research: Solid Earth, v. 92, p. 9215–9223.

Frehner, M., and Schmalholz S.M., 2010, Finite-element simulations of Stoneley guided-wave reflection and scattering at the tips of fluid-filled fractures: Geophysics v. 75, p. T23–T36.

Goloshubin, G.M., Krauklis, P.V., Molotkov, L.A., and Helle, H.B., 1994, Slow wave phenomenon at seismic frequencies: 63rd Annual International Meeting, SEG, Expanded Abstracts, p. 809–811.

Hamling, J.A., Glazewski, K.A., Leroux, K.M., Kalenze, N.S., Bosshart, N.W., Burnison, S.A., Klapperich, R.J., Stepan, D.J., Gorecki, C.D., and Richards, T.L., 2017, Monitoring 3.2 million tonnes of CO_2 at the Bell Creek oil field: Energy Procedia, v. 114, p. 5553–5561.

Hassan W., and Nagy P.B., 1997. On the low-frequency oscillation of a fluid layer between two elastic plates: Journal of the Acoustical Society of America, v. 102, no. 6, p. 3343–3348.

Korneev, V.A., and Bakulin, A., 2009, *Tube-wave seismic imaging*: U.S. Patent 7,602,669.

Korneev, V.A., 2008, Slow waves in fractures filled with viscous fluid: Geophysics, v. 73, no. 1, p. N1–N7.

Korneev, V.A., and Bakulin, A., 2009, Tube-wave seismic imaging: U.S. Patent 7,602,669.

Korneev, V.A., Bakulin, A., and Ziatdinov, S., 2006, Tube-wave monitoring of oil fields: 76th Annual International Meeting, SEG, Expanded Abstracts, p. 374–378.

Korneev, V.A., Goloshubin, G.M., Kashtan, B., Bakulin, A., Troyan, V., Maximov, G., Molotkov, L., Frehner, M., Shapiro, S., and Shigapov, R., 2012, Krauklis wave – half a century after: 5th Saint Petersburg International Conference and Exhibition – Geosciences: Making the Most of the Earth's Resources, Saint Petersburg, Russia, April 2–5, 2012.

Korneev, V., Parra, J., and Bakulin, A., 2005, Tube wave effects in cross-well seismic data at Stratton Field: SEG Technical Program Expanded Abstracts 2005, January, p. 336–339.

Krauklis, P.V., 1962, About some low frequency oscillations of a liquid layer in elastic medium: PMM, v. 26, no. 6, p. 1111–1115.

Krauklis, P.V., Goloshubin, G.M., and Kraulis, L.A., 1992, Slow wave in fluid-filled layer which imitates an oil collector: Trans. of LOMI Scientific Seminars, v. 22, p. 101–112.

Krylova, A., and Goloshubin, G., 2016, Reflectivity of isotropic fractured layer: SEG Technical Program Expanded Abstracts, p. 3379–3384.

Liang, C., O'Reily, O., Dunham, E.M., and Moos, D., 2017, Hydraulic fracture diagnostics from Krauklis-wave resonance and tube-wave reflections: Geophysics, v. 82, no. 3, p. D171–D186.

Nakagawa, S., Nakashima, S., and Korneev, V.A., 2016, Laboratory measurements of guided-wave propagation within a fluid saturated fracture: Geophysical Prospecting, v. 64, p. 143–156.

Scholte, J.G., 1942, On the Stoneley wave equation: Proceedings Nederlanse Akademic van Wetenschappen, v. 45, Pt. 2, p. 159–164.

Seismos, 2017, Cross-well reservoir monitoring using tube waves: Seismos unpublished report, Austin, Texas.

Shigapov, R., and Kashtan, B., 2011, Oscillations of a fluid layer sandwiched between different elastic half-spaces: 73rd EAGE Conference, p. P046, Vienna, Austria.

Tan, X.M., and Cheng, C.H., 1988, Wave propagation in a fluid-filled fracture – an experimental study: Geophysical Research Letters, v. 15, no. 13, p. 1463–1466.

APPENDIX A

GEOLOGIC MODELING

GEOLOGIC MODELING

Extensive analysis and interpretation of the reservoir geology at the Bell Creek field were done as part of the Energy & Environmental Research Center's (EERC's) Plains CO_2 Reduction (PCOR) Partnership Program large-scale CO_2 storage demonstration project. This geologic characterization effort resulted in a static geologic model that encompassed field development Phases 1–9 (Jin and others, 2017). As part of the K-wave study, the geologic model was clipped to encompass only the immediate project area, including portions of Phases 4 and 5, and modified to include more detailed information for applicable wells such as perforation data. This clipped geologic model was used to define structure and property distributions for dynamic reservoir simulations in order to ensure that meaningful predictive simulations of CO_2 enhanced oil recovery (EOR), associated storage and areal extent of the resulting CO_2 plume could be derived and compared to K-wave monitoring data and conventional 4-D data acquired as part of this study (Appendix E). To minimize any potential upscaling which may be required for detailed simulation work of this nature, dynamic reservoir simulations focused primarily on the Phase 5 area as extensive simulation work focusing on Phase 4 had previously been done as part of the Scalable Automated Semipermanent Seismic Array project (Burnison and others, 2017). This appendix discusses the geologic background and geologic interpretation of the Bell Creek Field related to the geologic modeling effort that is pertinent to understanding the 4-D seismic interpretation done as part of the K-wave project (Appendix B). Additionally, well log data and some of the geologic interpretations discussed in the appendix were used as part of the K-wave study to inform model parameters for numerical modelling of the K-wave method.

GEOLOGIC BACKGROUND

The study area for this project is located in the Bell Creek oil field, an oil field undergoing CO_2 EOR located in the Powder River Basin in southeastern Montana (Figure A-1). The field is mature and has been producing oil since 1967 (Jin and others, 2016). Production decline resulting from primary and secondary recovery led to tertiary recovery using CO_2 injection starting in May 2013 (Salako and others, 2017). Structurally, the field is on a shallow monocline dipping 1°–2° to the northwest, with a strike trending southwest to northeast. The target reservoir in the field is a ~30-foot-thick sand in the Muddy Formation, informally referred to as the Bell Creek sand, which is dominated by high-porosity (15%–35%), high-permeability (150–1175-mD) sandstones. The Lower Cretaceous Mowry Formation overlies the Muddy Formation and provides the primary seal (Figure A-1). Other low-porosity and low-permeability units such as the Upper Cretaceous Belle Fourche, Greenhorn, Niobrara, and Pierre Formations act as secondary seals. The reservoir is underlain by the Skull Creek Formation, which consists primarily of low-permeability shale.

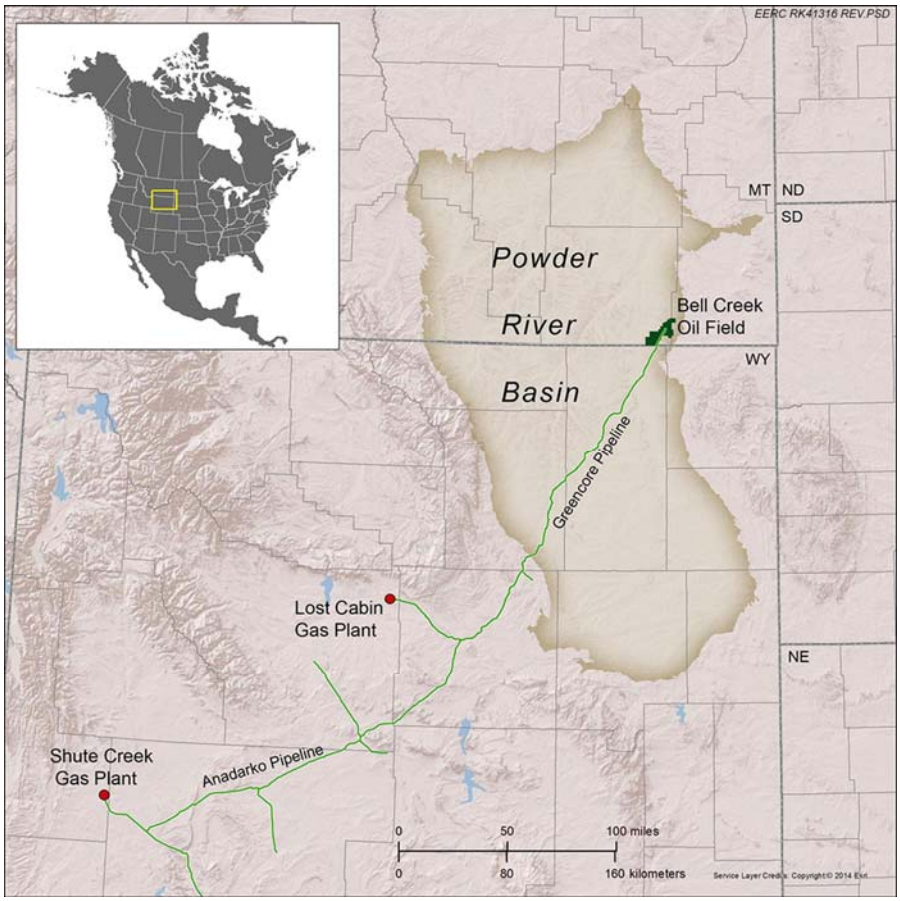

Figure A-1. The Bell Creek oil field in southeastern Montana lies on the eastern edge of the Powder River Basin. The CO_2 used for EOR is transported to the field through pipeline from ExxonMobil's Shute Creek gas-processing plant and ConocoPhillips' Lost Cabin natural gas-processing plant.

Through the course of acquiring and analyzing modern data sets (pulsed neutron logs, seismic data), Jin and others (2017) have proposed an updated interpretation of the Bell Creek reservoir's provenance (Figure A-2). The sand, in which the reservoir mostly resides, was deposited as two stratigraphic units. The two units are the result of a regressive–transgressive sequence divided by lower subaerial exposure and erosion. The lower sand was deposited as a deltaic/shoreline progradation (regression) from the northeast to the southwest during a period of relative sea fall. Higher seismic amplitude features on the eastern edge of the field in development Phase Areas 4 through 6 (Figure A-3) likely represent finer-grained material deposited at the edge of the prograding delta/shoreline during early Bell Creek sand deposition.

Following relative sea level fall, evidence of brief sea level rise is present, resulting in a relatively thin, fine-grained siltstone/mudstone layer overlying the regressive/prograding deposits below. A period of relative sea level fall and subaerial exposure is interpreted to follow. After relative sea level fall and the deposition of regressive sands, the seas began to transgress from the southwest, forming barrier bar and lagoonal deposits in the southwest part of the field. As the sea

level continued to rise, barrier bar and lagoonal environments continued to migrate to the northeast, forming a tidal channel complex.

A brief period of inactivity allowed a local barrier bar to form in Phase Areas 1 and 2 (Figure A-3), along with a connected lagoon to the northeast along the boundaries between Phase Areas 1 and 3 and Phase Areas 2 and 4. These features, which can be seen in seismic data, suggest shoreline orientation at this time to be northwest–southeast. Fluvial sediments, carried to the shallow marine environment seaward from the barrier bar, were transported southeast by longshore currents and covered an incised channel, which was developed previously, during lowstand subaerial exposure. Relative sea level rise then resumed, resulting in the deposition of transgressive sheet sands in the northern regions of the field. This final transgression appears to have occurred relatively quickly, preserving all these features (before wave-reworking made them indiscernible) during burial with the overlying estuarine–shallow marine Springen Ranch deposits.

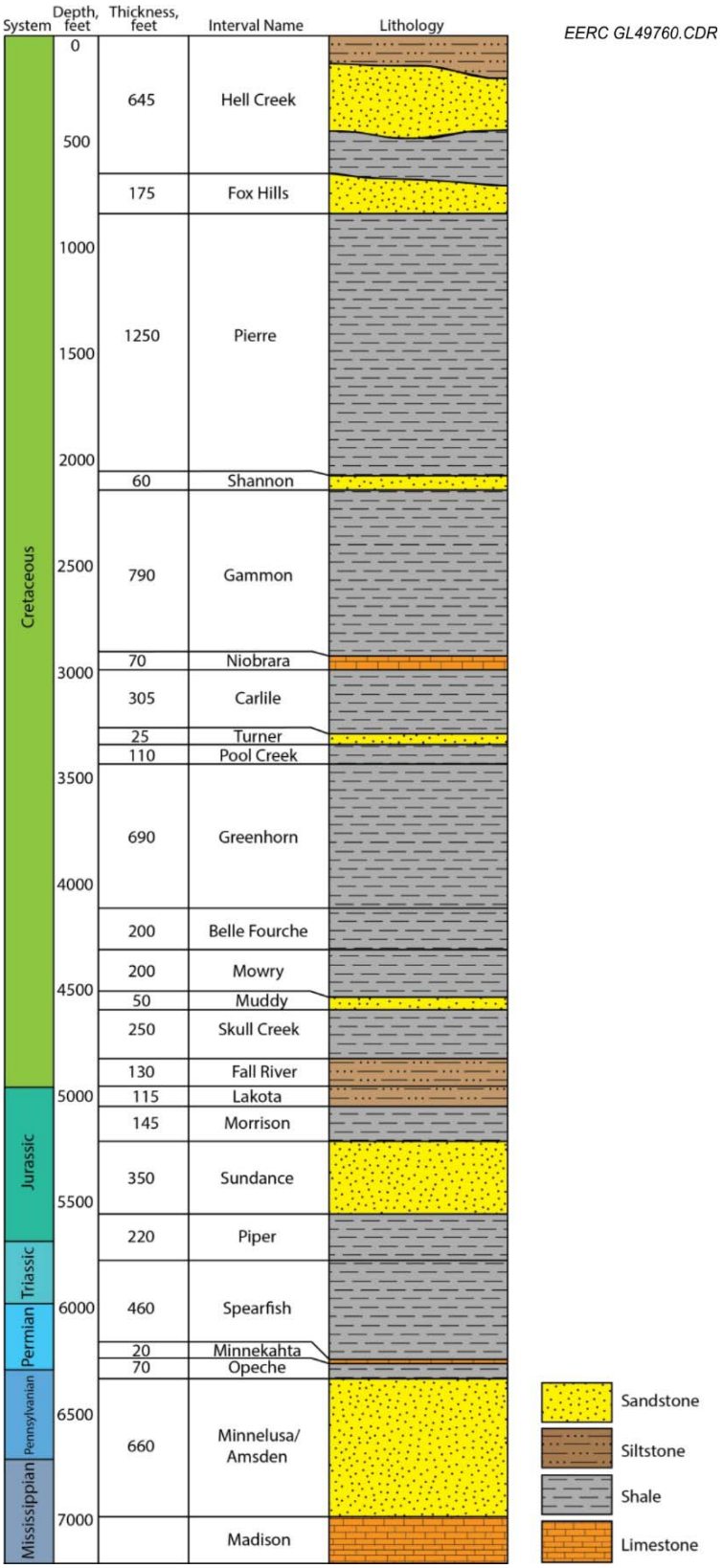

Figure A-2. Regional stratigraphy of the eastern Powder River Basin (Jin and others, 2017).

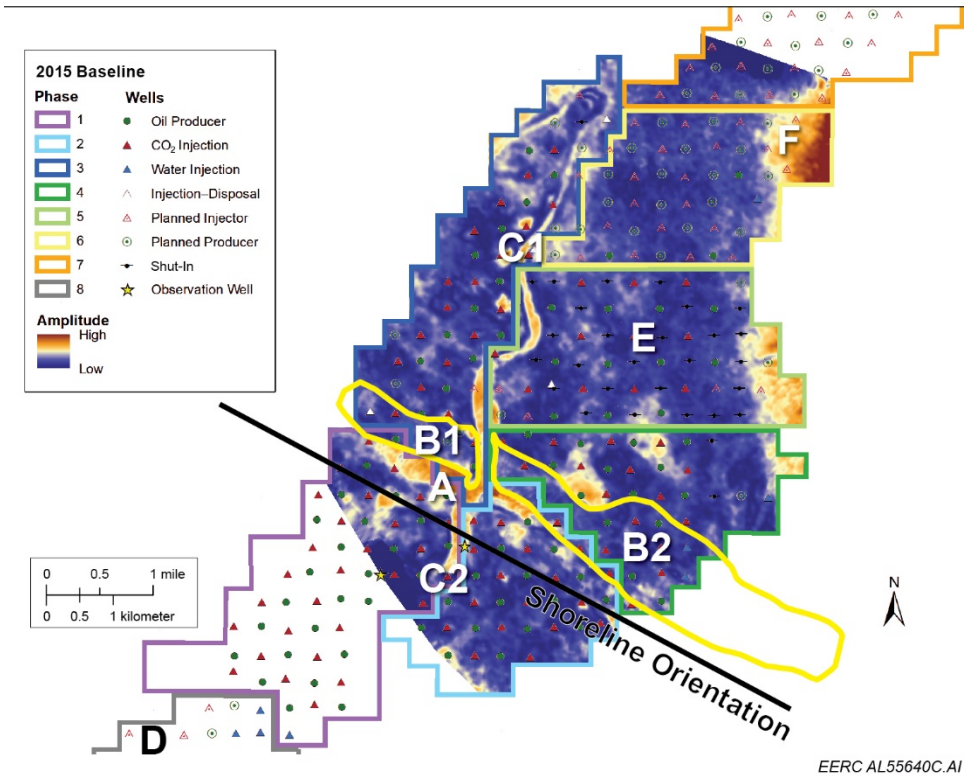

Figure A-3. Seismic amplitude root mean squared summation map of the Muddy Formation of Bell Creek Field from the 2015 surface seismic survey with labeled geobodies and shoreline orientation (from Bosshart and others, 2015). Geobody A represents the back-barrier silty sands of the interpreted barrier bar. Geobodies B1 and B2 represent lagoonal deposits that are bisected by the incised fluvial channel represented by C1. Geobody C2 represents shallow marine channel deposits. Geobody D represents an early lagoonal environment repurposed to a tidal channel complex as seas continued to transgress. Geobody E represents generally thicker regressive sands overlain by thinner transgressive sheet sands. Geobody F represents regressive silts, deposited on the margins of the northeast to southwest prograding deltaic/shorefront sands and overlain by thin transgressive sheet sands.

The Muddy Formation in the study area has previously been divided into several subintervals, based on basic well log and core analysis: the Rozet, Bell Creek Sand (reservoir), and the Springen Ranch (Jin and others, 2016). Log interpretation by Jin and others (2017), further divided the Muddy Formation into four main lithostratigraphic units: estuarine–shallow marine siltstone/shale, transgressive sand, mudstone, and regressive sand. A 3-D geocellular model of the Bell Creek Field was constructed based upon the revised geologic interpretation (Jin and others, 2017) which contains four Muddy Formation stratigraphic zones from the Shell Creek to the Rozet subinterval. These zones were correlated across 799 wells and picked from vintage well logs (gamma ray, spontaneous potential, sonic travel time, shallow and deep resistivity, and bulk density).

3-D and 4-D seismic data sets have allowed for the identification of seven geobody regions within the Bell Creek Sand interval (Jin and others, 2017, Figure A-4). Through log interpretation of each identified geobody, vertical and lateral facies associations were able to be determined. Fifteen facies have been classified in an attempt to capture the complex geologic heterogeneity throughout the Bell Creek field (Jin and others, 2017). Multiple-point statistics (MPS), a pixel-based modeling technique which allows for the use of large amounts of conditioning data to capture complex relationships between several facies (Strebelle and Journel, 2001; Caers and Zhang, 2004) was employed to distribute facies relationships throughout the model. The use of MPS has allowed for a more realistic representation of connectivity and compartmentalization of sand bodies in comparison to variogram-based methods.

Near the Phase 4 and 5 region, the study area and subject of this paper (see Figure A-4 for reference), three geobody regions are likely to be encountered (delta margin, sheet sand, and north/south trending channel). Each geobody differs from one another in both overall depositional setting and petrophysical character. The lower, prograding sand within the delta margin geobody

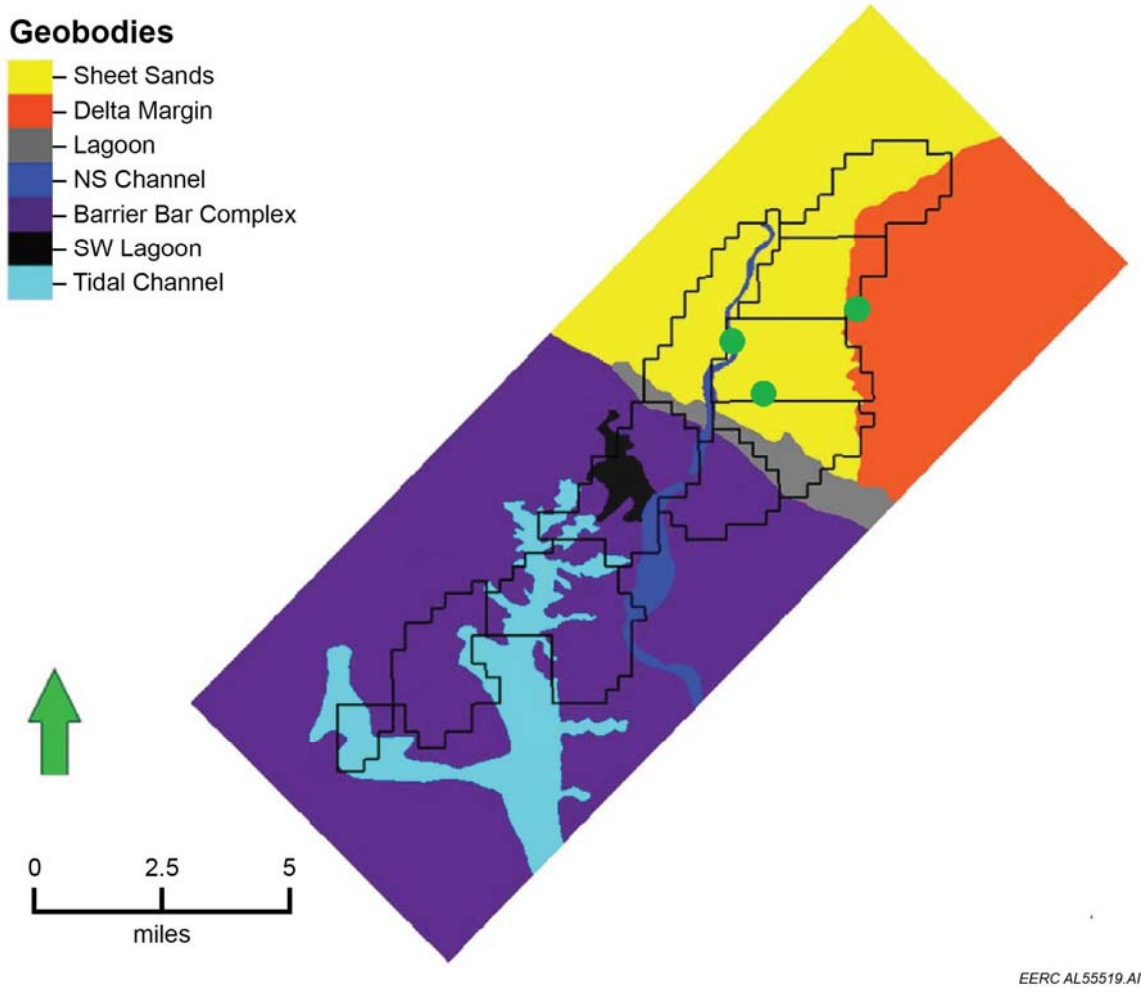

Figure A-4. Map view of modeled geobody regions within Bell Creek Field. Type log locations marked with green dots (updated from Jin and others, 2017).

(Figure A-5) becomes finer, siltier and thins in the eastward direction. Seismic amplitudes in this interval are higher, accompanied by higher gamma ray log values and decreased resistivity log measurements. Immediately above the silty sand facies, a laterally discontinuous mudstone separates the lower, prograding deposits from upper, retrograding deposits. The top of the reservoir in this geobody is characterized by a fining upward transition into siltstones and shales. Sheet sands (Figure A-6) were deposited during a period of inactivity, which was responsible for the deposition of barrier bar and lagoon sediments in Phase Areas 1 and 2. Because of onlappingretrogradation, the sheet sand deposits rest landward of the barrier bar complex and northeast of the lagoonal deposits. The transgressive sheet sands are mostly continuous in the northeastern region of the Bell Creek Field and can vary in thickness from 5 to 10 ft.

At the base of the reservoir, underneath the prograding sand, a sharp transition separates the sand from the siltstones. Laterally discontinuous mudstones may overlie or reside within the prograding sand. The mudstones themselves vary in stratigraphic position from the middle of the reservoir to approximately 5 feet from the top of the reservoir. Resting on top of the mudstone facies, retrograding sand facies eventually transition to siltstones and shales. During the same time period in which the transgressive sheet sands were being deposited, a fluvial valley incised a path along the eastern edge of Phase 3 and the border between Phases 1 and 2. This incised valley (Figure A-7) has caused transference of reservoir quality sand, leaving relatively poorer lag deposits behind. As the sea encroached landward, this channel was filled with low-permeability siltstones and shales which are referred to as the Springen Ranch Member (Farnham and Haddenhorst, 1972; Molnar, 1990).

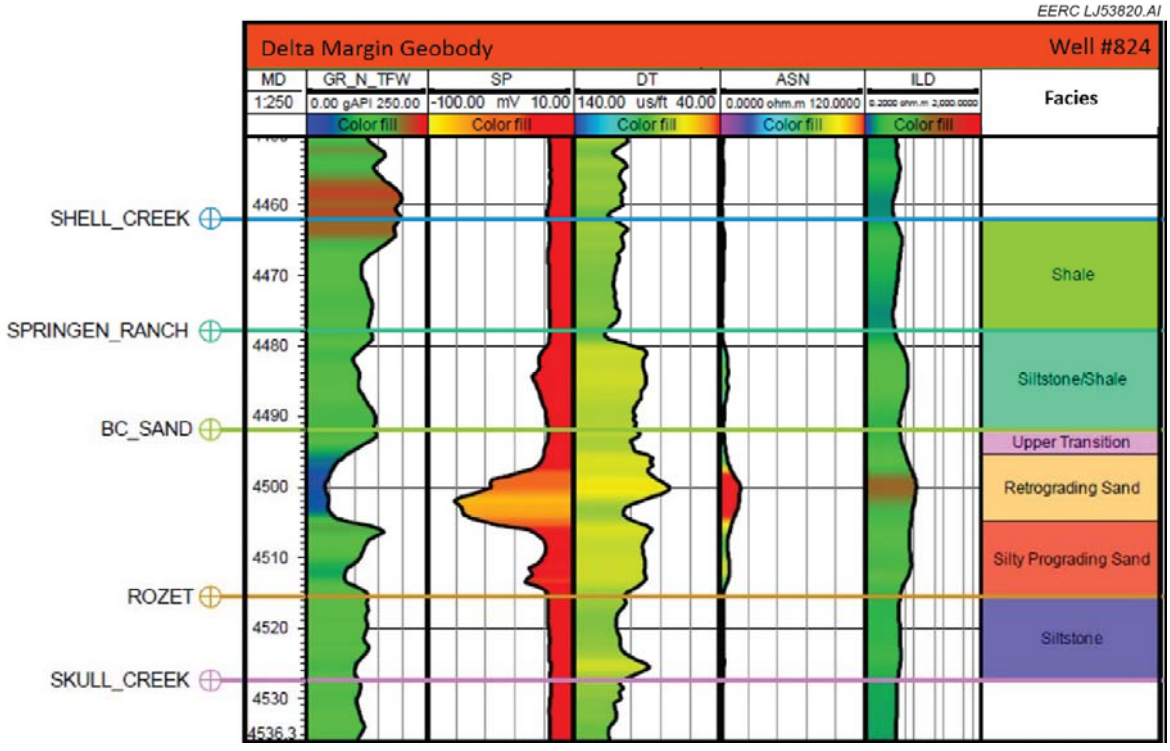

Figure A-5. Type log of the delta margin geobody (Jin and others, 2017).

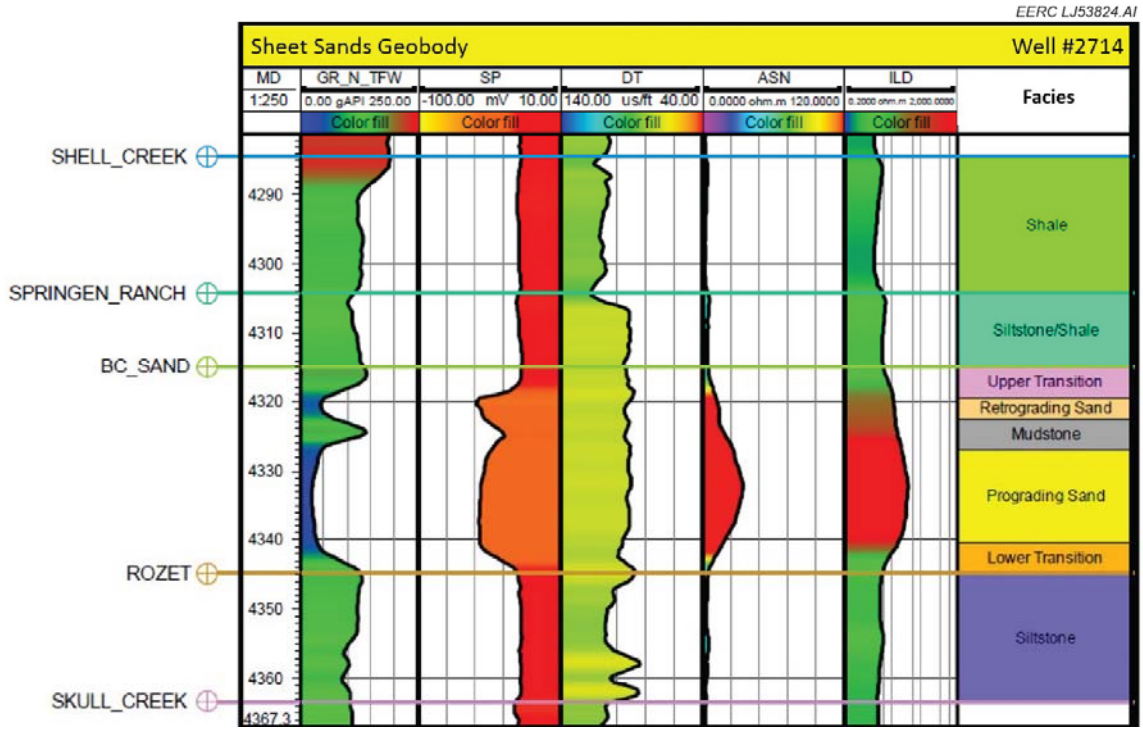

Figure A-6. Type log of the sheet sands geobody (Jin and others, 2017).

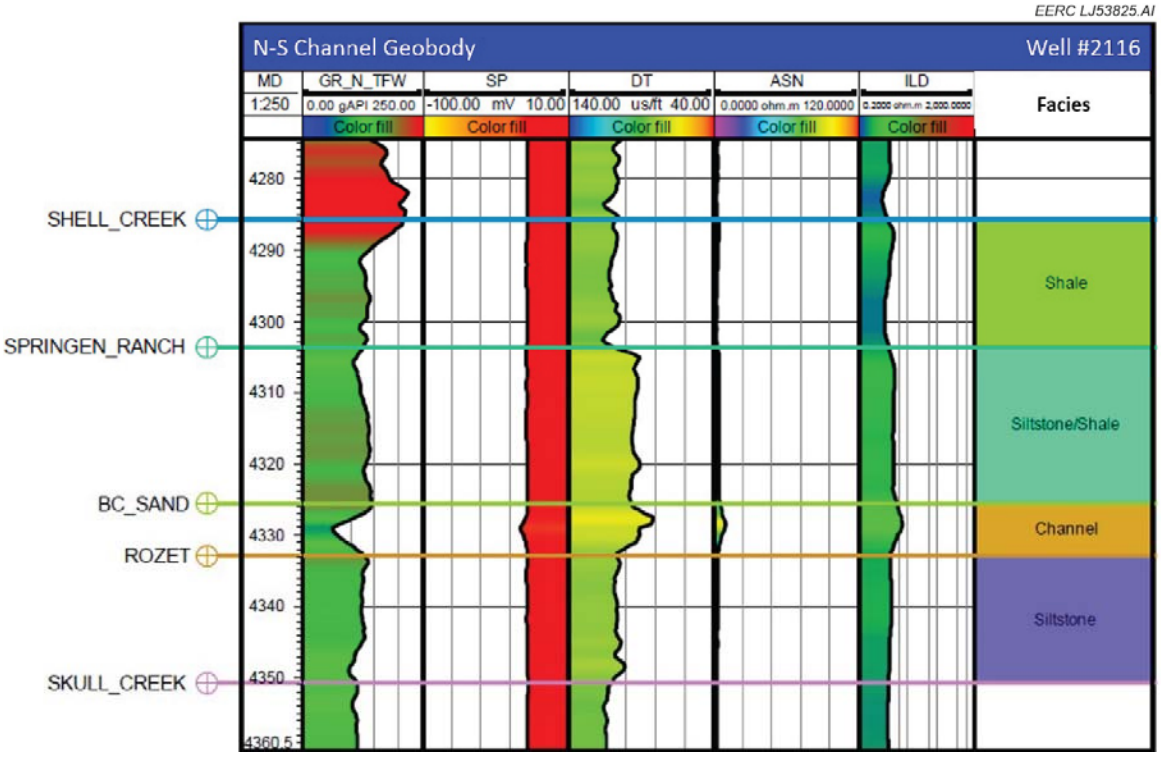

Figure A-7. Type log of the north/south trending channel geobody.

REFERENCES

Bosshart, N.W., Jin, L., Dotzenrod, N.W., Burnison, S.A., Ge, J., He, J., Burton-Kelly, M.E., Ayash, S.C., Gorecki, C.D., Hamling, J.A., Steadman, E.N., and Harju, J.A., 2015, Bell Creek test site—simulation report: Plains CO_2 Reduction (PCOR) Partnership Phase III Task 9 Deliverable D66 (Update 4) for U.S. Department of Energy National Energy Technology Laboratory Cooperative Agreement No. DE-FC26-05NT42592, EERC Publication: EERC-10-09, Grand Forks, North Dakota, Energy & Environmental Research Center, August.

Burnison, S.A., Livers-Douglas, A.J., Barajas-Olalde, C., Jin, L., Salako, O., Vettleson, H.M., Hamling, J.A., and Gorecki, C.D., 2017, Final report of a scalable, automated, semipermanent seismic array (SASSA) method for detecting CO_2 extent during geologic CO_2 injection: Final Report for Deliverable D4 Task 3 (October 1, 2016 – October 31, 2017) for U.S. Department of Energy National Energy Technology Laboratory Cooperative Agreement No. DE-FE0012665, EERC Publication 2017-EERC-12-02, Grand Forks, North Dakota, December.

Caers, J., and Zhang, T., 2004, Multiple point geostatistics—a quantitative vehicle for integrating geologic analogs into multiple reservoir models, *in* Integration of outcrop and modern analogs in reservoir modeling: AAPG Memoir, v. 80, p. 383–394.

Farnham, F.E., and Haddenhorst, F.A., 1972, Four and one-half years—discovery to unitized operation of the major, multi-reservoir Bell Creek field, *in* SPE Rocky Mountain Regional Meeting: Society of Petroleum Engineers, January 1.

Jin, L., Bosshart, N.W., Oster, B.S., Hawthorne, S.B., Peterson, K.J., Burton-Kelly, M.E., Feole, I.K., Jiang, T., Pekot, L.J., Peck, W.D., Ayash, S.C., and Gorecki, C.D., 2016, Bell Creek test site – simulation report: Plains CO_2 Reduction (PCOR) Partnership Phase III draft Task 9 Deliverable D66 (Update 5) executive summary for U.S. Department of Energy National Energy Technology Laboratory Cooperative Agreement No. DE-FC26-05NT42592, Grand Forks, North Dakota, Energy & Environmental Research Center, August.

Jin, L., Peterson, K.J., Bosshart, N.W., Pekot, L.J., Salako, O., Burnison, S.A., Smith, S.A., Mibeck, B. A., Oster, B.S., He, J., Peck, W.D., Hamling, J.A., Ayash, S.C., and Gorecki, C.D., 2017, Bell Creek test site—simulation report: Plains CO_2 Reduction (PCOR) Partnership Phase III draft Task 9 Deliverable D66 (Update 6) executive summary for U.S. Department of Energy National Energy Technology Laboratory Cooperative Agreement No. DE-FC26-05NT42592, Grand Forks, North Dakota, Energy & Environmental Research Center, August.

Molnar, P.S., 1990, Geologic reservoir study of the Bell Creek Field, Carter and Powder River Counties, Montana: Midland, Texas, Exxon Company.

Salako, O., Livers, A.J., Burnison, S.A., Hamling, J.A., Wildgust, N., Gorecki, C.D., Gladzewski, K.A., and Heebink, L.V., 2017, Analysis of expanded seismic campaign: Plains CO_2 Reduction (PCOR) Partnership Phase III Task 4 Deliverable D104 for U.S. Department of Energy National Energy Technology Laboratory Cooperative Agreement No. DE-FC26-05NT42592; EERC

Publication 2017-EERC-04-04; Energy & Environmental Research Center: Grand Forks, North Dakota, March.

Strebelle, S.B., and Journel, A.G., 2001, Reservoir modeling using multiple-point statistics, *in* SPE Annual Technical Conference and Exhibition: Society of Petroleum Engineers, January 1.

APPENDIX B

3-D SEISMIC

3-D SEISMIC

A prestudy 3-D surface seismic survey was acquired to compare with an existing baseline survey to create 4-D time-lapse difference displays and determine the extent of CO_2 in the portion of the study area where CO_2 had been injected prior to Krauklis wave (K-wave) data acquisition. The gained knowledge was intended to serve as a calibration for Seismos's monitoring efforts in the area where injection began before K-wave baseline data could be acquired in order to avoid possible underestimation of the plume extents. Additionally, a poststudy 3-D surface seismic survey was planned as part of this study to create 4-D time-lapse difference displays to help validate the K-wave monitoring results. Because of the no-go decision prior to acquisition of K-wave monitoring data, this poststudy 3-D survey was not acquired. This appendix contains a discussion about the prestudy 3-D surface seismic survey acquisition, processing, and the 4-D interpretation.

DATA ACQUISITION AND PROCESSING

The 4.7-square-mile prestudy 3-D surface seismic survey was acquired in late October/early November 2017 and is hence referred to as the 2017 monitor survey. The survey extent covers portions of development Phase Areas 4 and 5 and overlies an existing 3-D surface seismic survey acquired in 2015 (Figure B-1) (Salako and others, 2017). Acquisition parameters for this prestudy survey were selected to match the previously acquired 2015 baseline survey for 4-D interpretation purposes (Table B-1).

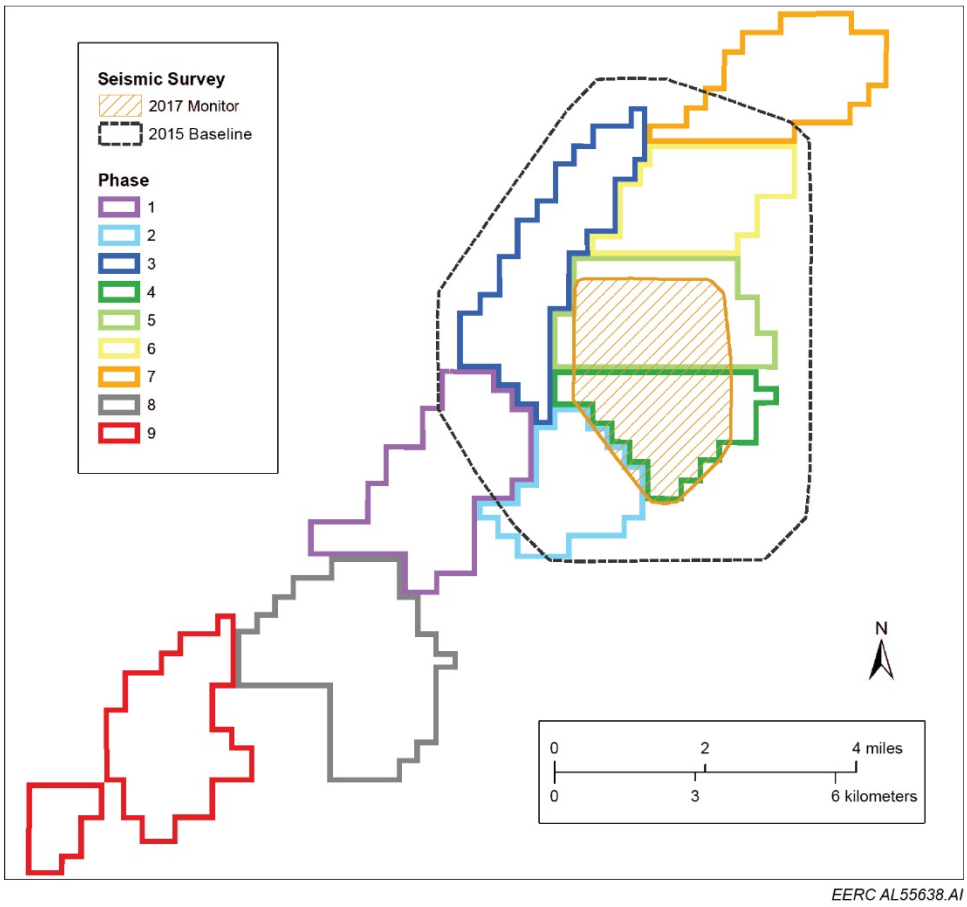

Figure B-1. Map of the Bell Creek Field showing the 2015 baseline and 2017 monitor survey extents

Table B-1. Acquisition Parameters for the 3-D Seismic Survey

	2017 Survey
Geophysical Contractor	Dawson
Energy Source	Two 64,000-lb AHV-IV Vibroseis
Source Interval	165 feet
Group Interval	165 feet
Geophone Pattern	One geophone
Total Preplan Source Stations	1262
Total Preplan Receiver Stations	1112
Sweep Parameters	Proprietary
Record Length	4 seconds
Sample Interval	2 millisecond

Arcis Seismic Solutions processed the prestudy 3-D surface seismic data using a similar processing sequence and parameters as previous seismic surveys acquired at the Bell Creek Field. A summary of the processing can be found in the SEG-Y format data file headers, and an in-depth discussion about the processing sequence is detailed by Salako and others (2017). A brief summary of the processing sequence is shown below:

- Minimum phase conversion
- Geometry assignment, trace edits, and 60-Hz noise removal
- Spherical divergence correction
- Surface consistent scaling, groundroll removal, and deconvolution
- Refraction statics, surface consistent statics
- Applying NMO (normal moveout)
  - Noise suppression across domains (shot, offset, CMP [common midpoint])
  - Surface consistent deconvolution
  - Noise suppression (offset and CMP)
  - Phase and statics compensation
  - Radon multiple attenuation
  - F-XY noise attenuation
  - 5-D interpolation
- Removing NMO
- Anisotropic velocity analysis
- Anisotropic Kirchhoff PSTM (prestack time migration)
- Front-end mute
- Stack, filter and AGC (automatic gain control) scaling

4-D ANALYSIS

4-D analysis of the 2015 baseline and 2017 monitor data included data conditioning involving calibration of the data using a workflow designed to minimize the differences where they are not expected to occur, such as above or below the injection zone. The calibration process involved cross-equalization operations that included phase and time-shift estimations between the baseline and monitor, application of the estimated phase and time-shifts, and a shaping filtering. The design window used for phase and time-shift estimations and the shaping filter was a 550-ms window ending at the Springen Ranch horizon. Normalized root mean square (NRMS) maps of the baseline and the monitor data sets, before and after cross-equalization, were generated over a window above and below the reservoir to quantify the differences between the data sets and assess improvements made after each process was applied.

For interpretation purposes, a phase rotation was applied to the data. Burnison and others (2014) recognized that the reservoir reflection manifests as a thin-bed seismic response, characterized by an entering reflection followed immediately by an exiting reflection of opposite polarity. This results in the situation where the reservoir sand is located at the middle zero-crossing of the reflection. Applying a 90-degree phase shift to the data rotates the reflection so that a positive peak is centered on the reservoir sand, with its amplitude related to the reservoir character or content. The bounding horizons of Springen Ranch and Skull Creek then fall on either side of the

reflection peak. Understanding the impact of CO_2 on the reservoir reflection becomes much more intuitive.

Maps were generated for 4-D interpretation by calculating the RMS amplitude values over a 12-ms window below the Springen Ranch horizon (Figure B-2 and B-3). To create a map showing the time-lapse changes between the 2015 baseline and 2017 monitor data, the baseline data were subtracted from the monitor data (Figure B-4). The amplitude distribution of the resulting 4-D amplitude difference map represents changes in the reservoir due to injection and production activities. Key findings from the 3-D and 4-D interpretation include identification of geobodies in the study area, a greater understanding of heterogeneities in the reservoir and how they influence CO_2 migration and pressure build-up, and a better sense of how injection volumes influence detectability of time-lapse changes in the reservoir.

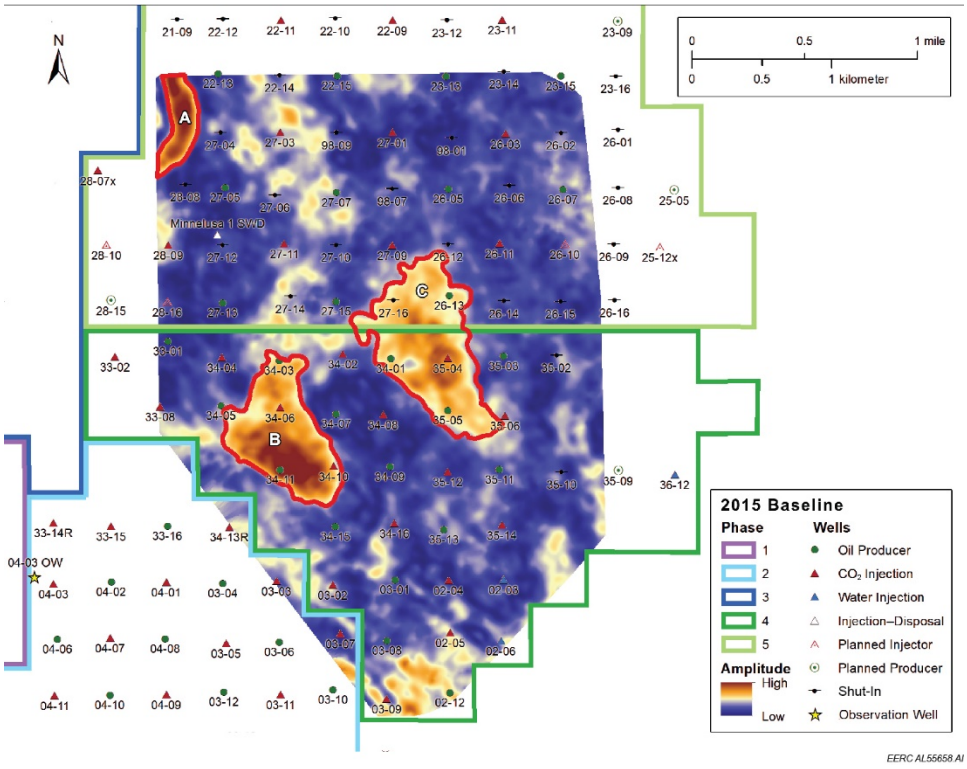

Figure B-2. The RMS average amplitude map of the Bell Creek reservoir for the pre-CO_2 injection 2015 baseline survey (where it overlaps the 2017 monitor) generated between the Springen Ranch and Skull Creek horizons. High-amplitude anomalies are outlined in red.

Conventional 3-D interpretation of the 2015 baseline survey data in the project area resulted in identification and interpretation of three high-amplitude features (Figure B-2). The high amplitude anomaly labeled A in Figure B-2 is a small section of the N–S-oriented channel described in Appendix A. The high-amplitude anomalies labeled B and C are not representative of

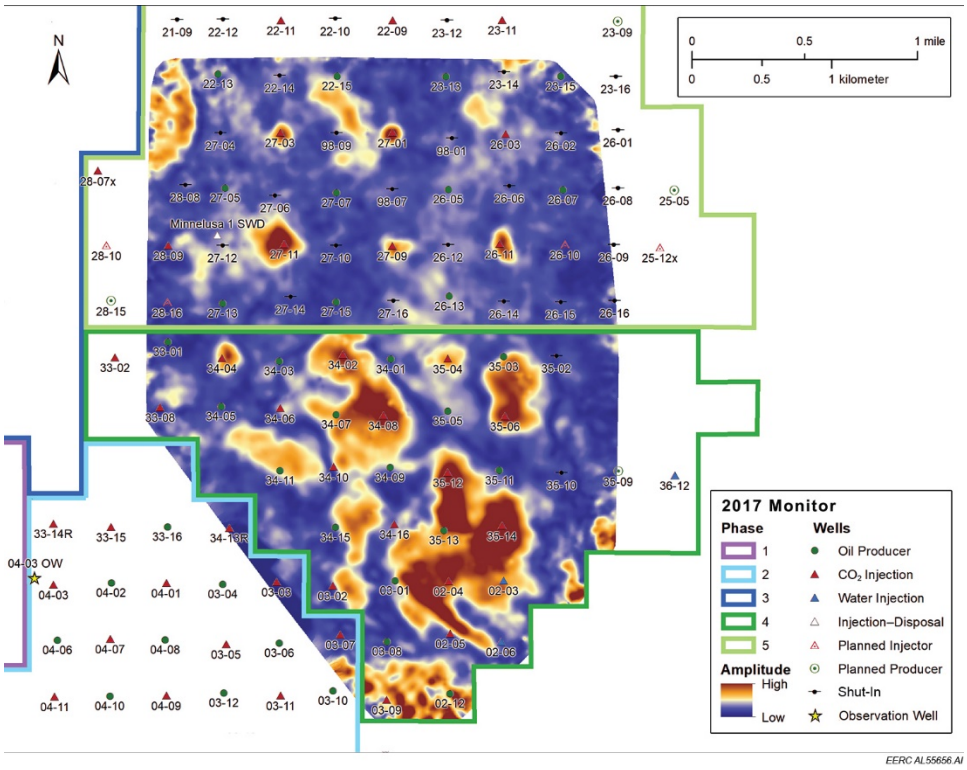

Figure B-3. The RMS average amplitude map of the Bell Creek reservoir for the 2017 monitor survey generated between the Springen Ranch and Skull Creek horizons.

geobodies but rather a specific stratigraphic sequence. These high-amplitude anomalies are associated with the stratigraphic sequence highlighted in Figure B-5. This sequence consists of deltaic channel deposits at the base overlain by deltaic channel margin deposits and transgressive sands at the top. High-amplitude values correlate to areas where the top transgressive sand is thin or not present. This trend can be seen on several cross sections in the project area. These high-amplitude values provide insight into the thickness of the transgressive sand interval between wells.

The 4-D difference map indicates that CO_2 migration is influenced by this lateral variation in the thickness of the top transgressive sand (Figure B-4). In injection Wells 34-06 and 34-10 that fall within the boundaries of the high-amplitude anomaly labeled B, injected CO_2 appears to migrate cross-dip away from the thinner sands. The thickness of this top transgressive sand interval and the deltaic channel sands interval appears to influence CO_2 migration in other areas of the field as well. To the south of injection Well 34-06, the deltaic channel sand interval thins, whereas to the north, the thickness does not change. The 4-D difference and breakthrough at Producer 35-03 show that CO_2 preferentially migrated across dip to the north instead of updip in the direction of the thinning sands. Similarly, other small-scale heterogeneities in the reservoir in the project area influence the migration of CO_2. As injection volumes increase over time, these heterogeneities will likely be better illuminated on subsequent 4-D seismic surveys.

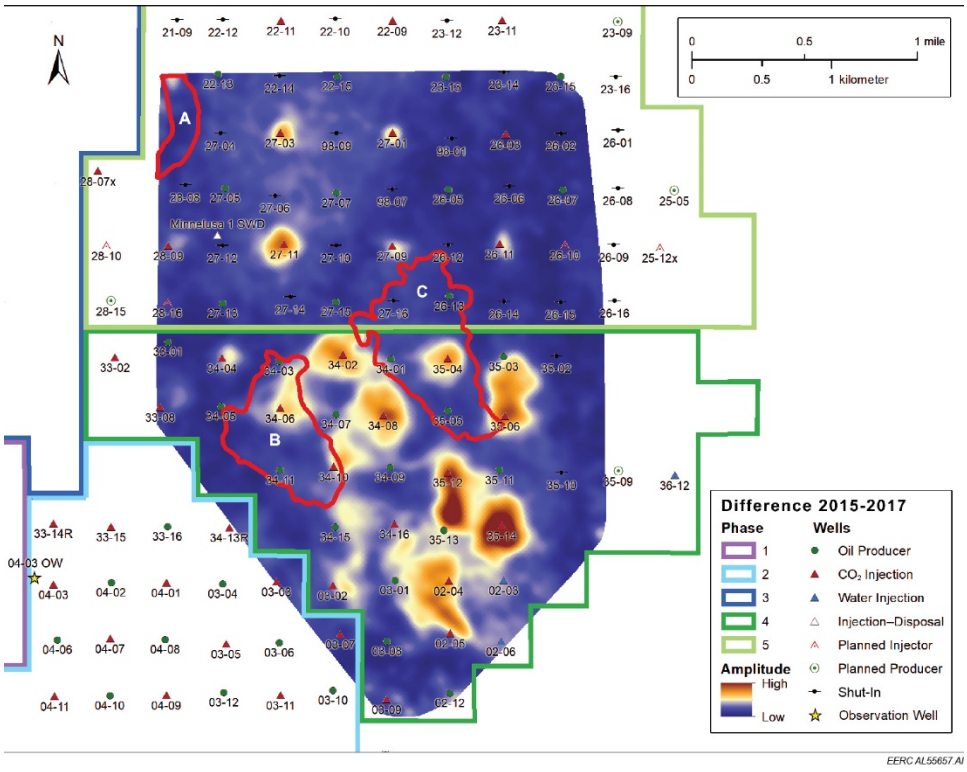

Figure B-4. 4-D amplitude difference map of the Bell Creek reservoir created by subtracting the 2015 baseline from the 2017 monitor survey. High-amplitude anomalies identified using the 2015 baseline survey are outlined in red.

In addition to illuminating potential preferred pathways in the reservoir, the 4-D difference provides insight into the pressure response in the reservoir due to injection. Previous studies in the Bell Creek Field have demonstrated that pressure buildup due to water injection also affects the seismic signature in the reservoir, producing differences on 4-D seismic displays (Salako and others, 2017). Although the pressure response is not easily distinguishable from change due to an increase in CO_2 saturation, the magnitude of the 4-D difference amplitude values provides some insight into pressure buildup in the reservoir. The 4-D difference amplitude values in Phase 4 appear to be affected by pressure buildup in wells near the updip pinchout of the reservoir sands in addition to an increase in CO_2 saturation (Figure B-4). For example, during the period between the 2015 and 2017 seismic surveys, injector Well 35-14 had approximately the same amount of CO_2 than injector Well 35-04 but has significantly higher 4-D difference amplitude values. Well 35-14 is near the updip pinchout of the reservoir sands has higher 4-D difference amplitude values than at Well 35-04 likely indicating a higher increase in reservoir pressure around this well.

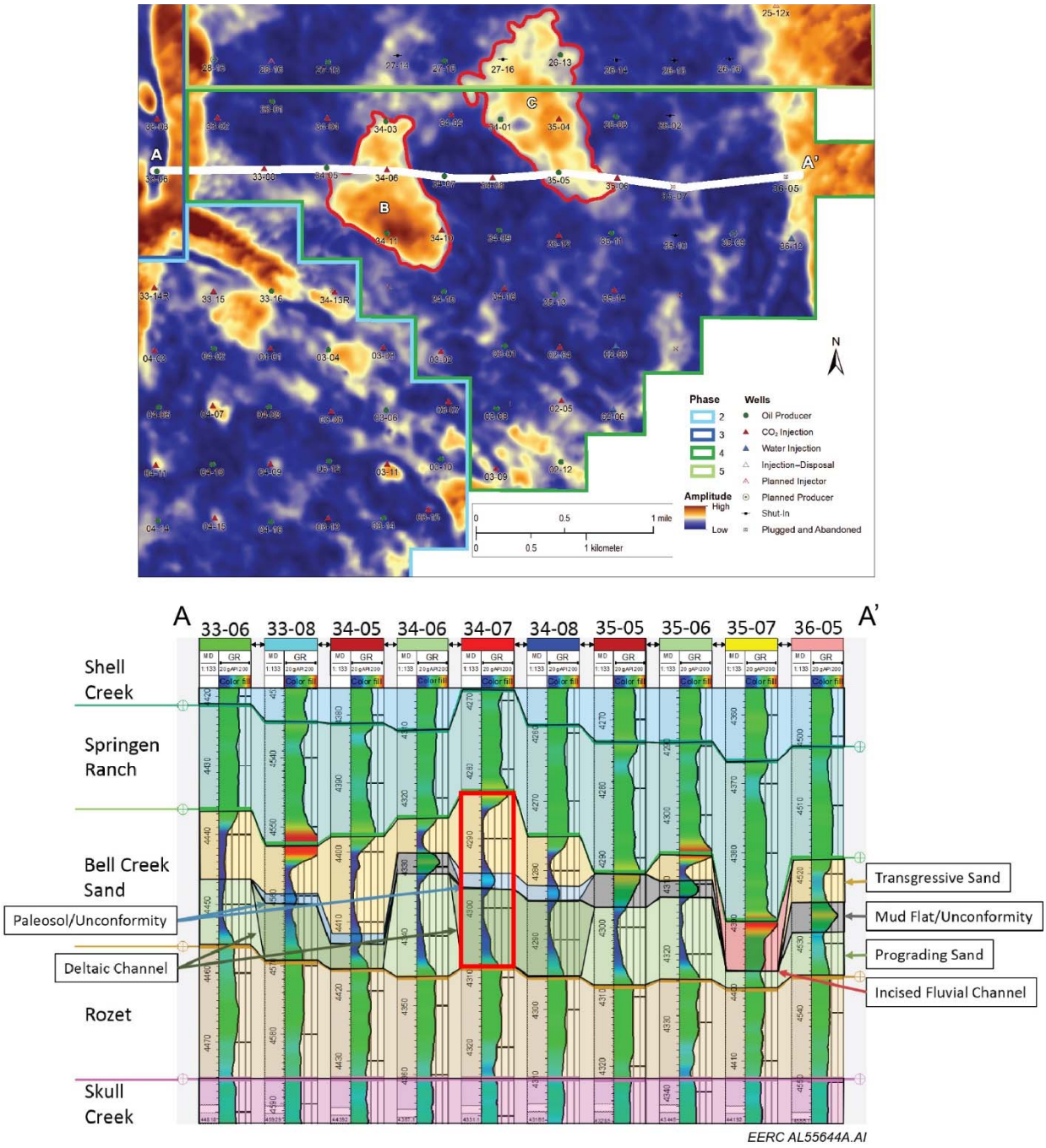

Figure B-5. Top: cropped RMS average amplitude map of the Bell Creek reservoir for the pre-CO_2 injection 2015 baseline survey generated between the Springen Ranch and Skull Creek horizons. Cross section A-A' is indicated by the white line. Bottom: gamma ray logs for the wells along cross section A-A' showing formation top correlations and interpretation of depositional sequences.

Another key finding from this 4-D analysis is a better sense of how injection volumes influence detectability of time-lapse changes in the reservoir. The 2017 monitor survey provides a unique look at injection volumes and detectability as Phase 5 had only been undergoing CO_2 injection for 2 months prior to the acquisition of the seismic data set. Previously 4-D data sets were acquired over phases that had been undergoing CO_2 injection for a year or more. The 4-D difference amplitude map in Figure B-4 shows that time-lapse changes due to CO_2 injection can be detected around injectors in Phase 5 that had as little as 156,000 mscf of CO_2 injected (Table B-2).

Table B-2. CO_2 Injected in the Reservoir in Phase 5 Within the Extent of the 2017 Monitor Survey (Montana Board of Oil and Gas Conservation, 2018) at the Time the Survey Was Acquired

Well Name	Cumulative CO_2 Injected, mscf
26-11	155,715
27-01	116,996
27-03	189,029
27-09	167,725
27-11	257,094
28-09	111,478

Although the 3-D seismic data were not used in this study to help validate K-wave monitoring data, they provide great value-added information to the operator and other research being conducted at the Bell Creek Field. The 3-D and 4-D interpretation can better inform injection and production operations in the project area and help the operator maximize sweep efficiency and better understand well performance. This insight into injection volumes and seismic detectability will help the field operator plan future 4-D seismic surveys. The 4-D data in the project area will also help inform another study being done in the Phase 5 area. One example is the Colorado School of Mines project, Charged Wellbore Casing–Controlled Source Electromagnetics (CWC–CSEM) on Reservoir Imaging and Monitoring that is being conducted in Phase 5.

REFERENCES

Montana Board of Oil and Gas Conservation, 2017, MBOGC online oil and gas information system: www.bogc.dnrc.mt.gov/WebApps/DataMiner (accessed October 2018)

Burnison, S.A., Burton-Kelly, M.E., Zhang, X., Gorecki, C.D., Steadman, E.N., and Harju, J.A., 2014, Bell Creek test site – 3-D seismic and characterization report: Plains CO_2 Reduction (PCOR) Partnership Phase III Task 4 Deliverable D96 for U.S. Department of Energy National Energy Technology Laboratory Cooperative Agreement No. DE-FC26-05NT42592; EERC Publication 2015-EERC-04-04; Energy & Environmental Research Center: Grand Forks, North Dakota, March.

Salako, O., Livers, A.J., Burnison, S.A., Hamling, J.A., Wildgust, N., Gorecki, C.D., Glazewski, K.A., and Heebink, L.V., 2017, Analysis of expanded seismic campaign: Plains CO_2 Reduction (PCOR) Partnership Phase III Task 4 Deliverable D104 for U.S. Department of Energy National Energy Technology Laboratory Cooperative Agreement No. DE-FC26-05NT42592; EERC Publication 2017-EERC-04-04; Energy & Environmental Research Center: Grand Forks, North Dakota, March.

APPENDIX C

SEISMOS MODELING

seismos
8868 Research Boulevard, Suite 401, Austin, TX 78758, tel. 512-903-4375, www.seismos.com

Update: November 15, 2017

Cross-well reservoir monitoring using tube waves

1. Overview of Modeling Objectives

The motivation for this overall project is to monitor reservoir properties using tube wave sources and receivers placed on multiple wellheads. The sources will generate tube waves, which will propagate down the well, convert to seismic waves at perforations, the well bottom, and changes in lithology, propagate through the reservoir to adjacent wells, convert back to tube waves, and then propagate up the well to be recorded at the wellhead. While the conversion between tube waves and seismic waves is known to be rather inefficient, past studies have observed such conversions in real data. The objective of this specific modeling effort is to perform numerical simulations to quantify signal amplitudes for conditions relevant to the Bell Creek Field.

To perform these simulations requires completing the following tasks:

1. Identify processes that control conversion between tube waves and seismic waves.
2. Describe these processes in terms of mathematical equations.
3. Develop a numerical method for solving these equations.
4. Implement the numerical method in a parallelized code.
5. Run the code, using material properties and parameters values con- strained by available data, to simulate wave propagation.
6. Examine simulation results to quantify signal amplitudes.

It is essential to recognize that this is a major effort that involves the creation of new knowledge. While several processes (and associated equations) governing conversion between tube waves and seismic waves have been identified in the literature, no publications we have found consider cased wells with perforations.

Thus the first two tasks are nontrivial.

In addition, we must develop numerical methods and the associated software codes to solve the governing equations. Numerical method development and programming are also challenging tasks, particularly for the equations that arise in this project.

The purpose of this report is to document the Seismos progress on this project since we began work on it in April 2017. We also provide a tentative timeline for future results, bearing in mind that a research project of this type is likely to experience unanticipated breakthroughs or delays.

2. Processes controlling conversion between tube waves and seismic waves

Most of the energy carried by tube waves remains within the well; only a small fraction (likely only 1% or even 0.1%) is converted to seismic waves. There is a similar conversion efficiency from seismic waves back to tube waves. Quantifying the conversion efficiency requires identifying the processes responsible for coupling between the well and reservoir.

Our first step, completed within the first few weeks of the project, was to identify these processes. We label them here as follows:

• Coupling 1, at the well bottom. Pressure changes carried by tube waves reflecting from the bottom of the well generate a downward force on the reservoir. This force generates seismic waves. Correspondingly, displacement of the reservoir rocks by an incident seismic waves pushes the bottom of the well, and the fluid within it, up or down to generate tube waves.

• Coupling 2, at perfs. Pressure changes carried by tube waves pushes fluid through perforations in the casing into the reservoir. These fluids dilate the solid and generate seismic waves. Correspondingly, incident seismic waves squeeze the fluid-saturated rocks surrounding the well, pushing fluids into the well through the perforations.

• Coupling 3, along the length of the well. Pressure changes carried by tube

waves can slightly expand the well, along its entire length, and the resulting strains in the solid serve as a source for seismic waves. Similarly, seismic waves can squeeze the well and push fluid within the well up or down, generating tube waves. Note that there is no fluid exchange between the well and reservoir in this coupling, unlike coupling 2.

Couplings 1 and 3 have been described previously in the literature, but coupling 2 has not.

Coupling 1 is considerably simpler to describe mathematically, and to implement in a code, than the other two couplings. Coupling 3 is most relevant in uncased wells; the presence of a stiff casing will limit the ability of the wellbore to expand or contract, decreasing this form of coupling. For these reasons, we decided to begin with coupling 1, then to proceed to coupling 2, and to finish with coupling 3.

3. Numerical method development and soft- ware implementation, coupling 1

The major computational expense in this project comes from simulating seismic wave propagation in a 3-D medium. Therefore we deemed it essential to use the most efficient numerical method for solving the 3-D elastic wave equation: the staggered grid finite difference method. Rather than writing our own code, we decided to begin with an open-source code, AWP- ODC-OS, available under the BSD-2 license: http://hpgeoc.github.io/ awp-odc-os/. The code is written in C and CUDA; the latter enables the code to be run on GPU clusters. The code is parallelized.

Approximately two weeks were spent learning how to run this code, at the same time we were identifying the coupling processes. We had seismic wave simulation capabilities by early May. At the same time we added wells to the code, providing us with the ability to model tube waves within the wells. At this point we had the ability to simultaneously model tube waves and seismic waves, but without any coupling.

From mid-May to mid-June, we implemented coupling 1 into the code. Initial simulations during this period later proved to be invalid due to some bugs in the

code. These bugs were related to improperly specifying boundary conditions at the wellhead and incorrectly specifying the source. In addition, we encountered a major software issue that required about two weeks of de- bugging to resolve. In early June we switched from prototype simulations using a single GPU to production-scale simulations on a high-performance GPU cluster. Simulations on the cluster were inconsistently crashing. Ultimately we traced the issue to a memory allocation routine in the open-source seismic wave propagation code. With the assistance of the original code developers, we resolved this issue.

4. Simulations with coupling 1

In mid-June we began production simulations with coupling 1. The purpose of these simulations was to quantify the efficiency of conversions between tube waves and seismic waves through the well bottom. This was done for both a homogeneous medium and for media with a horizontal low-velocity layer. We anticipated that the latter might be important for creating guided waves through the reservoir. We also wanted to quantify signal amplitudes as a function of distance between the wells.

These simulations were carried out during the end of June and throughout July. The initial simulations were incorrectly set up; the low-velocity layer was placed at the wrong depth and our computational mesh was too coarse to properly resolve high frequency waves. So we had to run those simulations again. Each production simulation takes over one day of wall clock time to finish.

In Figure 1 we show results from a representative simulation. In this simulation, there are two wells, 400 m (about 1300 ft) apart, one filled with water and the other with more compressible and less dense CO2. There is a low-velocity layer near the bottom of the wells that is 84 m (about 275 ft) thick in which seismic wave speeds are reduced by about 20% relative to the surrounding rock. (This example is merely to investigate the role of guided waves; the layer thickness and material contrast are not based on well logs or other data.)

We also show, in Figure 2, a record section of particle velocity in the receiver well. This figure is useful for identifying the different seismic wave arrivals at the bottom of the receiver well, and separating these from the tube wave reverberations in the receiver well.

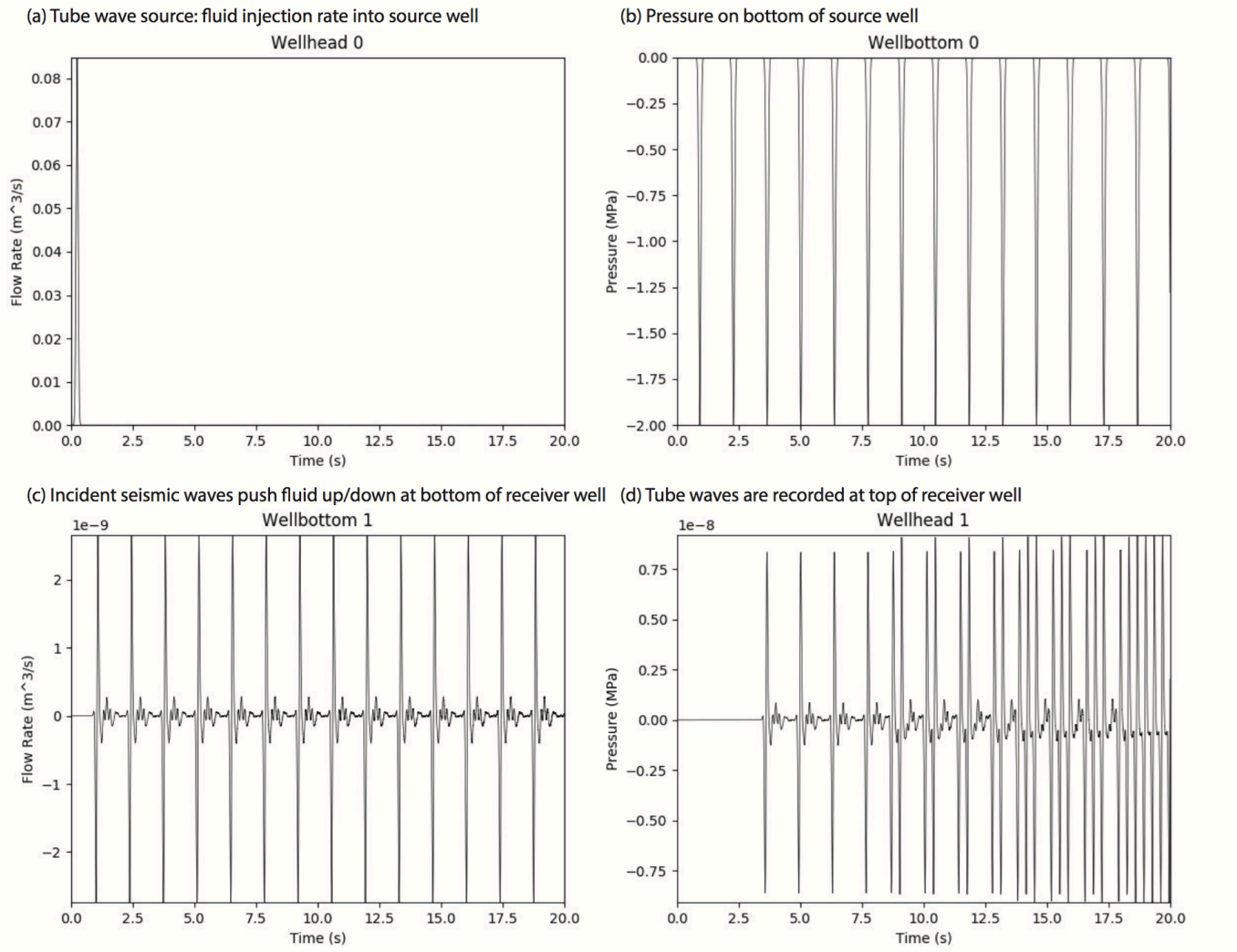

Figure 1: Simulation with coupling 1 (at the well bottom). (a) Tube waves are generated in the source well by injecting fluid at the wellhead. (b) Tube waves bounce between the wellhead and well bottom in the source well, creating a pressure on the well bottom. The downward force from this pressure generates seismic waves that propagate across the reservoir. (c) Seismic waves arrive at the receiver well and push its bottom up and down. This pushes the fluid in the well up and down, generating tube waves in the receiver well. (d) Tube waves bounce between the well bottom and wellhead in the receiver well, and are recorded at the wellhead

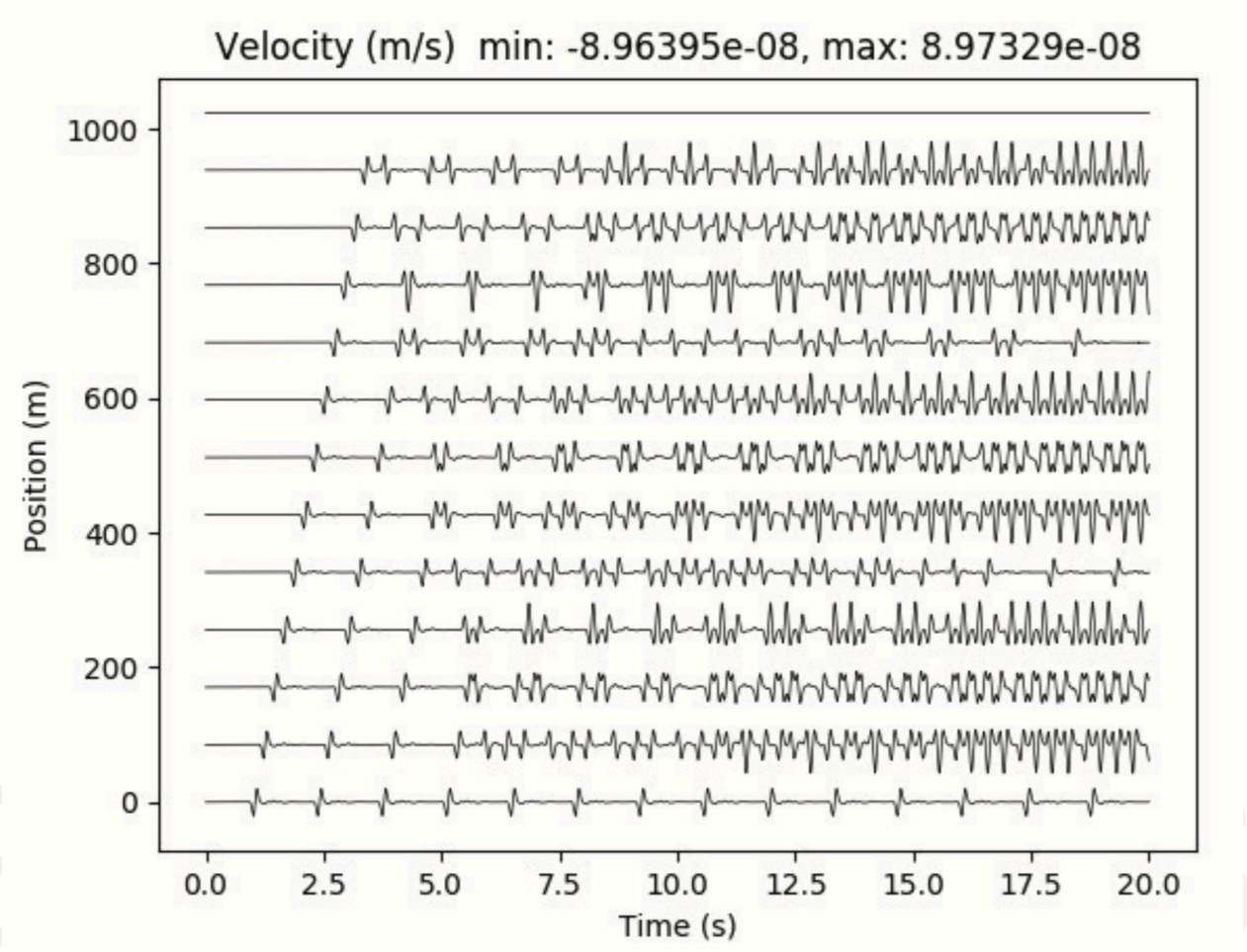

Figure 2: Record section of particle velocity in receiver well, from same simulation as in Figure 1.

The source amplitude, duration, and frequency content are approximately consistent with the current Seismos source. The resulting signal at the receiver wellhead (Figure 1d) shows pressure changes of approximately 0.01 Pa or 10^{-6} psi. These low amplitude signals would require considerable stacking to rise above the noise. The waveform shape is approximately the time derivative of the input source time function, consistent with theoretical expectations. In addition to the main arrivals (seismic body waves) there are smaller amplitude signals arriving soon after that are identified as the guided waves. The guided waves are many times smaller than the direct body waves.

We performed additional simulations exploring the influence of the layer thickness and well separation distance. Even for rather thick low-velocity layers (up to several hundred feet thickness), the guided waves have smaller

amplitudes than the direct waves. This is likely because the source has negligible power above 10 to 20 Hz, and low frequency waves are not efficiently trapped within the low-velocity layer. We also confirmed that signal amplitudes are inversely proportional to well separation distance, as expected for seismic body waves.

These simulations were completed at the end of July.

During July, we also examined well log data for the Bell Creek Field. No evidence for low-velocity reservoir layers, of thickness likely to influence seismic wave propagation, were found in the well logs.

5. Progress on coupling 2

Starting in mid-July we began work on coupling 2. Because this coupling process was previously undescribed in the literature, we began by developing a mathematical theory for how fluid exchange between the well and reservoir couples tube waves and seismic waves. We have made substantial progress on this front, culminating in a set of partial differential equations that describe the poroelastic near-wellbore response. We also understand how to convert the resulting strains in the near-wellbore solid into a seismic moment tensor (i.e., the seismic source term for the 3-D elastic wave equation).

We are now developing a numerical method to solve these equations and implementing the method in the code. We anticipate having initial results with coupling 2 by the end of August. After we confirm that everything is working with the code, we will begin a parameter-space study to quantify the efficiency of conversion via coupling 2. There is more uncertainly in this coupling that comes from uncertainty in near-wellbore poroelastic properties.

Our strategy will be to explore a range of parameter choices, guided as best possible by available poroelastic property constraints. Having tube wave data from representative source and receiver wells would provide useful constraints on the poroelastic properties.

A complete parameter-space study of coupling 2 will likely be completed during September, though preliminary results should be available in August that will

give us some sense of signal amplitudes.

6. Coupling 3

Coupling 3 is likely to be negligible for cased wells, so we have left this for last. Only after completing coupling 2 will we investigate coupling 3.

7. September 1, 2017 Update

This section describes work during the month of August 2017. Focus has been on coupling 2. Our understanding of this type of coupling has improved after formulating the near-wellbore problem using the dynamic Biot theory of a fluid-saturated porous solid. We now distinguish between two types of coupling through the perfs:

- Coupling 2a, total stress coupling at perfs. Total stress refers to the forces per unit surface area exerted through the solid matrix and pore fluid. At the perf opening, fluid pressure in the well is balanced by an equal and opposite total normal stress from the solid outside the well. Changes in fluid pressure directly couple to the solid to generate seismic waves, even in the absence of fluid flow through the pores.
- Coupling 2b, fluid flow coupling at perfs. When oscillatory fluid flow occurs in the reservoir, due to tube wave pressure changes at the perfs, pressure gradients within the fluid act also on the solid matrix. This process can also generate seismic waves.

Coupling 2a would dominate when pore fluid pressure perturbations, induced by tube waves, do not penetrate far from the well. It is likely that we are in this limit, though this depends on the near-wellbore poroelastic structure and connectivity between the well and the reservoir. The Seismos reflection analysis for a single well would help determine the near-wellbore poroelastic structure.

During August 2017 coupling 2a was implemented into the Seismos simulations. Preliminary results are shown below. Coupling 2a is remarkably similar to coupling 3, in the sense that no fluid flow through the porous solid needs to be modeled and we are primarily concerned with how dilation of the source wellbore generates seismic waves and how normal stresses carried by seismic

waves squeeze the receiver well to generate tube waves. As a simple first approximation, the cased well with perforations is modeled as having perfectly rigid casing over most of its length, except for the perfed interval. This region is modeled as if it is uncased and therefore more compliant. A similar approach was taken by Wu and Harris (2004) in their crosswell imaging study of the interaction between tube waves and seismic waves.

The modeling procedure adopted is similar to that in the work of Burridge et al. (1993) and Kurkjian et al. (1994), classic studies by the Schlumberger group of this problem. Tube waves in the source well create pressure changes at the location of the perfs, p(t). These pressure changes are converted into a point seismic moment tensor (the source term for the elastic wave equation),

$$M(t) = LAp(t) \begin{bmatrix} (\lambda+2\mu)/\mu & 0 & 0 \\ 0 & (\lambda+2\mu)/\mu & 0 \\ 0 & 0 & \lambda/\mu \end{bmatrix}, \qquad (1)$$

where L is the length of the perfed interval, A is the borehole cross-sectional area, and λ and μ are the elastic moduli of the solid.

Seismic waves emanate from that point source and propagate to the receiver well. The normal strains (or, equivalently, the normal stresses) carried by these seismic waves are converted into a source term for the tube wave equation in the receiver well:

$$\rho_f \frac{\partial v}{\partial t} + \frac{\partial p}{\partial z} = 0, \qquad (2)$$

$$\beta \frac{\partial p}{\partial t} + \frac{\partial v}{\partial z} = S(z,t), \qquad (3)$$

$$S(z,t) = -\frac{1}{\mu}\left[(\lambda+2\mu)(\dot{\epsilon}^I_{11}+\dot{\epsilon}^I_{22}) + \lambda\dot{\epsilon}^I_{33}\right] L\delta(z-z_p), \qquad (4)$$

where ϱf is fluid density, v is fluid particle velocity in the well, p is pressure, β is the sum of fluid compressibility and borehole compliance, ε ïj are strain rates in the solid carried by incident seismic waves, and δ(z − zp) is a delta function that localizes the source to the perf location. Tube waves in the receiver well are modeled by solving the above equations.

Pressure changes in the source well are identical to those shown in Figure 1 so are not shown again. Figure 3 shows the source well pressure rate dp/dt at perfs, receiver well source term, and pressure at the receiver wellhead. Perhaps the most important result from these simulations is that the signal amplitudes for coupling 2a are two orders of magnitude larger than those for coupling 1.

The next step at this point would be to continue by implementing coupling 3. Wu and Harris (2004) found quite substantial tube-seismic-tube coupling via this process, even for cased wells. Their field data contradict our earlier speculation that coupling 3 was negligible for cased wells. We would also want to investigate coupling 2b by estimating the contribution to seismic wave generation from fluid flow. Finally, we have not investigated any "cross-coupling;" that is, waves that leave the source well by coupling 1 and enter the receiver well by coupling 2a (and similar combinations).

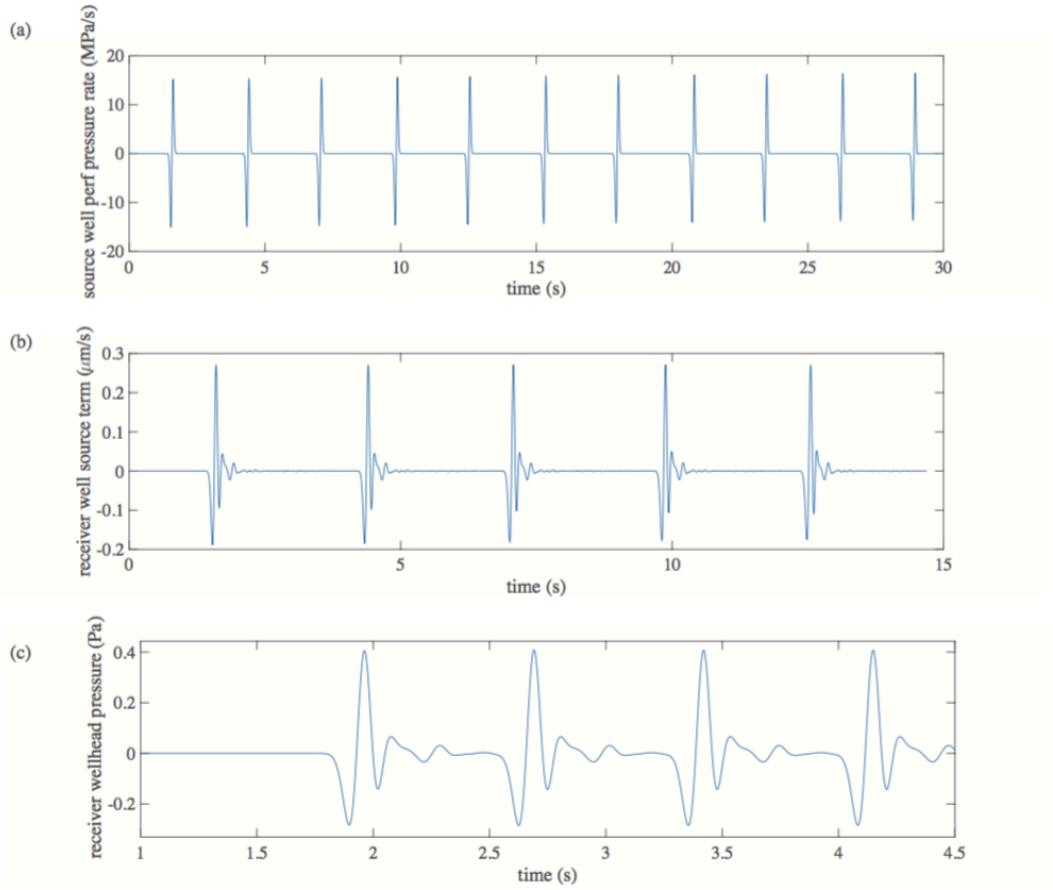

Figure 3: (a) Source well pressure rate dp/dt at perfs, (b) receiver well source term S(t) without the delta function, and (c) pressure at the receiver well- head. Time t = 0 is different for each plot. The source well is filled with CO2 and the receiver well with water or oil, which accounts for the different two-way travel times (time delay between successive pulses) in the two wells.

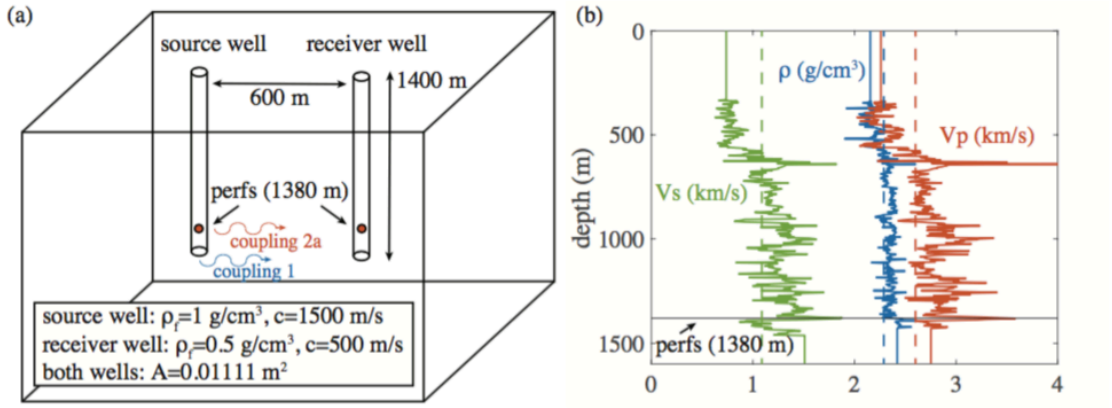

Figure 4: (a) 3D elastic solid containing two wells. Coupling from tube waves to seismic waves (and vice versa) occurs at both the well bottom (coupling 1) and at the perfs (coupling 2a). (b) Layered structural model based on well logs (solid lines) and homogeneous half-space model (dashed lines).

8. November 1, 2017 Update (Final Results)

This section of the report documents modeling results conducted specifically for the Bell Creek site. The previous work was conducted for either a homogeneous half-space or a half-space containing a low-velocity layer. In contrast, the new results are for simulations utilizing a depth-varying or layered structural model based on well logs. These results are compared to results using a homogeneous half-space with average properties from the well logs. The purpose of this comparison is to identify and isolate waveform characteristics that are sensitive to details of the material structure. In addition, over the past two months, we have done extensive verification tests of the code and fixed a few bugs. Thus all results and conclusions presented in this final report supersede those in previous reports/updates.

A schematic of the overall model is shown in Figure 4a. Well log data from DENBURY_0506_OW_SEMBLANCE.las and associated Excel files provided by Nick Bosshart (EERC) in early October 2017 were used to construct the layered structural model shown in Figure 4b. Also shown are properties of the homogeneous half-space model (ρ = 2289 kg/m3, Vs = 1088 m/s, and Vp = 2600 m/s, average values of the layered model). At depths where log data were not available, the material properties were extrapolated with constant values. We employ a coordinate system with origin at the source wellhead and vertical is

positive down.

Two couplings were used: coupling 1 (well bottom) and coupling 2a (perfs). For coupling 1 out of the source well, the fluid pressure changes exerted by the tube wave on the formation at the well bottom are converted into a downward force

$$F(t) = Ap(t), \quad (5)$$

where A is the borehole cross-sectional area and p(t) is the pressure on the well bottom. For coupling 1 into the receiver well, the solid moves with vertical particle velocity v(t) at the well bottom, and the fluid in the borehole there moves with the same velocity. Coupling 2a is described by equations (1) and (4) with length of perfed interval L = 5 m.

The tube wave source is assumed to be a Gaussian pulse producing volumetric flow rate into the well Q(t) = Q0e−0.5(f0t)2 with amplitude Q0 = 7.4 m3/s and characteristic frequency f0 = 10 Hz. This Q0 will generate a pressure wave with maximum amplitude of 1 MPa in the source well (and that amplitude will double upon reflection from the closed bottom end of the well). Tube wave parameters are given in Figure 4a and the tube wave equations are (4). The tube wave speed is c = 1/ ϱfβ. No attenuation of tube waves is accounted for in our simulations. Fluid velocity (or, equivalently, flow rate) is specified at the top and bottom of the source and receiver wells. The velocity is zero unless otherwise stated. The tube wave equations are solved using a high-order staggered grid, time-domain finite difference method.

Seismic wave propagation is simulated using the 3D viscoelastic wave equation code AWP-ODC-OS described previously, accounting for frequency-independent attenuation with P- and S-wave quality factors of 100. This time-domain code is based on the classic fourth order staggered grid velocity- stress method with attenuation incorporated using memory variables. The top boundary is a traction-free surface, and absorbing boundary conditions are used on all other boundaries. Extensive tests were conducted to verify the accuracy of the method in simulating wave propagation from point forces and moment tensor sources, by comparing solution results to analytical solutions for waves in a homogeneous medium. These tests also helped us select the size of the computational domain to avoid reflections from the absorbing boundaries, as

well as the grid spacing (3.125 m) required for accuracy up to 10 Hz.

Each simulation requires three consecutive steps:

1. Simulate tube waves in the source well from a source at the wellhead. Input: Source time function (flow rate at wellhead). Output: Pressure time series in the source well at the perfs and well bottom.
2. Convert pressure at the bottom of the source well to a force on the solid using equation (5). Convert fluid pressure at the perfs to a point seismic moment tensor source using equation (1). Simulate seismic waves from the source well to the receiver well. Input: Force F (t) and moment tensor M(t). Output: Vertical particle velocity at the receiver well bottom and strain rates at the receiver well perf location.
3. Simulate tube waves in the receiver well. Input: Solid particle velocity as a boundary condition on fluid velocity at the well bottom and "squeezing" source term S(z,t) in the tube wave equations (4). Output: Pressure, p(t), and pressure rate, dp/dt, time series at the receiver wellhead.

Steps 1 and 3 are relatively fast, since they only require solving a 1D wave equation, whereas step 2 takes considerable computational time. The seismic wave simulations were performed on the XStream GPU Cluster at Stanford University (http://xstream.stanford.edu).

Figure 5 shows the source well simulation (step 1). Note that this simulation is independent of the choice of reservoir structural model. Tube waves are generated at the wellhead, propagate down the well, reflect from the bottom (doubling the amplitude of pressure), and return to the surface. This process would continue indefinitely since the model neglects tube wave attenuation, so only a single reflection is modeled. Pressure at the well bottom and perfs (Figure 5b) is stored and used to calculate the source terms for the seismic wave simulation (downward force and seismic moment tensor).

The seismic wave simulation (step 2) provides boundary conditions and a source term for the receiver well tube wave problem. Figure 6 explains seismic wave arrivals at the receiver well. At these distances and low frequencies, there is no clear separation between P and S waves at locations near the bottom of the receiver well. In fact, it is customary in seismology to distinguish between near-

field and far-field terms in the response to a point force (and near-, intermediate-, and far-field terms in the response to a point moment tensor). At these distances and frequencies, all terms contribute with equal amplitude to the total response. We also observe that couplings 1 and 2a contribute with comparable amplitude (Figure 7)

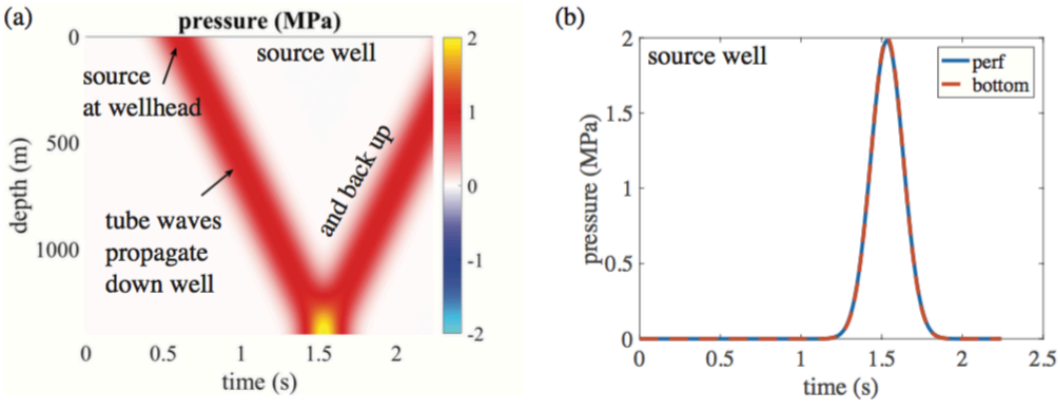

Figure 5: Source well simulation. (a) Space-time plot showing excitation of tube waves by the wellhead source, propagation down the well, reflection at the bottom, and propagation back up the well. (b) Time series of pressure at the well bottom and perfs, used for couplings 1 and 2a, respectively. Because these two locations are separated by a distance much less than the tube wave wavelength, the time series are effectively identical. (c) Downward force on the formation exerted by the fluid at the bottom of the source well (coupling 1). (d) Seismic moment tensor at the perf location in the source well (coupling 2a).

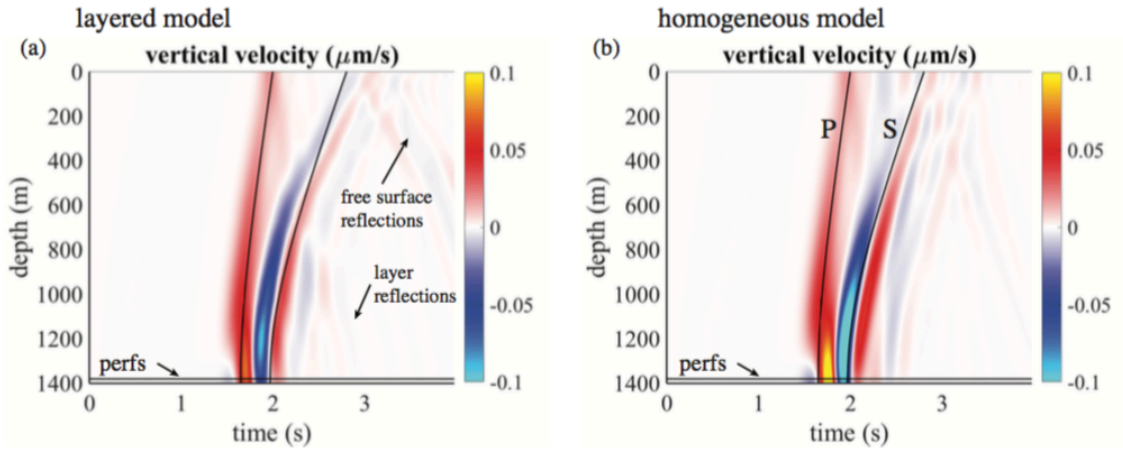

Figure 6: Seismic wave simulations. Space-time plots of vertical particle velocity (positive down) in the solid along the length of the receiver well. This is the incident seismic wavefield that couples to tube waves. Horizontal black line marks perf depth. Black curves show theoretical P- and S-wave arrivals (for the homogeneous model). (a) Layered structural model. (b) Homogeneous half-space model. For the layered case, note the delayed arrivals near the free surface due to lower near-surface velocities. Reflections from individual layers are present, but of small amplitude. There are no obvious features indicative of reservoir guided waves at these low frequencies.

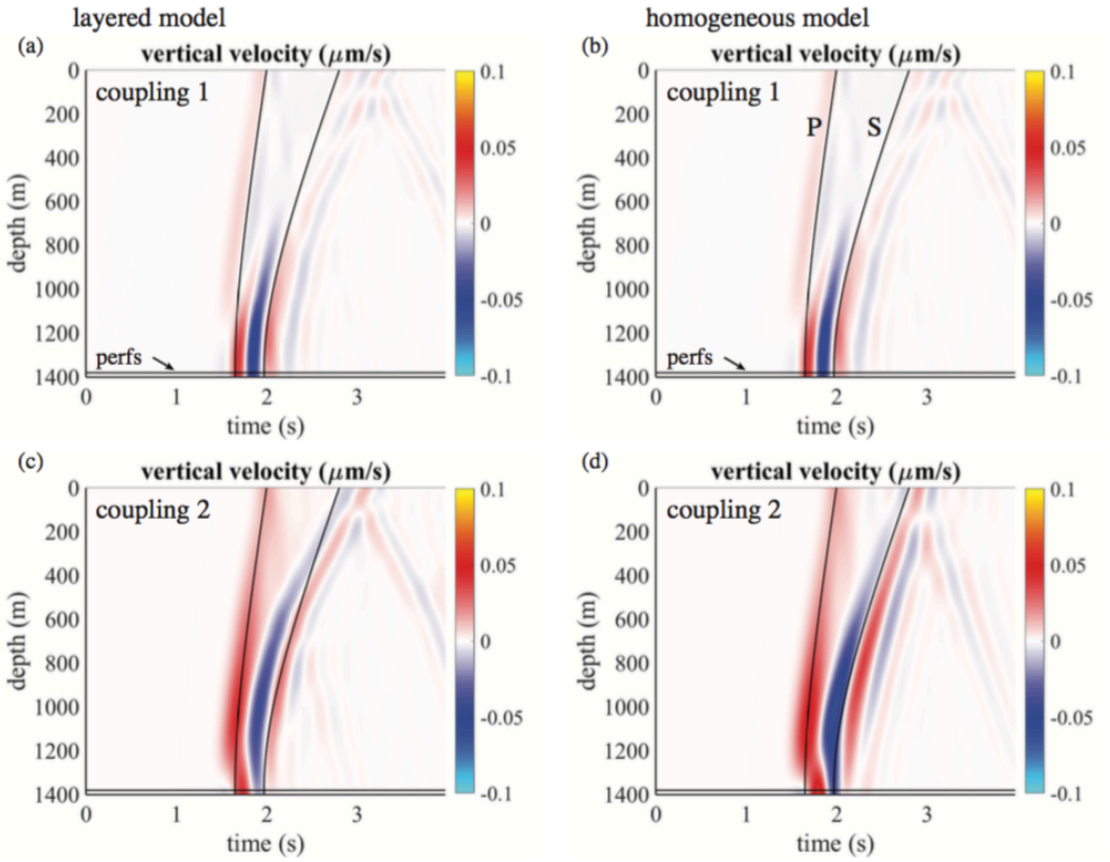

Figure 7: Similar to Figure 6, but showing contributions from couplings 1 and 2a separately. Both couplings produce similar amplitude signals at these frequencies and well separation distance.

Figure 8 shows results from the receiver well simulations (step 3). The homogeneous model produces amplitudes that are about twice as large as the layered models, but the general waveform shapes are remarkably similar and dominated by direct arrivals rather than layer reflections or guided waves. This is a consequence of the seismic wavelengths generally being larger than the vertical length scales over which material properties exhibit significant variation. In other words, at the low frequencies in this study, the seismic waves are only sensitive to a low-pass filtered version of the material structure in Figure 4b. There are no obvious waveform features to indicate reservoir guided waves, again likely a consequence of the low frequencies studied.

Finally, because the well separation distance is comparable to seismic

wavelengths, the incident waves are not simply far-field body waves. Instead there is a complicated superposition of near-, intermediate-, and far-field arrivals. It is therefore not possible to identify specific waveform features as P waves or S waves, as is often done for travel time tomography.

Overall this study has demonstrated several challenges that arise when using low frequency waves for cross-well imaging at the Bell Creek Field site:

1. The first challenge comes from the unique properties of the reservoir layer and surrounding rocks, which prevent the reservoir layer from acting as a wave guide. The reservoir layer is considerably faster than the surrounding rocks, exactly the opposite of the desired low-velocity wave guide. There are interface waves (Stoneley waves) that exist at some material interfaces, such as at the boundary between the reservoir layer and one of the bounding units. However, these waves do not exist for all material pairs (existence depends on the constrast in properties), nor for all frequencies, and no evidence was found in the simulations for such waves. Wave guide effects are mostly likely for wavelengths comparable to or smaller than the reservoir layer thickness (i.e., for sufficiently high frequencies). Taking this thickness as 10 m, we estimate that frequencies of 100 Hz or greater would be required for wave guide effects to become apparent at the Bell Creek Field.
2. The second challenge is a low signal amplitude, arising from the low efficiency of tube wave to seismic wave conversions out of the source well and similarly low efficiency for coupling back into the receiver well. Analysis of the governing equations (described in more detail below), shows that coupling is more efficient at higher frequencies, up to the point where attenuation along the seismic wave propagation path becomes significant. There have been several cross-well imaging studies demonstrating that tube wave to seismic wave to tube wave conversions can be measured in offset wells. But those studies employed higher frequency sources (e.g., airguns). In Appendix A we provide estimates of the signal amplitude as a function of frequency, which might be used to design future experiments. If we know instrument noise levels and the source spectrum, these formulas can be used to select the optimal source spectrum and frequency band.

3. The third challenge is a lack of distinct P- and S-wave arrivals at the receiver well, preventing easy identification of related arrivals in the tube wave time series recorded at the wellhead. Again, the situation would be more favorable at higher frequencies. Higher frequencies would also provide more sensitivity to short wavelength details of the structural model.

A/ Estimates of Signal Amplitude

In this appendix we provide simple formulas for estimating signal amplitude as a function of frequency, well separation distance, and borehole properties. These estimates are conservative in the sense that they assume that the relevant seismic waves are far-field body waves, not possibly larger amplitude guided waves. The derivation parallels the three steps taken in the simulation procedure, and is carried out in the frequency domain. Subscripts s and r denote fields in the source and receiver wells, respectively, and 1 and 2 denote coupling 1 and 2a, respectively.

The first step is to estimate tube wave amplitudes in the source well. For wellhead source volumetric flow rate Q(t), the spectral amplitude of pressure in the well (e.g., at the well bottom or perfs) is

$$\hat{p}_S(\omega) \sim Z_S \hat{Q}(\omega). \quad (6)$$

The second step is use this pressure in equations (5) and (1) for point source and moment tensor sources as

$$\hat{F}(\omega) \sim A_S Z_S \hat{Q}(\omega) \quad (7)$$

and

$$\hat{M}(\omega) \sim A_S L Z_S \hat{Q}(\omega), \quad (8)$$

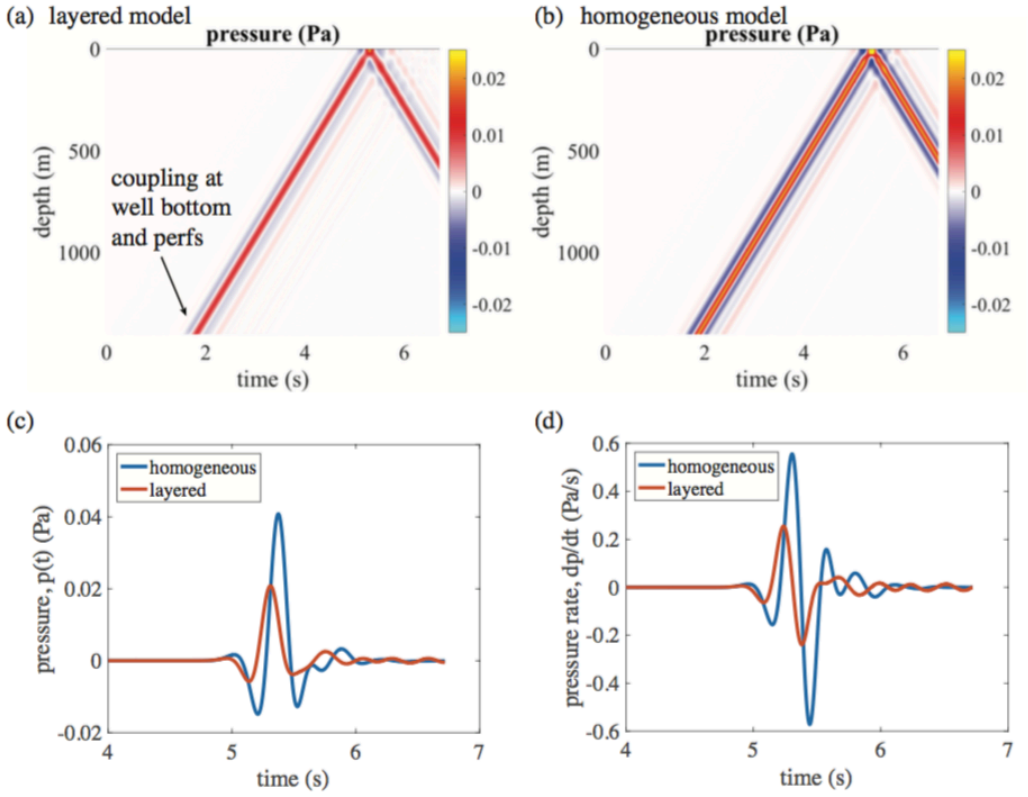

Figure 8: Receiver well simulations. (a) Space-time plot showing excitation of tube waves by seismic wave coupling at the well bottom (coupling 1) and perfs (coupling 2a), for layered structural model. Because the perfs are so close to the well bottom, it is impossible to distinguish between these two receiver couplings in the plot. Note change of units from MPa for source well to Pa for receiver well. (b) Same as (a) but for homogeneous half-space structural model. (c) Time series of pressure, p(t), at receiver wellhead. (d) Same as (c) but plotting pressure rate, dp/dt, as would be recorded by a hydrophone. Waveforms from the layered structural model are similar in amplitude and waveform shape to those from a homogeneous model. There are no obvious guided wave arrivals.

respectively. Note that AsZs = ϱscs, the product of fluid density and tube wave speed in the source well. Next we use far-field body wave solutions for seismic waves to estimate fields in the solid at a distance r, specifically particle velocity and strain rate

$$\hat{v}(\omega) \sim \frac{\omega \hat{F}(\omega)}{4\pi\rho c^2 r} \sim \frac{\omega \rho_s c_s \hat{Q}(\omega)}{4\pi\rho c^2 r} \tag{9}$$

$$\hat{\dot{\epsilon}}(\omega) \sim \frac{\omega^3 \hat{M}(\omega)}{4\pi\rho c^4 r} \sim \frac{\omega^3 L \rho_s c_s \hat{Q}(\omega)}{4\pi\rho c^4 r}, \tag{10}$$

where ϱ and c are solid density and wave speed (e.g., P or S wave speed). The third step is to couple into the receiver well by applying the velocity at the well bottom (coupling 1) or using the squeezing source term in equation (4) for coupling 2a. The resulting tube wave amplitude in the receiver well is for coupling 1 and

$$\hat{p}_{r1}(\omega) \sim \rho_r c_r \hat{v}(\omega) \sim \frac{\omega(\rho_s c_s)(\rho_r c_r)\hat{Q}(\omega)}{4\pi\rho c^2 r} \tag{11}$$

$$\hat{p}_{r2}(\omega) \sim \rho_r c_r L \hat{\dot{\epsilon}}(\omega) \sim \left(\frac{\omega L}{c}\right)^2 \frac{\omega(\rho_s c_s)(\rho_r c_r)\hat{Q}(\omega)}{4\pi\rho c^2 r} \tag{12}$$

for coupling 2a. These can be converted to spectral amplitudes of hydrophone signals (i.e., records of dp/dt) by multiplying by ω.

From this exercise we learn that the relative amplitude of coupling 2a to coupling 1 is (ωL/c)2. Thus coupling 2a (through the perfs) becomes the dominant coupling at frequencies higher than some critical frequency. Taking L ~ 5 m and c ~ 1 km/s, the critical frequency is f = ω/2π ~ c/2πL ~ 30 Hz. Around this frequency, signal amplitudes from both couplings are comparable, as found in our simulations. The estimates provided above can be used to design future experiments in the following manner. First determine instrument noise levels. Then determine the minimum acceptable signal to noise ratio, taking into account that this ratio can be increased by stacking. Finally, use the provided

formulas to calculate the source amplitude and frequency required to reach the desired signal level.

APPENDIX D

SEISMOS FIELD TEST RESULTS

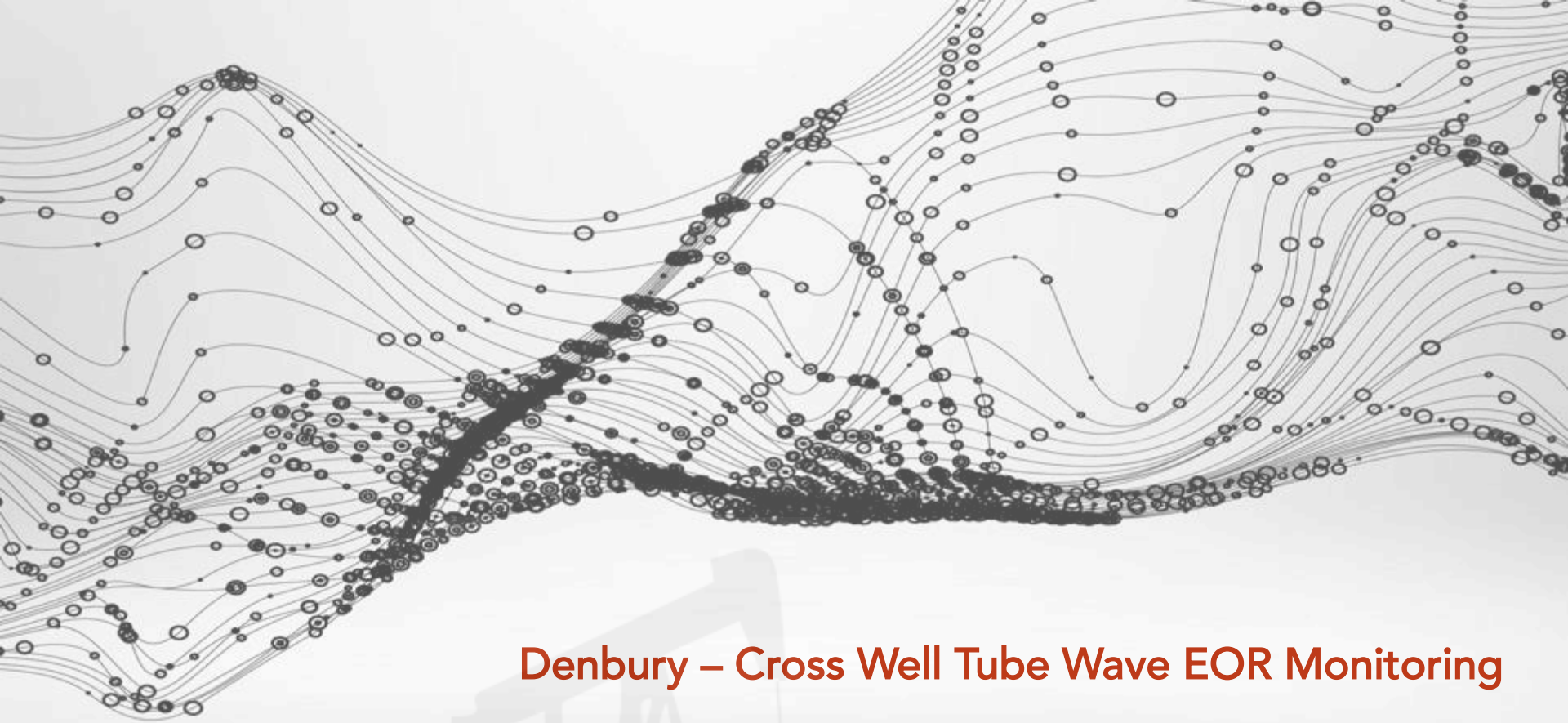

Denbury – Cross Well Tube Wave EOR Monitoring

November 20, 2017

seismos

Summary

- Signals between Wells B (33-02) and C (34-04) are seen
- Need to verify what are these signals

Basemap

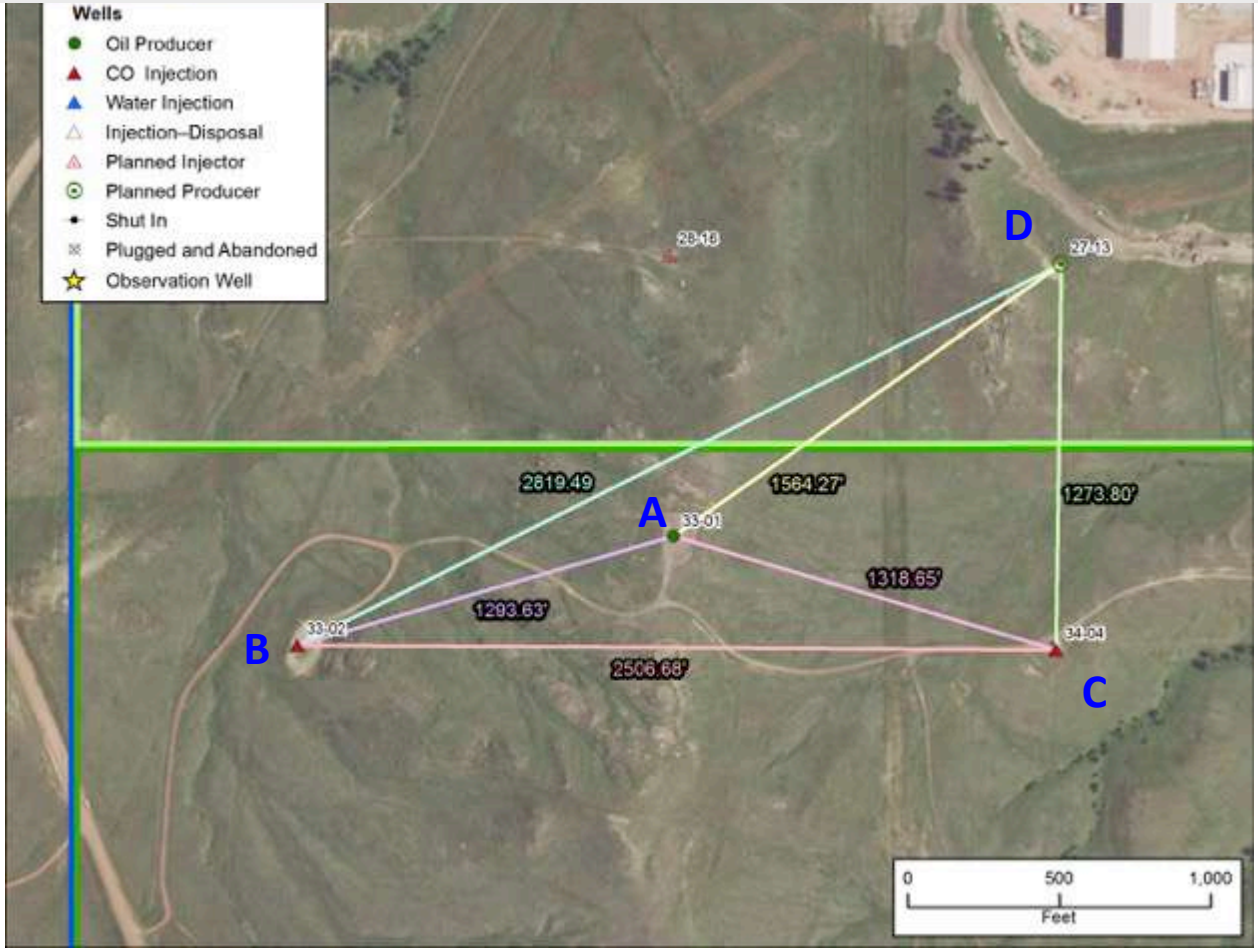
Wells
Oil Producer
CO Injection
Water Injection
Injection–Disposal
Planned Injector
Planned Producer
Shut In
Plugged and Abandoned
Observation Well
28-18
D
27-13
2819.49
1584.27'
1273.80'
A
33-01
1318.65'
1293.63'
33-02
34-04
B
2506.68'
C
0
500
1,000
Feet

Pipeline Map

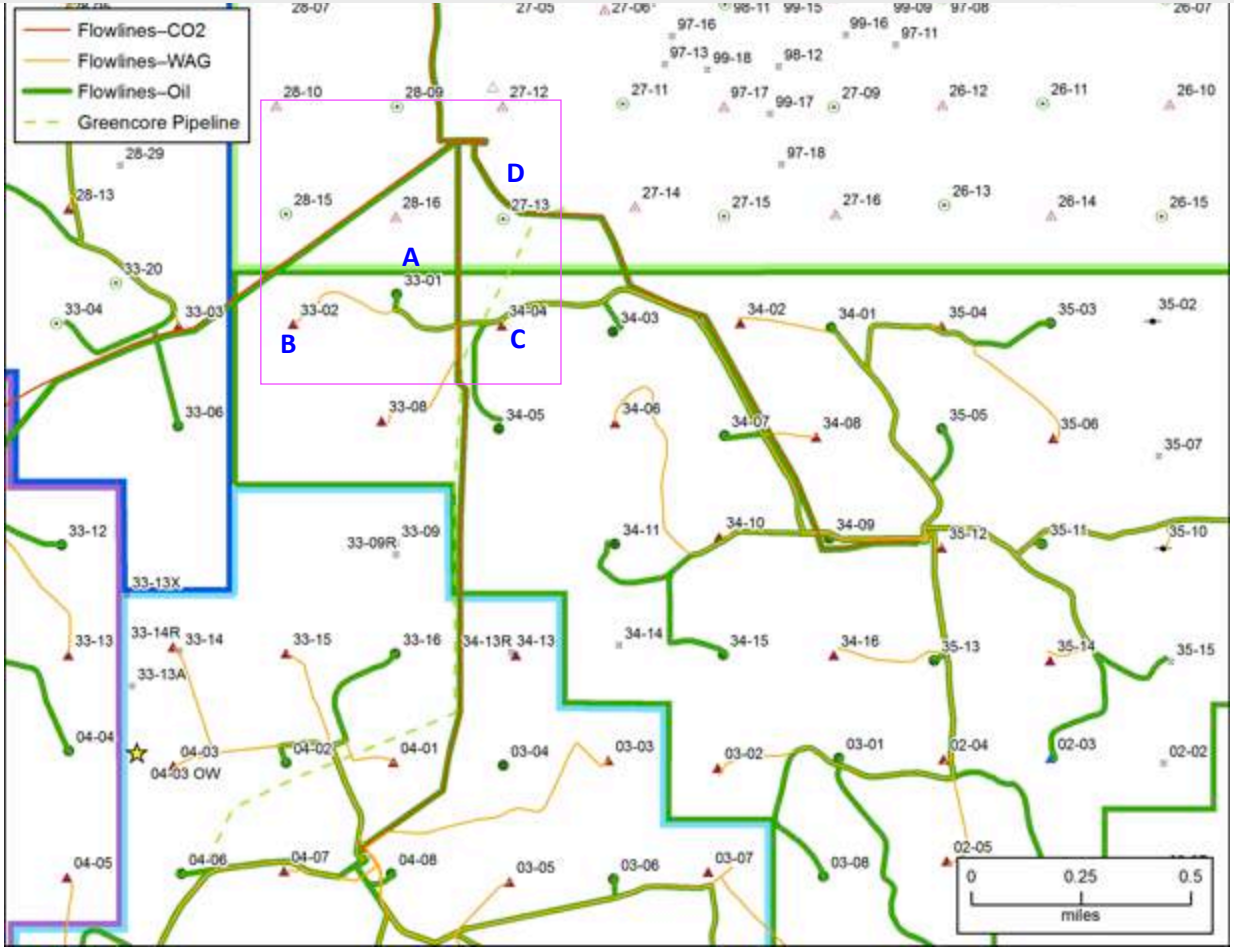

Signals between Wells B and C

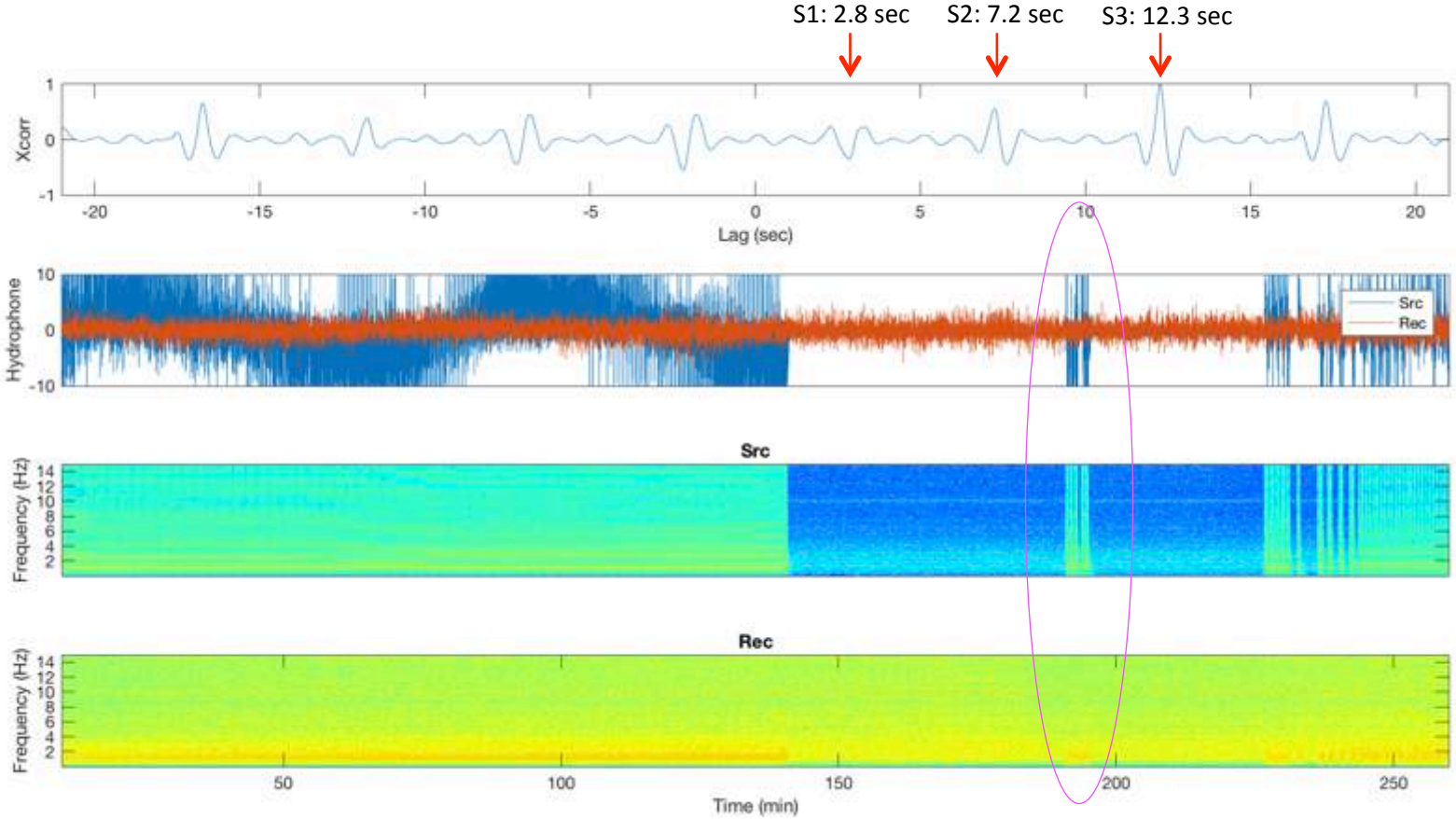

Next slide shows the zoom-in

Wells B -> C

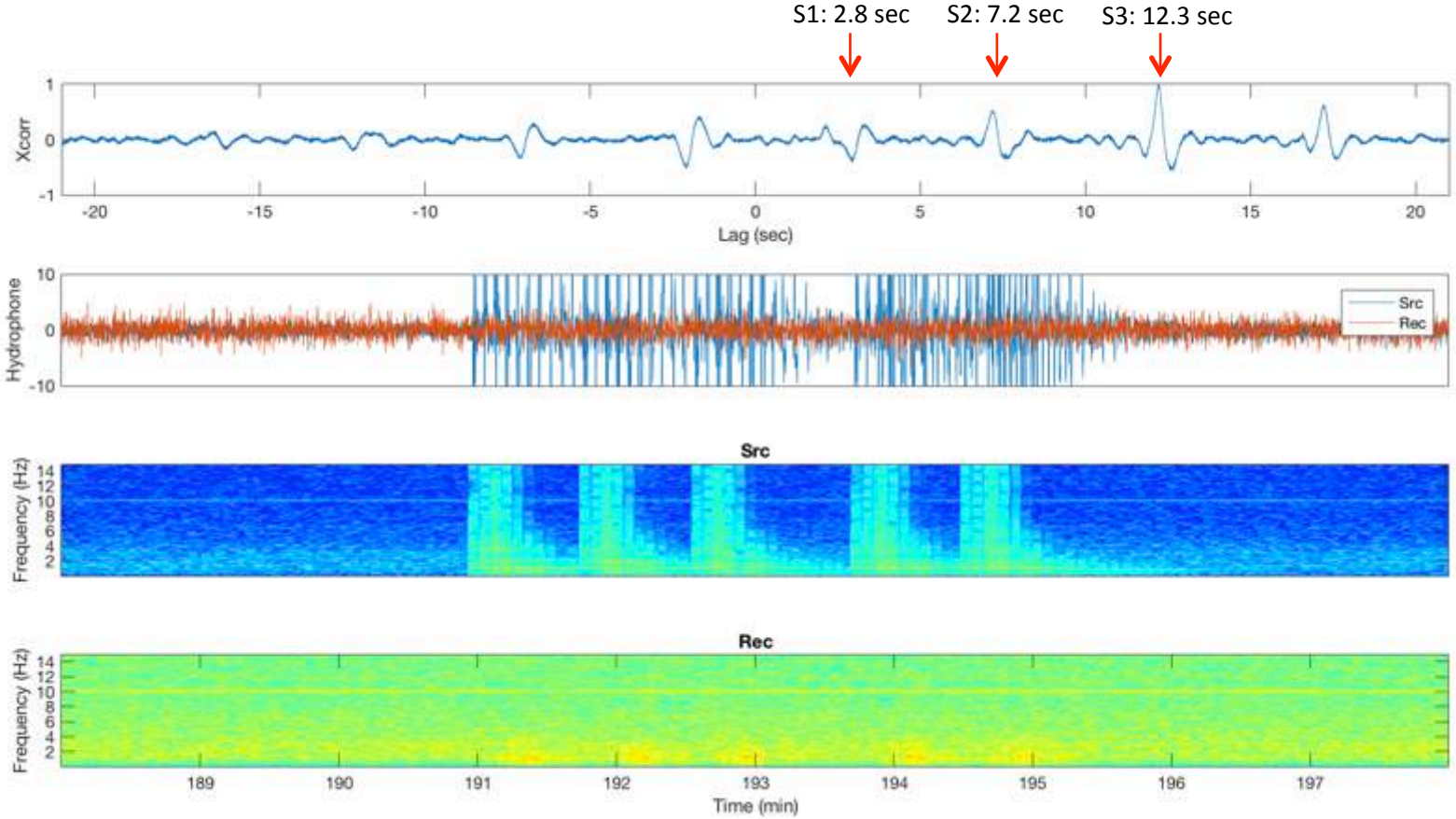
S1: 2.8 sec
S2: 7.2 sec
S3: 12.3 sec
Xcorr
Lag (sec)
Hydrophone
Src
Rec
Src
Frequency (Hz)
Rec
Frequency (Hz)
Time (min)

Pipeline Info

Distances between wells

From	To	Distance (feet)	Distance (miles)
33-02	33-01	1293.63	0.245
33-02	34-04	2506.68	0.475
33-02	27-13	2819.49	0.534
34-04	33-01	1318.65	0.250
34-04	27-13	1273.80	0.241
27-13	33-01	1564.27	0.296

Distance from Phase 4 manifold to respective well

33-02 (B)	9721.31	1.841
34-04 (C)	6951.64	1.317
33-01 (A)	8472.58	1.605

Two possible wave paths

Wells B -> C: Tube wave – Formation guided wave – Tube wave

0.3048*(4475/1500+2500/2300+4408/1500) -> 2.14 sec

Wells B -> C: Pipelines

0.3048*(9721/1500 + 6952/1500) -> 3.4 sec

Appendix

- Raw Data
- All possible cross-well pairs

Source Well 3301 (A)

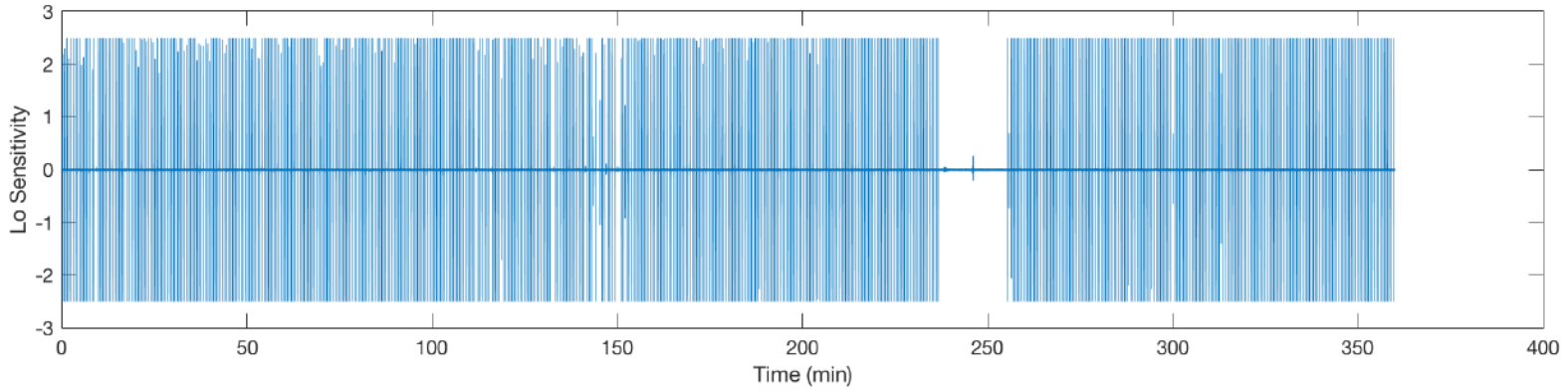

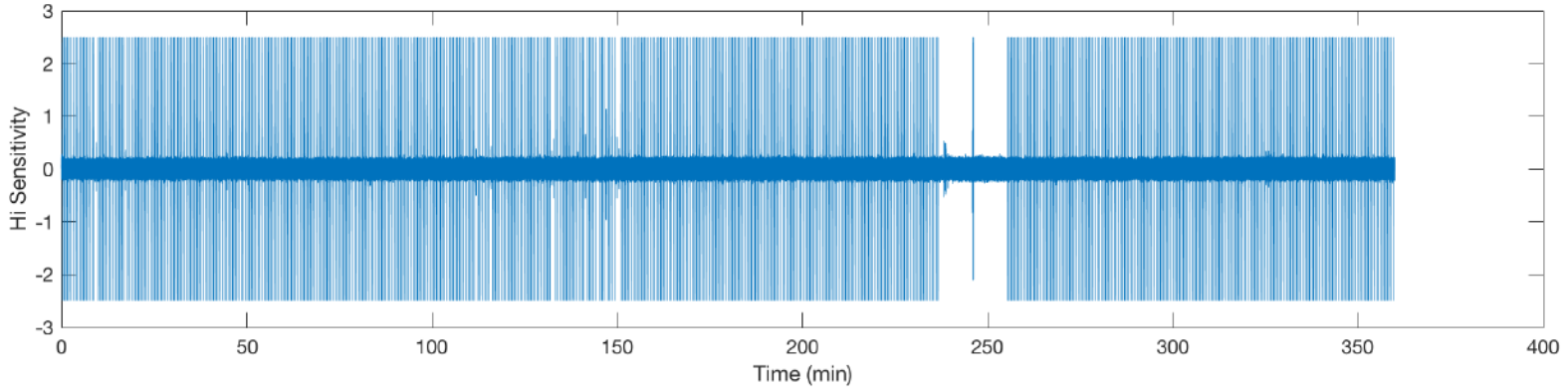

Source Well 3302 (B)

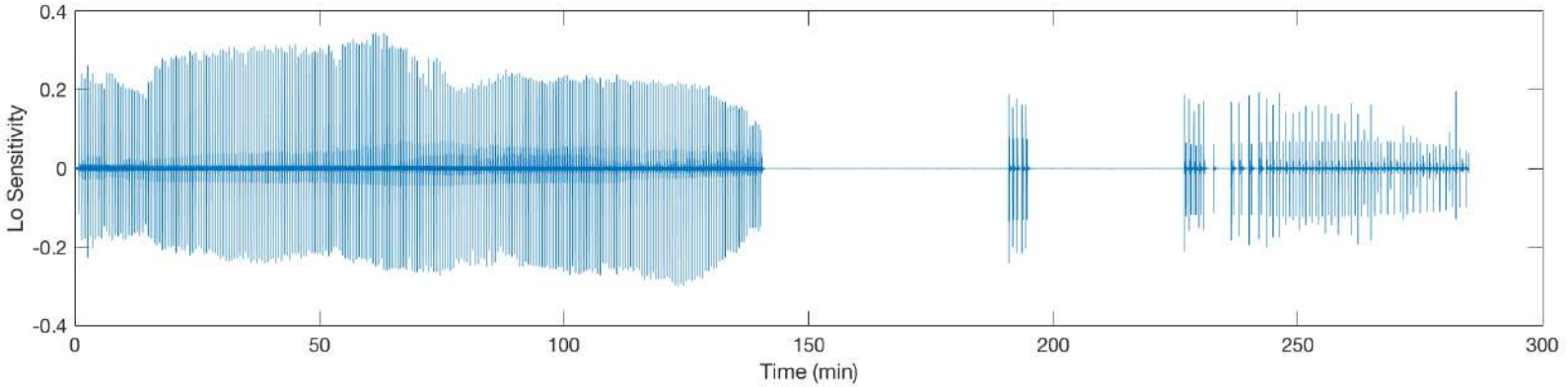

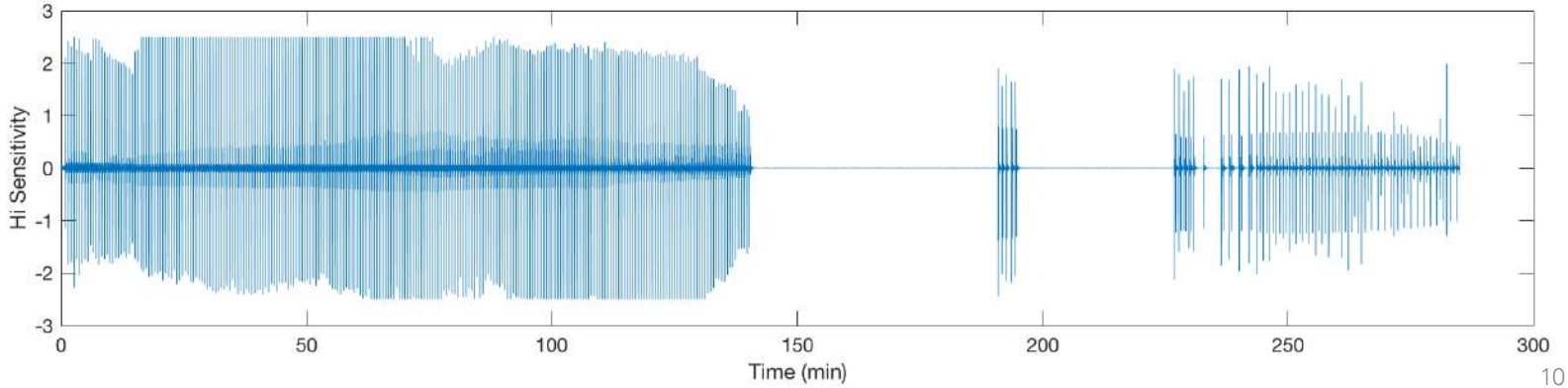

Source Well 3404 (C)

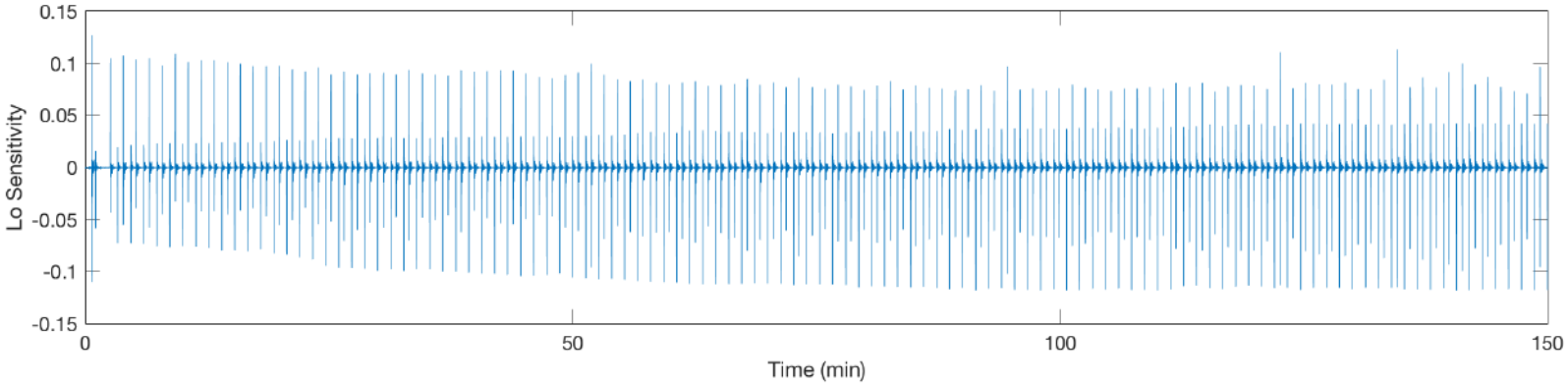

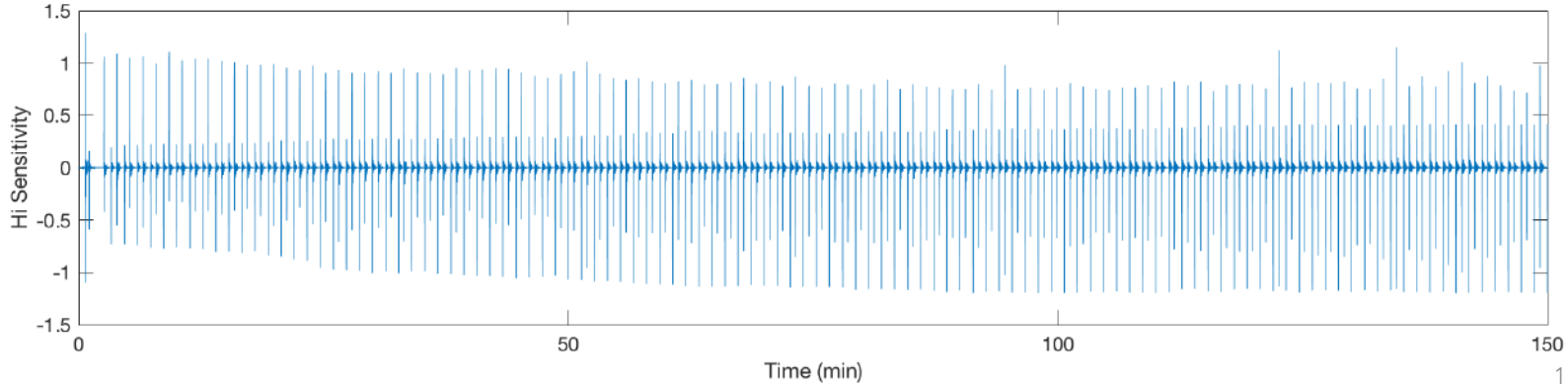

Source Well 2713 (D)

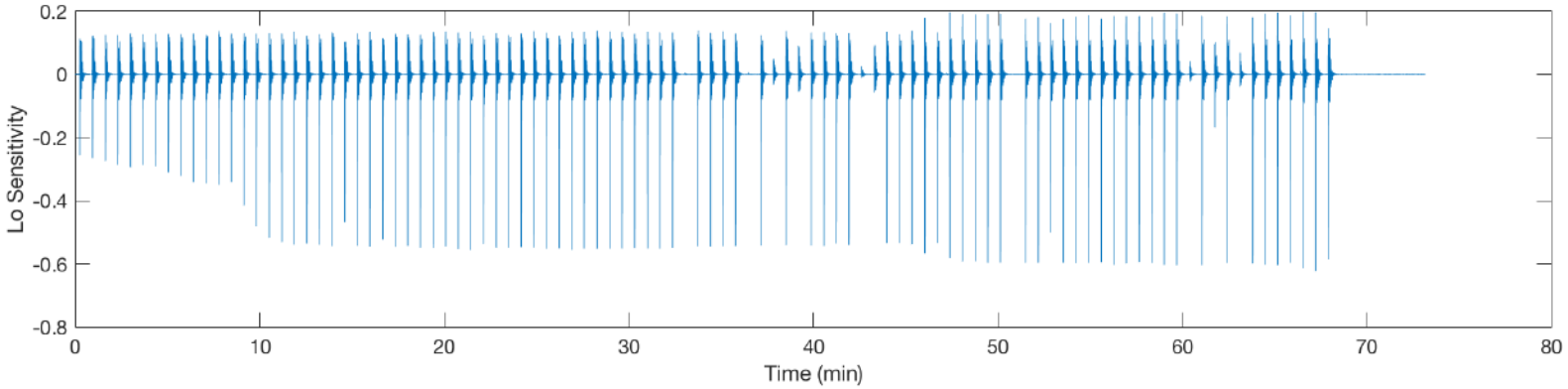

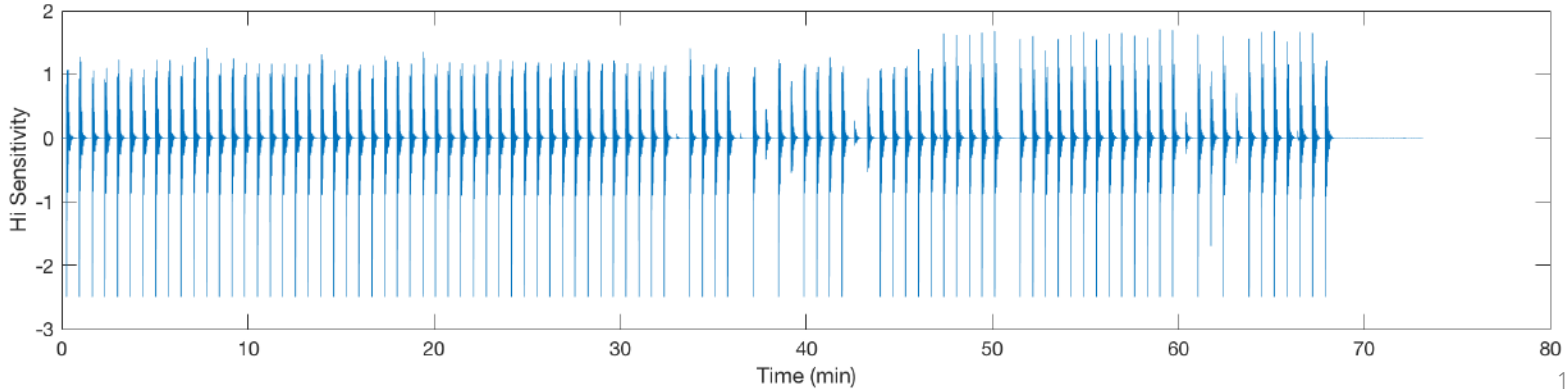

Wells A -> B

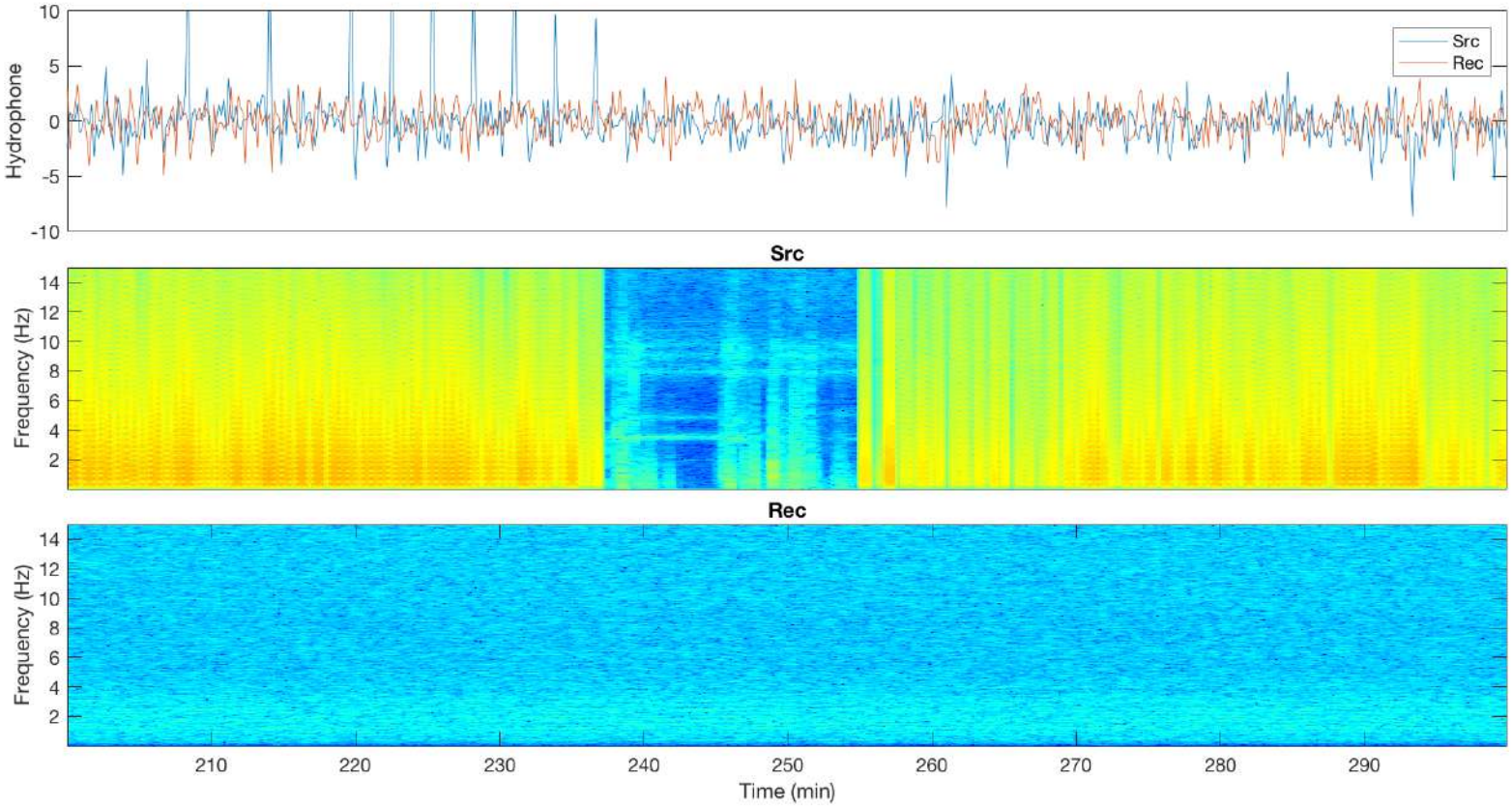
Hydrophone
10
5
0
-5
-10
Src
Rec
Src
Frequency (Hz)
14
12
10
8
6
4
2
Rec
Frequency (Hz)
14
12
10
8
6
4
2
210
220
230
240
250
260
270
280
290
Time (min)

Wells A -> C

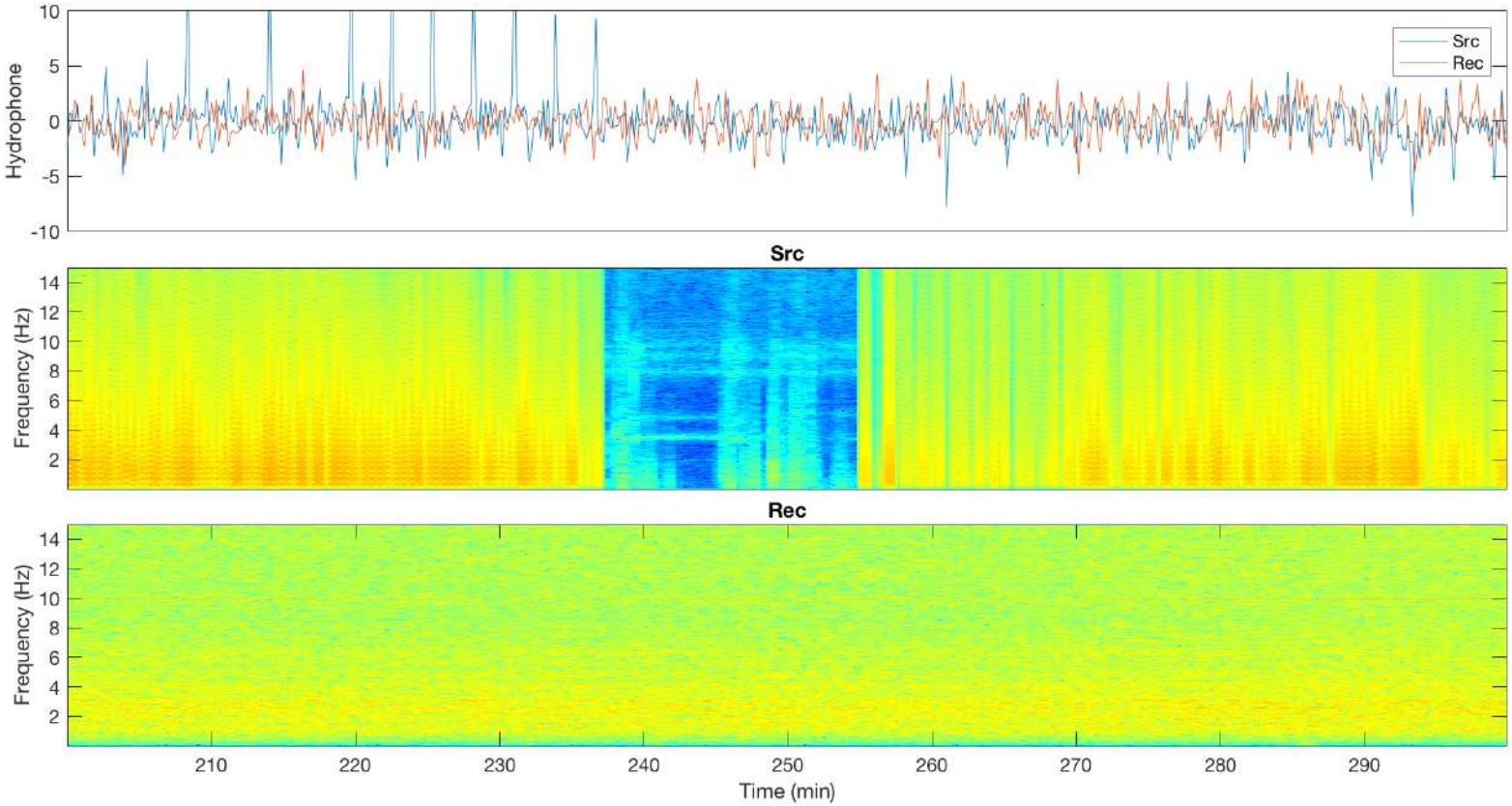
Hydrophone
10
5
0
-5
-10
Src
Rec
Src
Frequency (Hz)
14
12
10
8
6
4
2
Rec
Frequency (Hz)
14
12
10
8
6
4
2
210
220
230
240
250
260
270
280
290
Time (min)

Wells A -> D

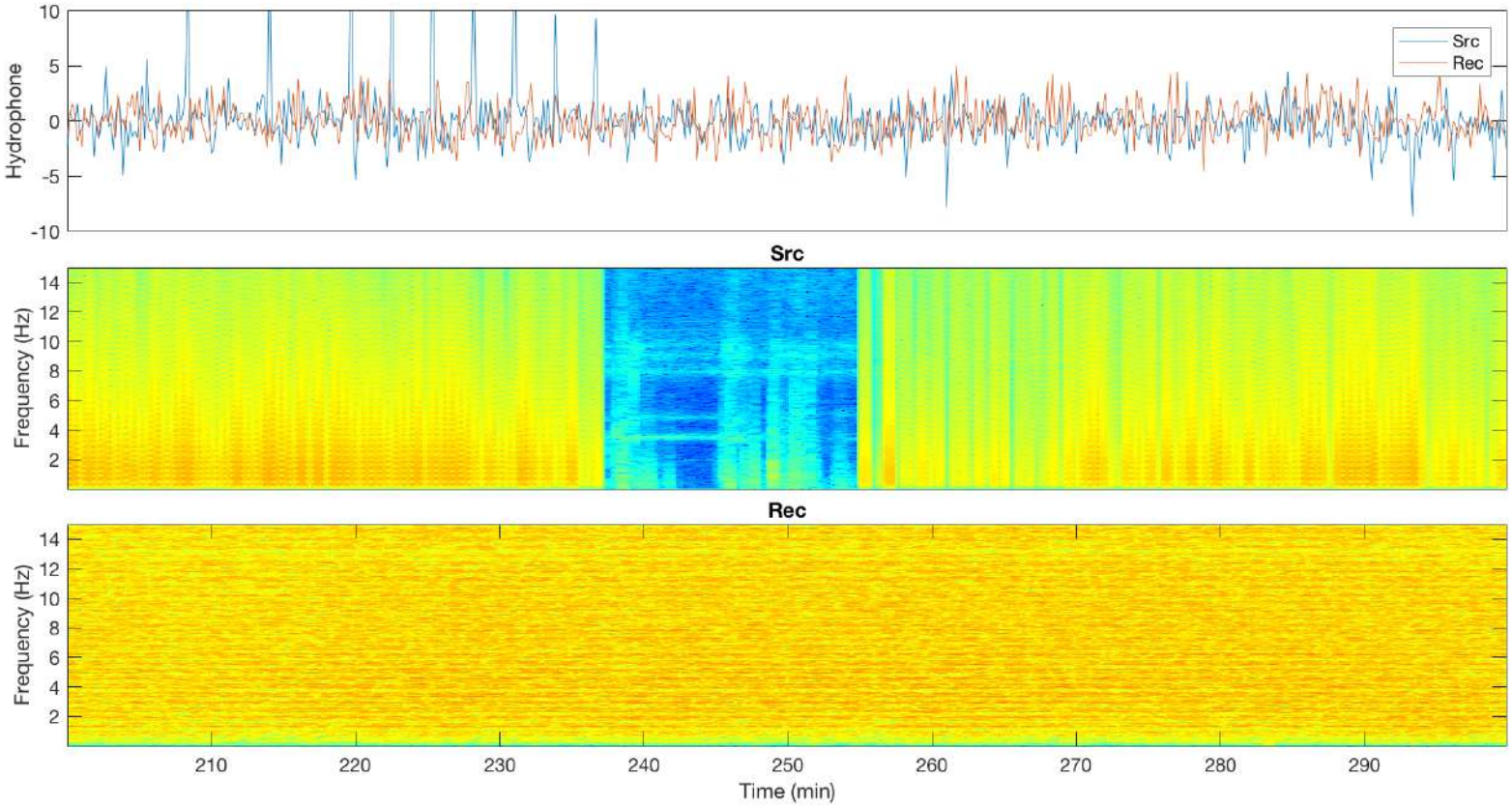
Hydrophone
10
5
0
-5
-10
Src
Rec
Src
Frequency (Hz)
14
12
10
8
6
4
2
Rec
Frequency (Hz)
14
12
10
8
6
4
2
210
220
230
240
250
260
270
280
290
Time (min)

Wells A -> D

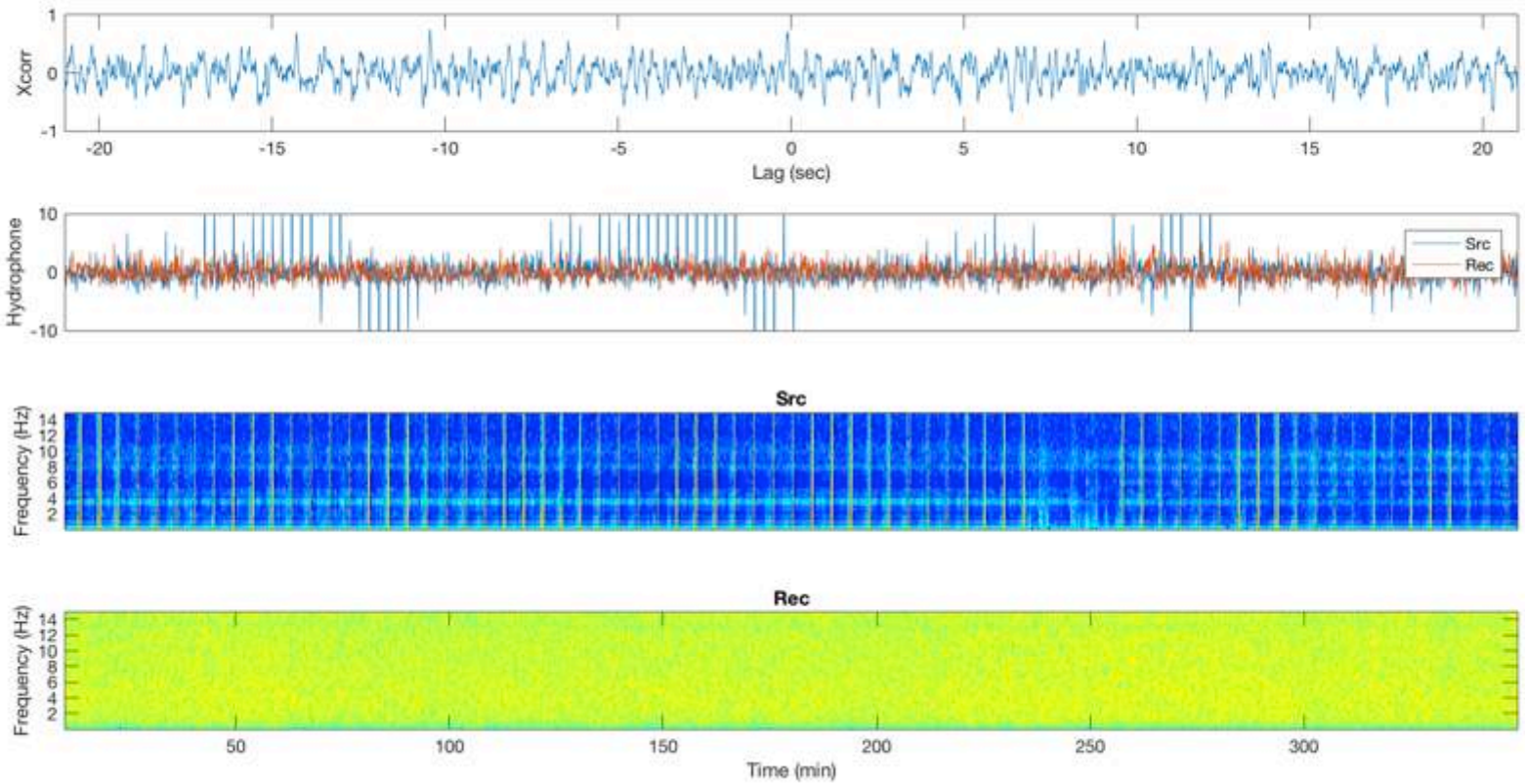
Xcorr
1
0
-1
-20
-15
-10
-5
0
5
10
15
20
Lag (sec)
Hydrophone
10
0
-10
Src
Rec
Src
Frequency (Hz)
14
12
10
8
6
4
2
Rec
Frequency (Hz)
14
12
10
8
6
4
2
50
100
150
200
250
300
Time (min)

Wells B -> A

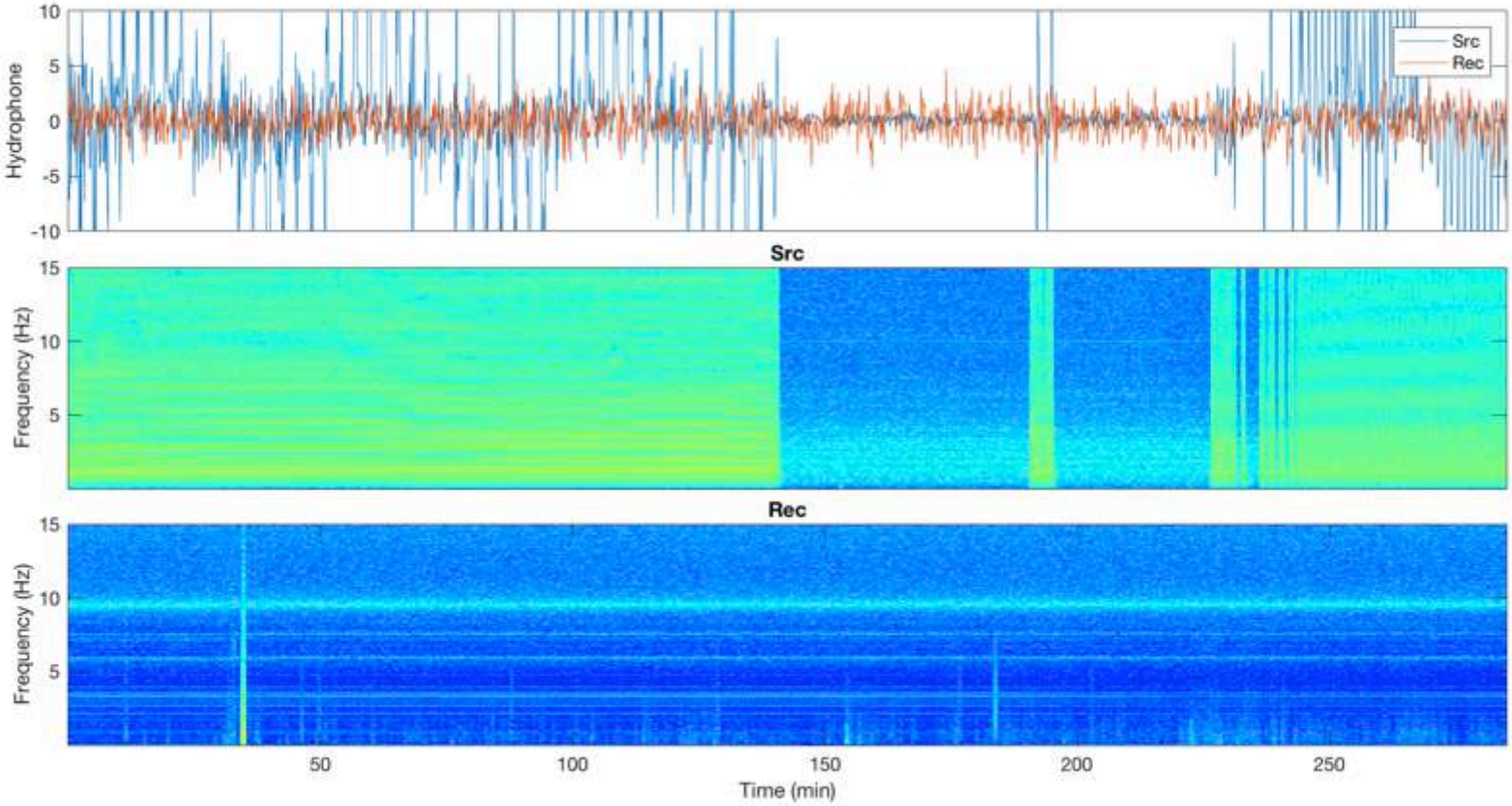
Hydrophone
10
5
0
-5
-10
Src
Rec
Src
Frequency (Hz)
15
10
5
Rec
Frequency (Hz)
15
10
5
50
100
150
200
250
Time (min)

Wells B -> D

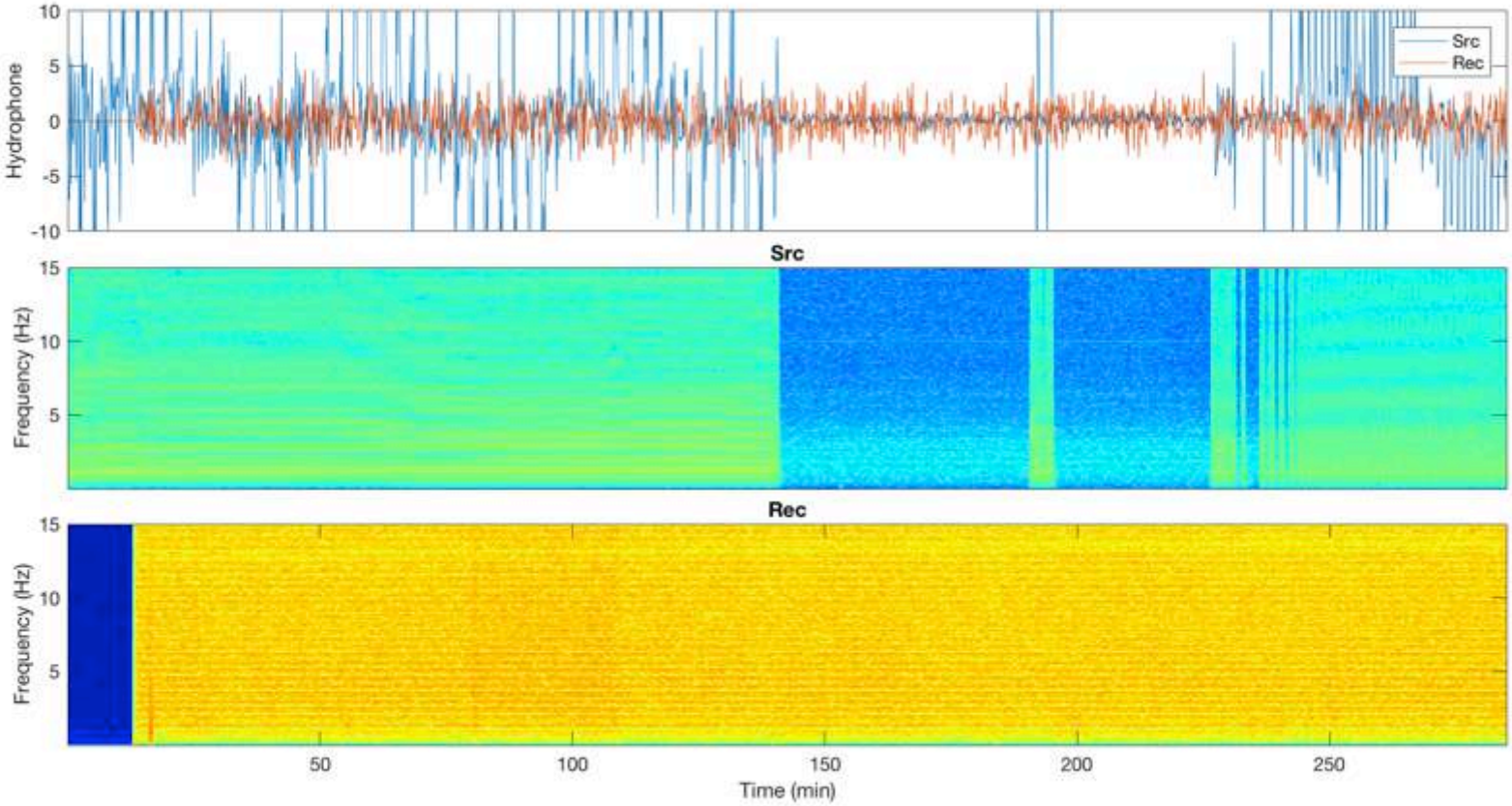
Hydrophone
10
5
0
-5
-10
Src
Rec
Src
Frequency (Hz)
15
10
5
Rec
Frequency (Hz)
15
10
5
50
100
150
200
250
Time (min)

Wells B -> C

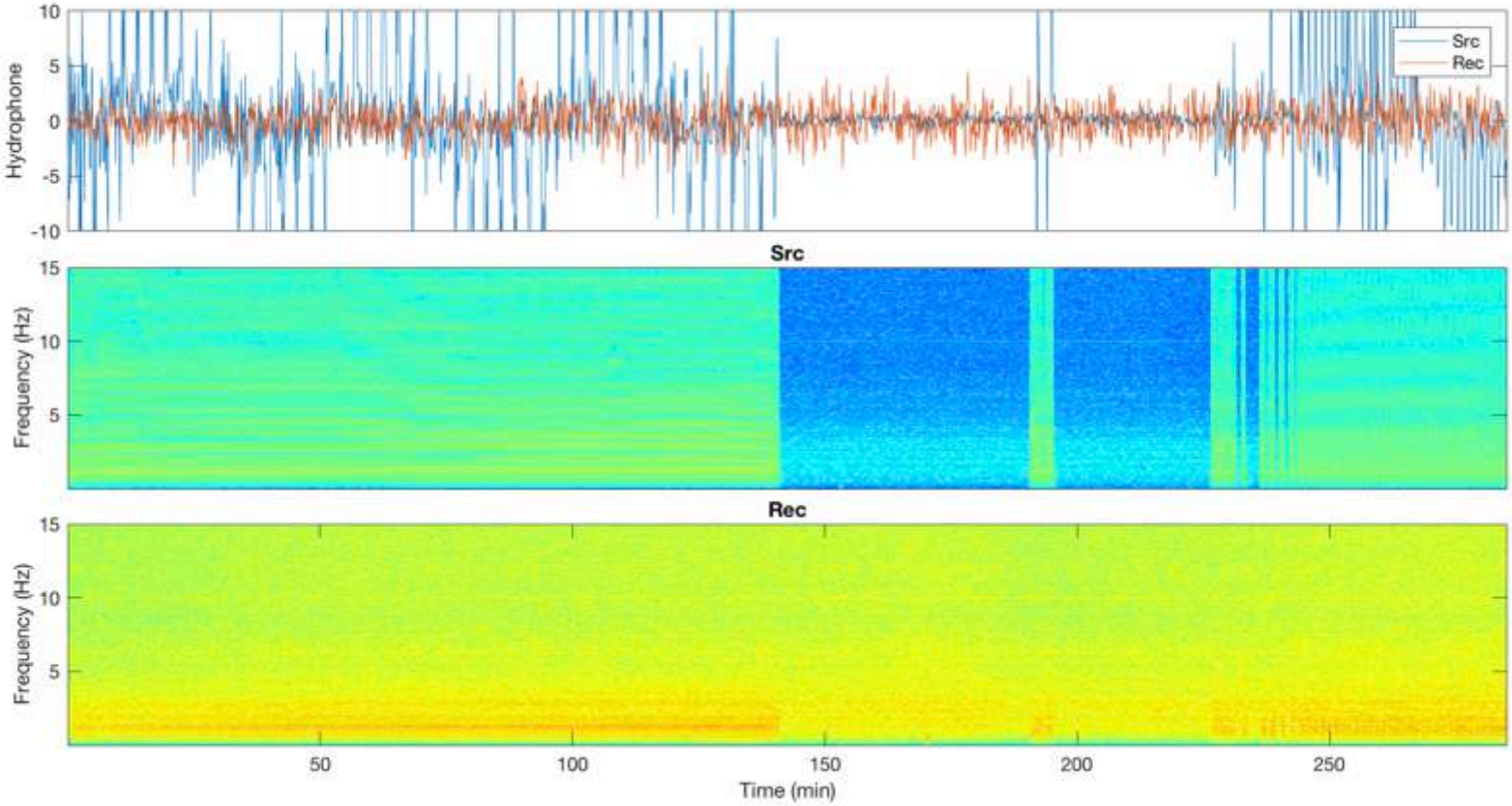
Hydrophone
10
5
0
-5
-10
Src
Rec
Src
Frequency (Hz)
15
10
5
Rec
Frequency (Hz)
15
10
5
50
100
150
200
250
Time (min)

Wells B -> C

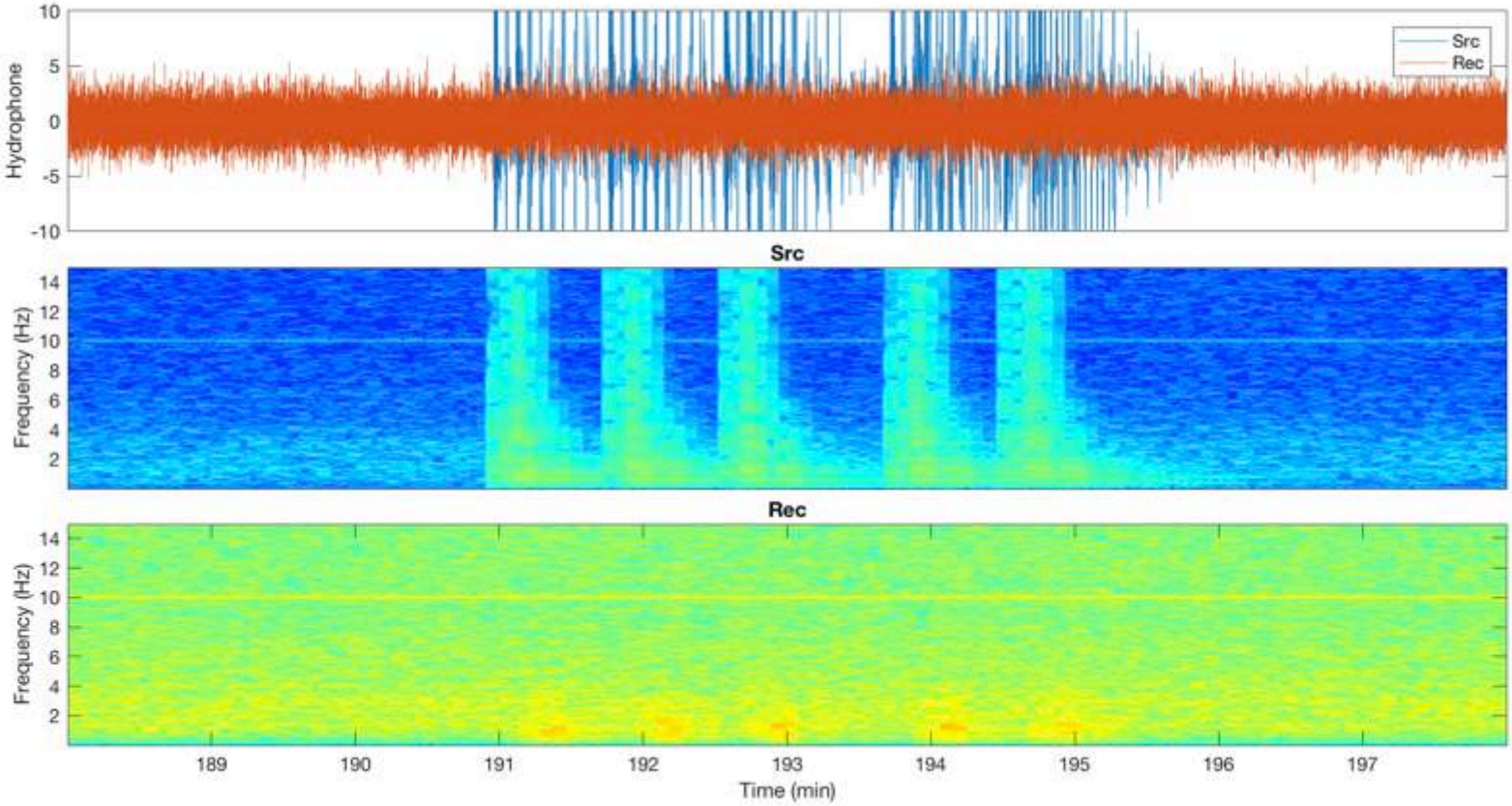
Hydrophone
10
5
0
-5
-10
Src
Rec
Src
Frequency (Hz)
14
12
10
8
6
4
2
Rec
Frequency (Hz)
14
12
10
8
6
4
2
189
190
191
192
193
194
195
196
197
Time (min)

Wells B -> C

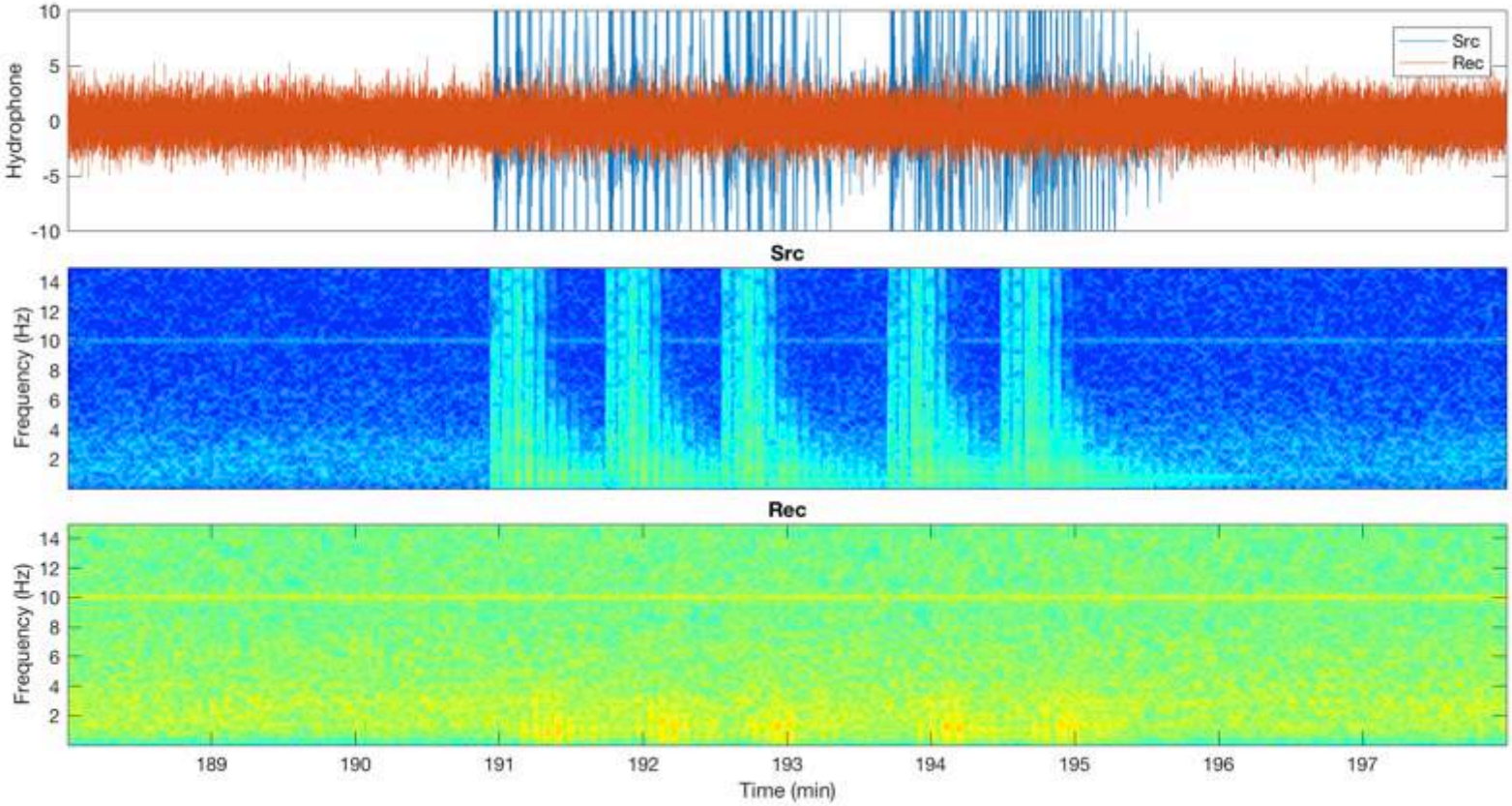
Hydrophone
10
5
0
-5
-10
Src
Rec
Src
Frequency (Hz)
14
12
10
8
6
4
2
Rec
Frequency (Hz)
14
12
10
8
6
4
2
189
190
191
192
193
194
195
196
197
Time (min)

Wells B -> C

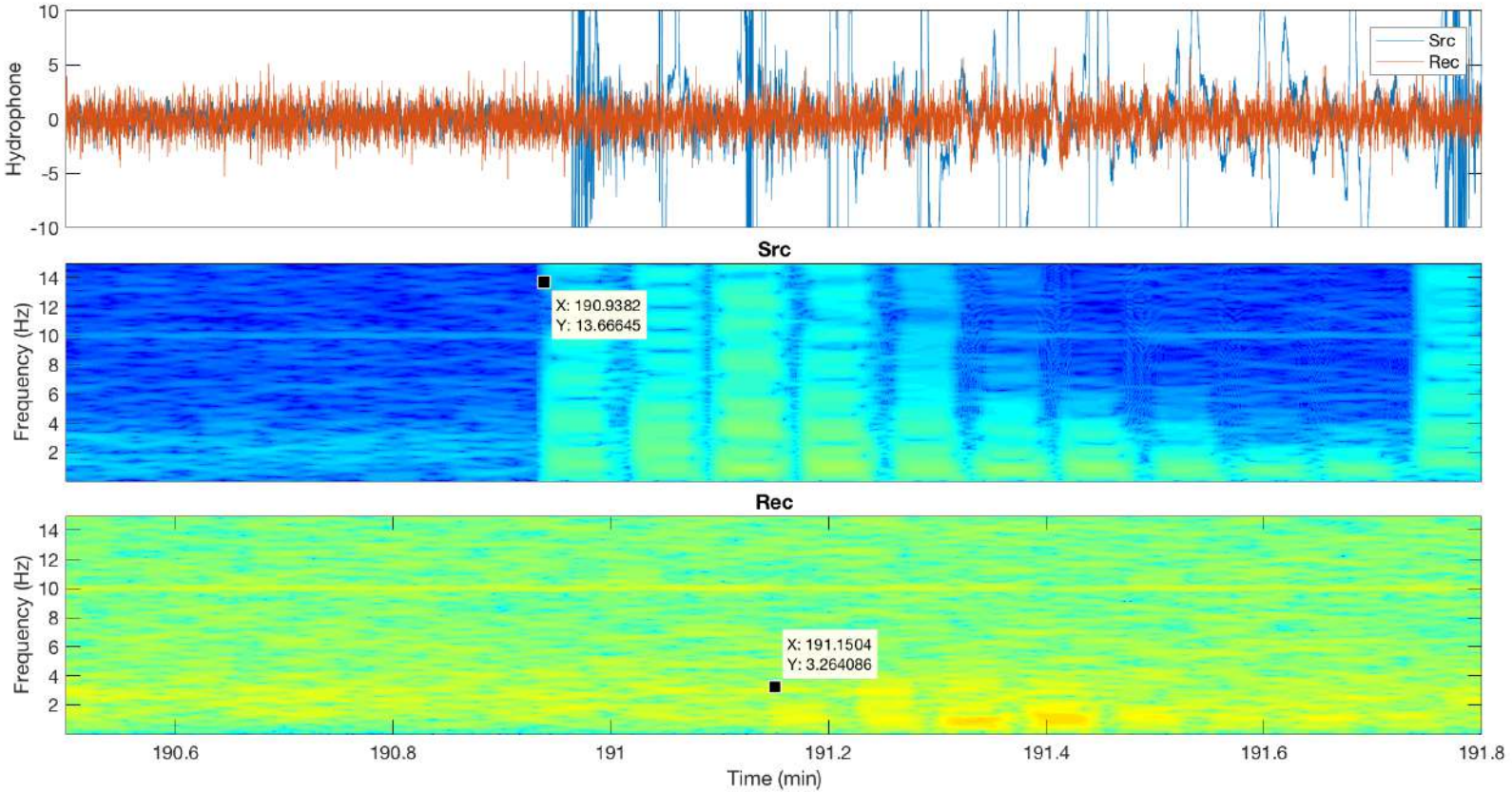

1500*(191.1504-190.9382)*60 -> 12 sec (quite long?)

Wells B -> C

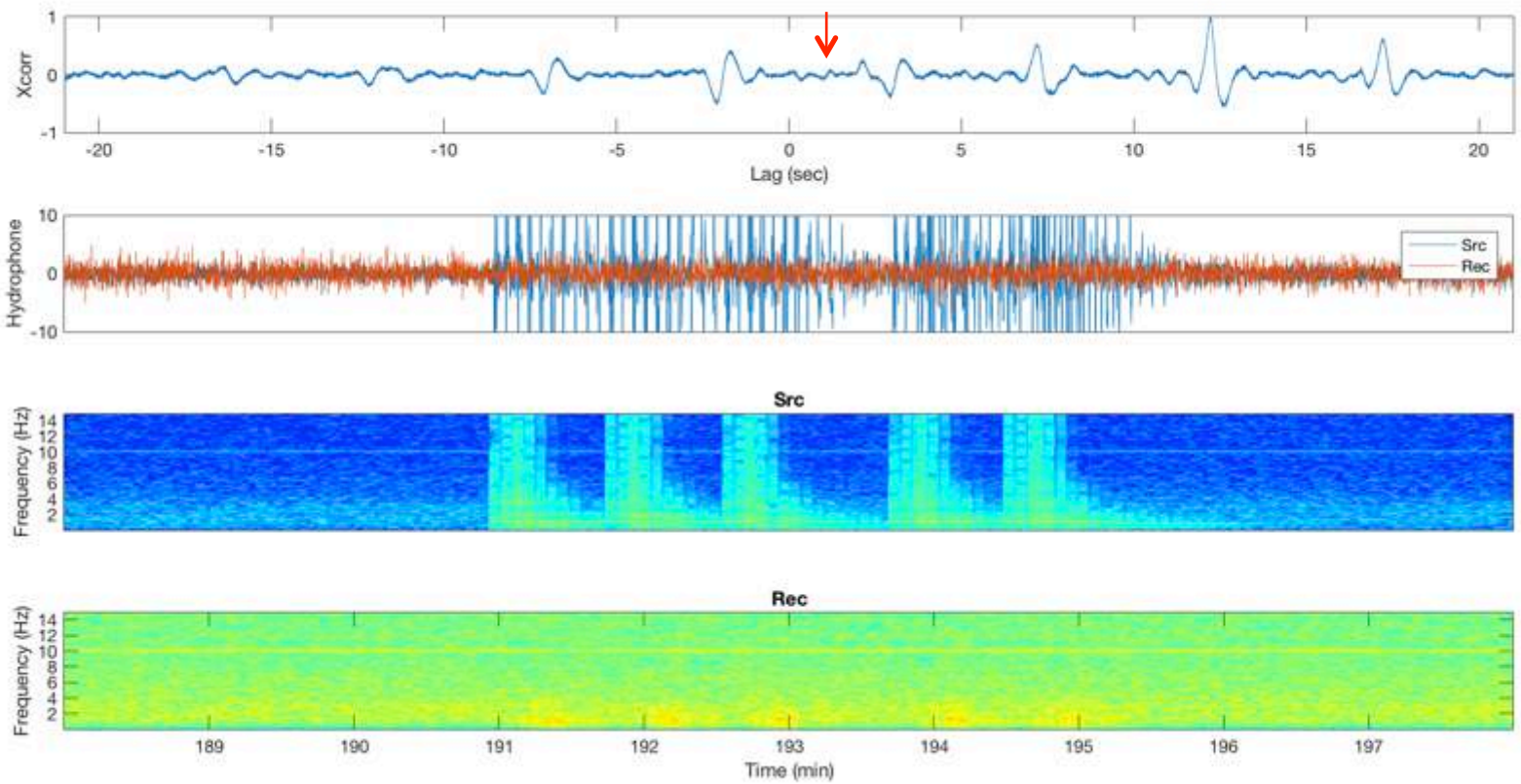
Xcorr
1
0
-1
-20
-15
-10
-5
0
5
10
15
20
Lag (sec)
Hydrophone
10
0
-10
Src
Rec
Src
Frequency (Hz)
14
12
10
8
6
4
2
Rec
Frequency (Hz)
14
12
10
8
6
4
2
189
190
191
192
193
194
195
196
197
Time (min)

Wells B -> C

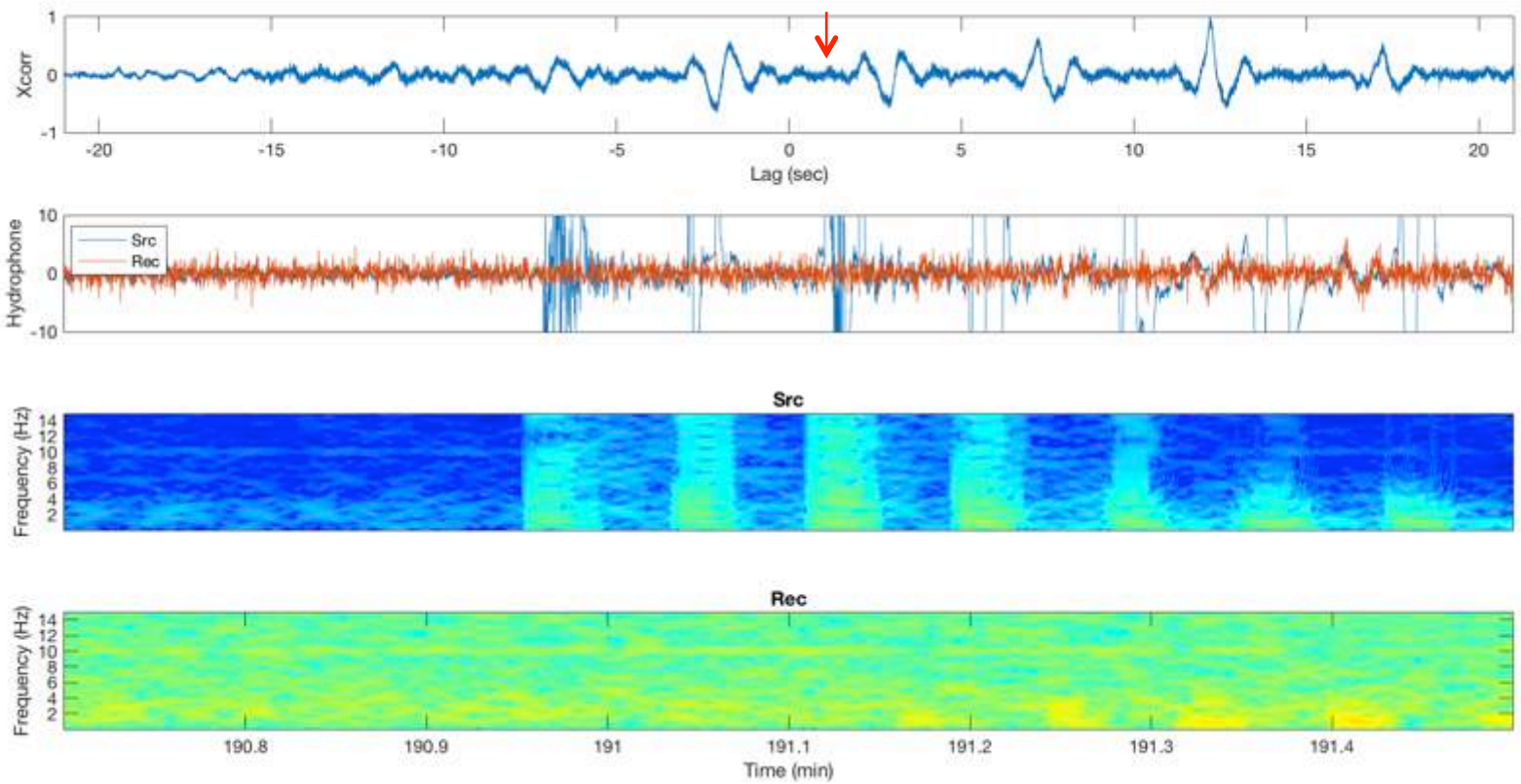
Xcorr
1
0
-1
-20
-15
-10
-5
0
5
10
15
20
Lag (sec)
Hydrophone
10
0
-10
Src
Rec
Src
Frequency (Hz)
14
12
10
8
6
4
2
Rec
Frequency (Hz)
14
12
10
8
6
4
2
190.8
190.9
191
191.1
191.2
191.3
191.4
Time (min)

Wells B -> C

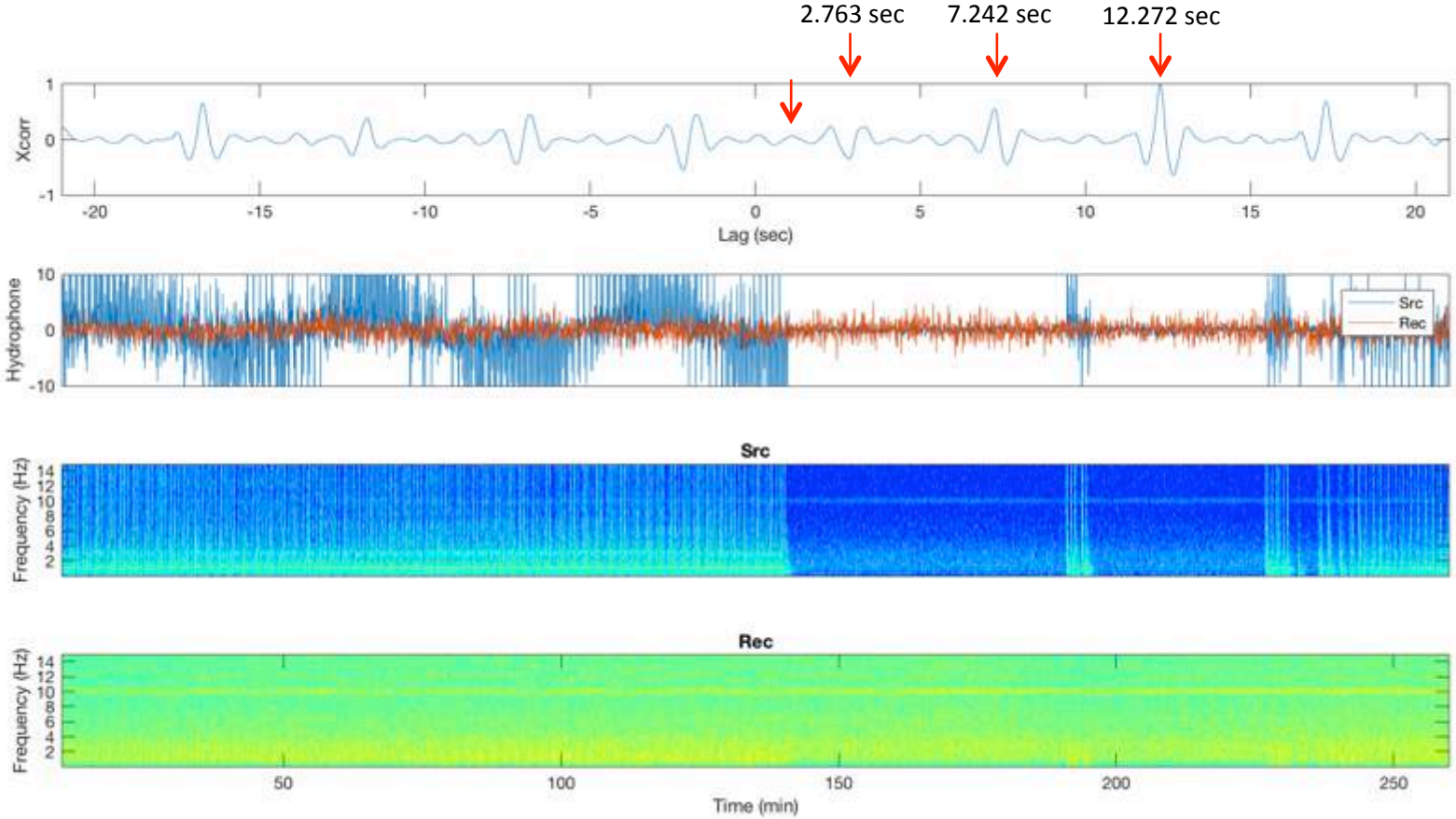
2.763 sec
7.242 sec
12.272 sec
Xcorr
Lag (sec)
Hydrophone
Src
Rec
Src
Rec
Frequency (Hz)
Time (min)

Wells C -> A

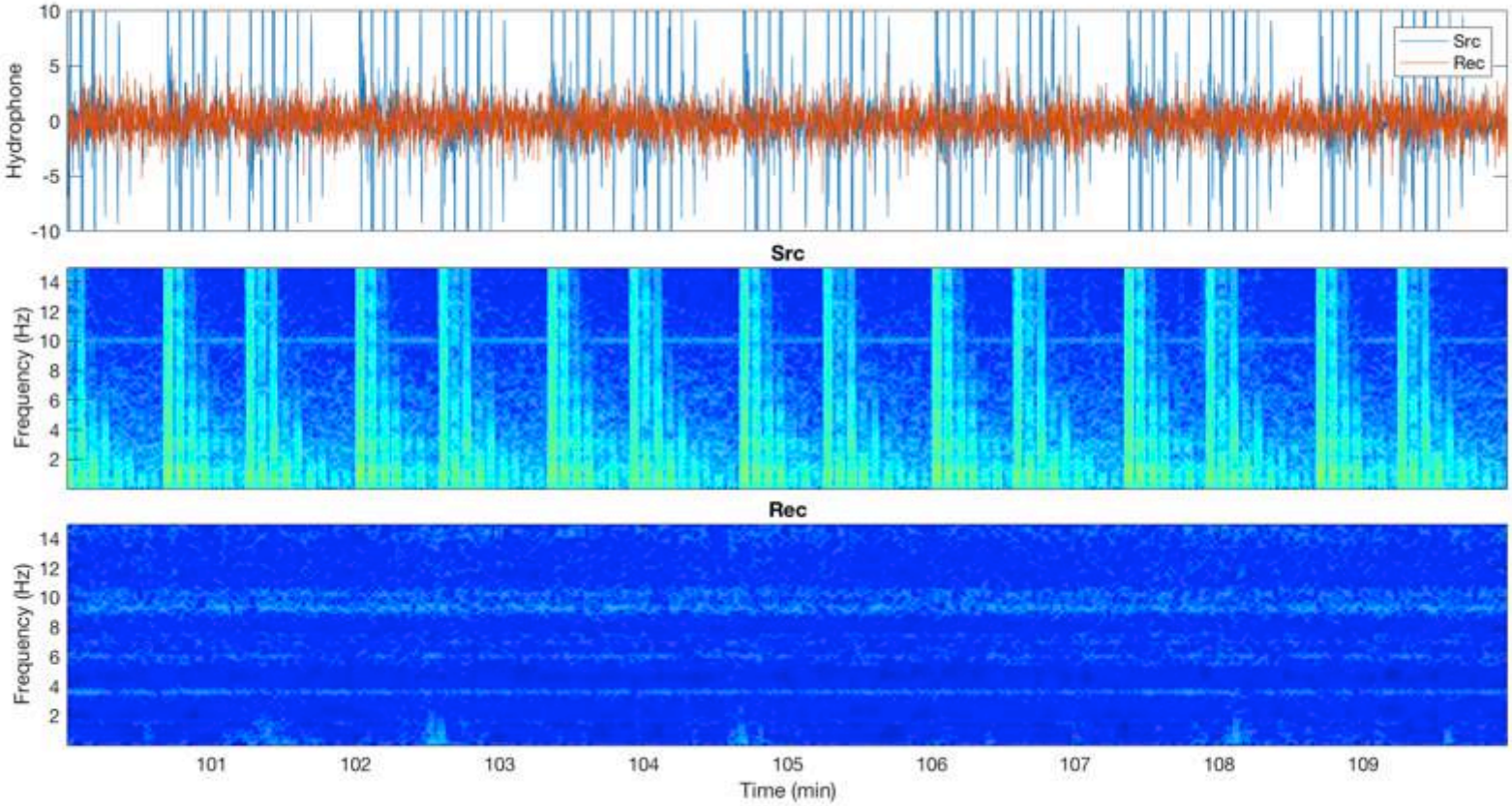
Hydrophone
10
5
0
-5
-10
Src
Rec
Src
Frequency (Hz)
14
12
10
8
6
4
2
Rec
Frequency (Hz)
14
12
10
8
6
4
2
101
102
103
104
105
106
107
108
109
Time (min)

Wells C -> A

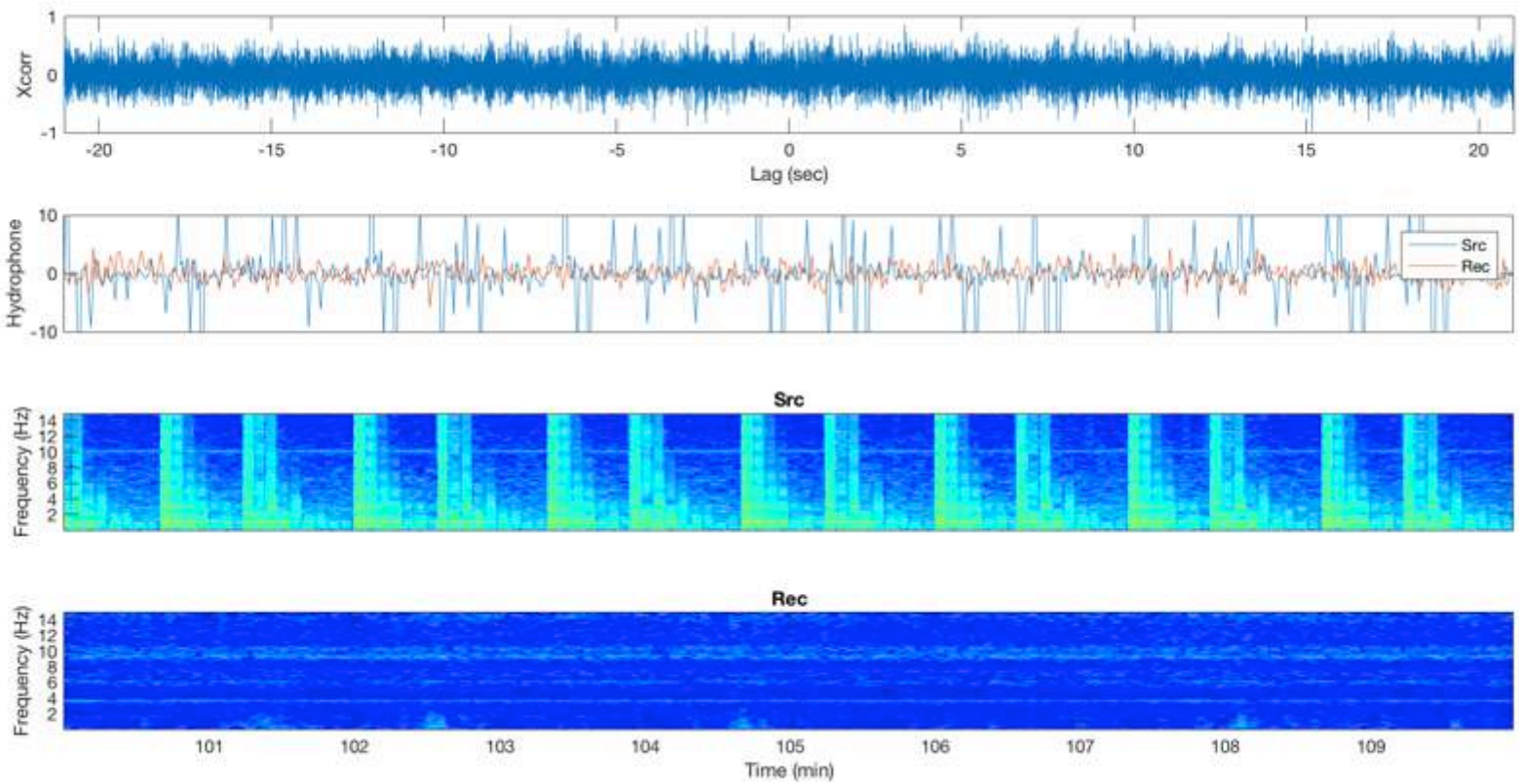
Xcorr
1
0
-1
-20
-15
-10
-5
0
5
10
15
20
Lag (sec)
Hydrophone
10
0
-10
Src
Rec
Src
Frequency (Hz)
14
12
10
8
6
4
2
Rec
Frequency (Hz)
14
12
10
8
6
4
2
101
102
103
104
105
106
107
108
109
Time (min)

Wells C -> B

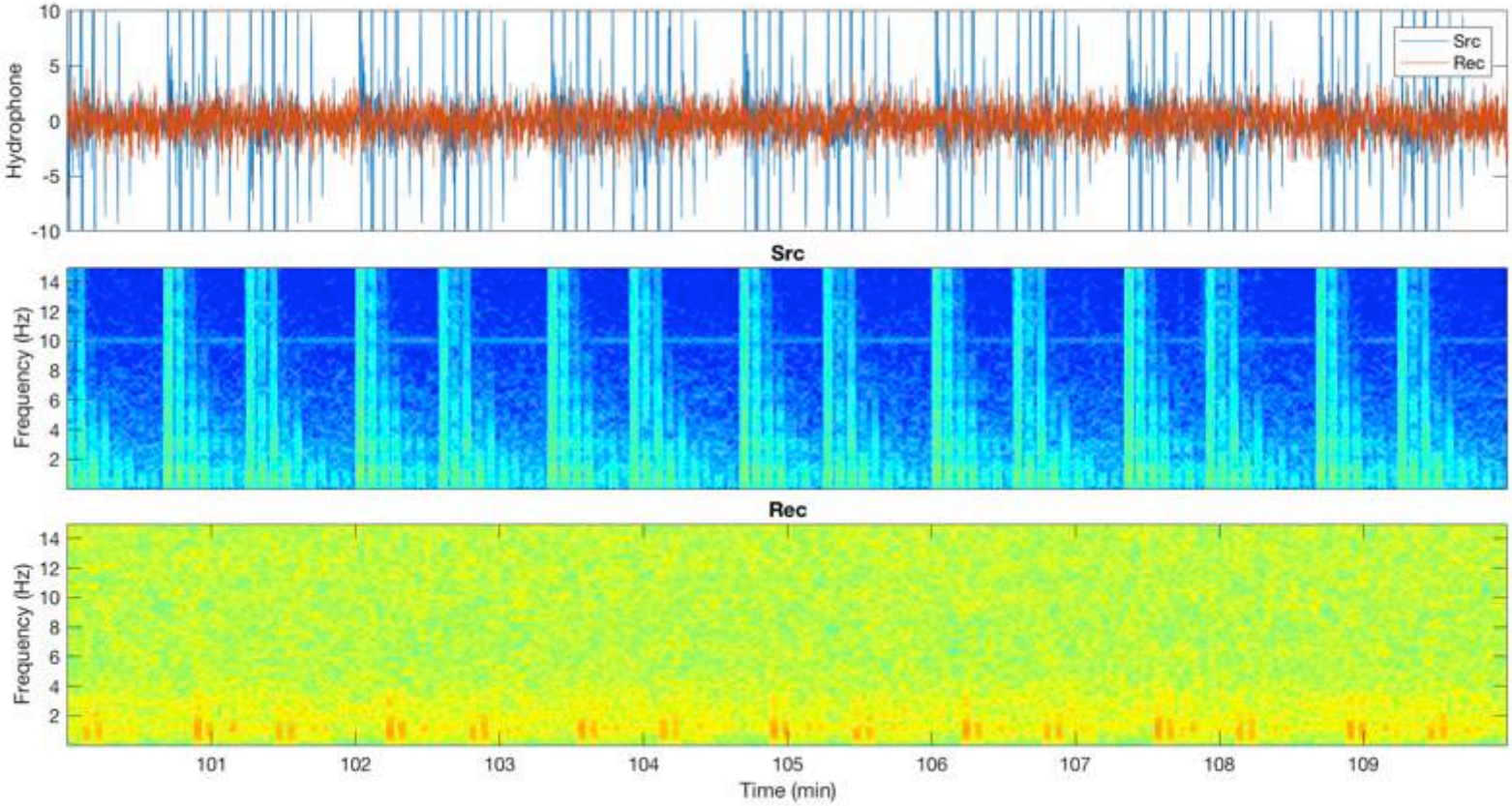
Hydrophone
10
5
0
-5
-10
Src
Rec
Src
Frequency (Hz)
14
12
10
8
6
4
2
Rec
Frequency (Hz)
14
12
10
8
6
4
2
101
102
103
104
105
106
107
108
109
Time (min)

Wells C -> B

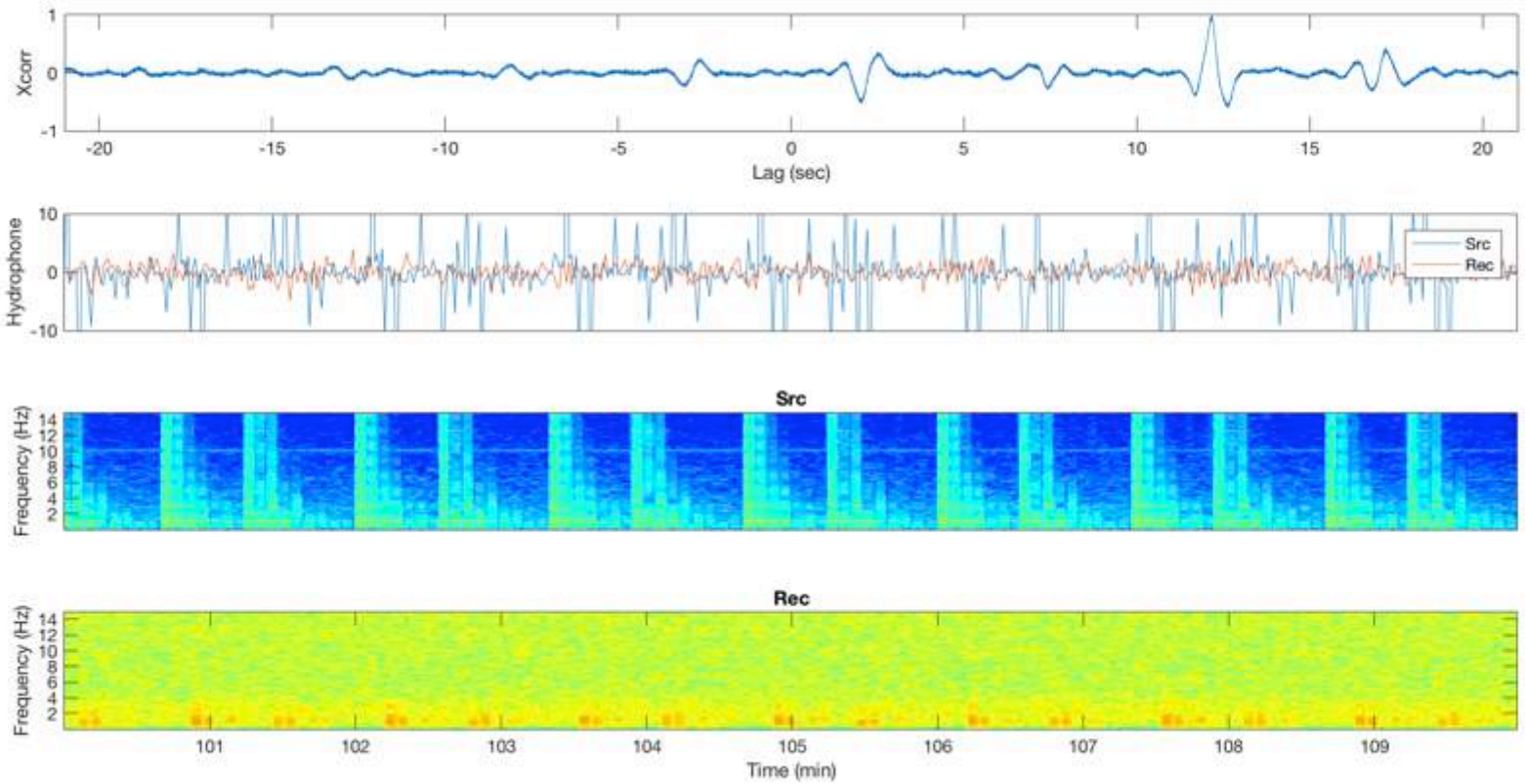
Xcorr
1
0
-1
-20
-15
-10
-5
0
5
10
15
20
Lag (sec)
Hydrophone
10
0
-10
Src
Rec
Src
Frequency (Hz)
14
12
10
8
6
4
2
Rec
Frequency (Hz)
14
12
10
8
6
4
2
101
102
103
104
105
106
107
108
109
Time (min)

Wells C -> B

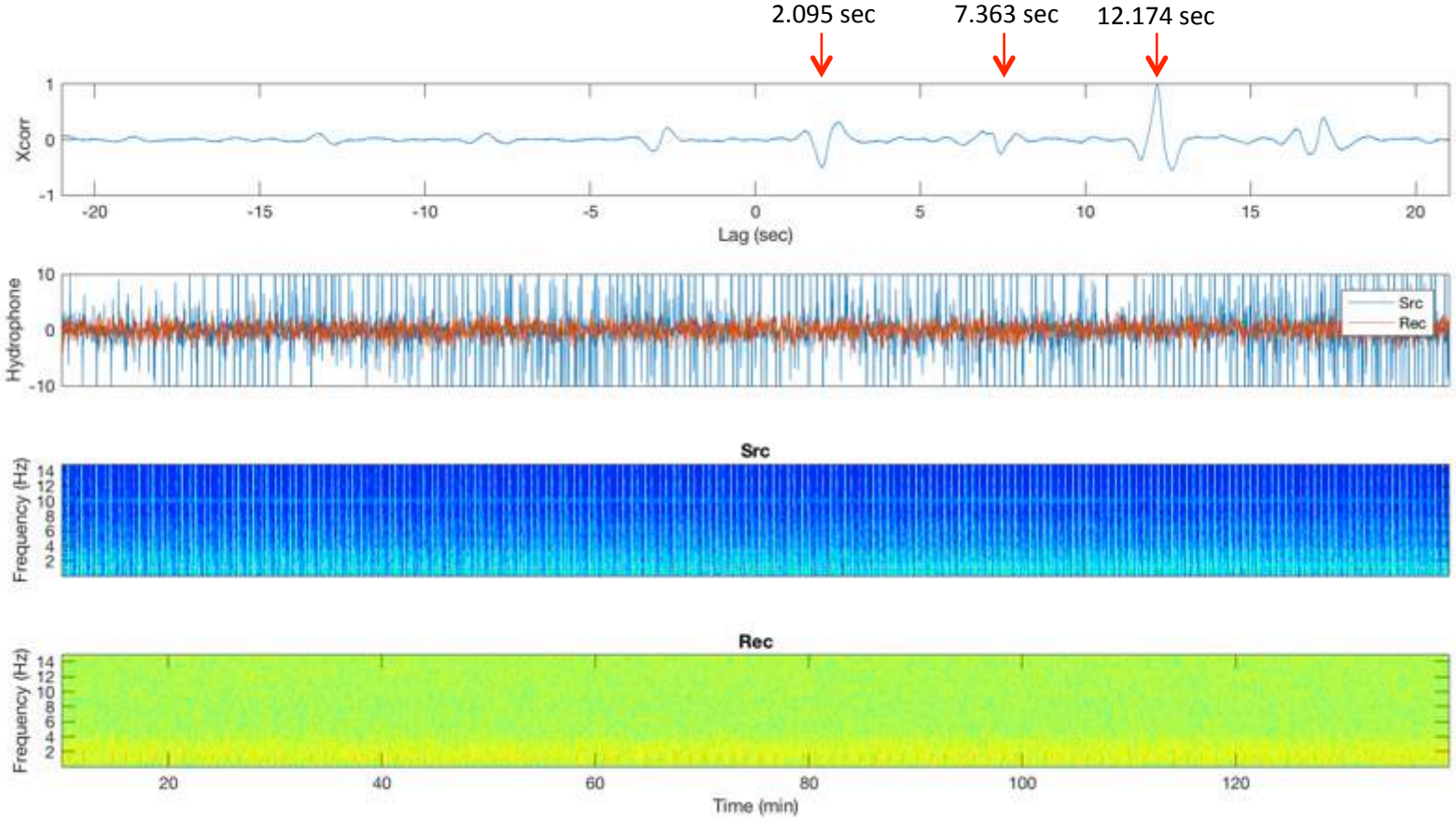
2.095 sec
7.363 sec
12.174 sec
Xcorr
Lag (sec)
Hydrophone
Src
Rec
Src
Frequency (Hz)
Rec
Frequency (Hz)
Time (min)

Wells C -> D

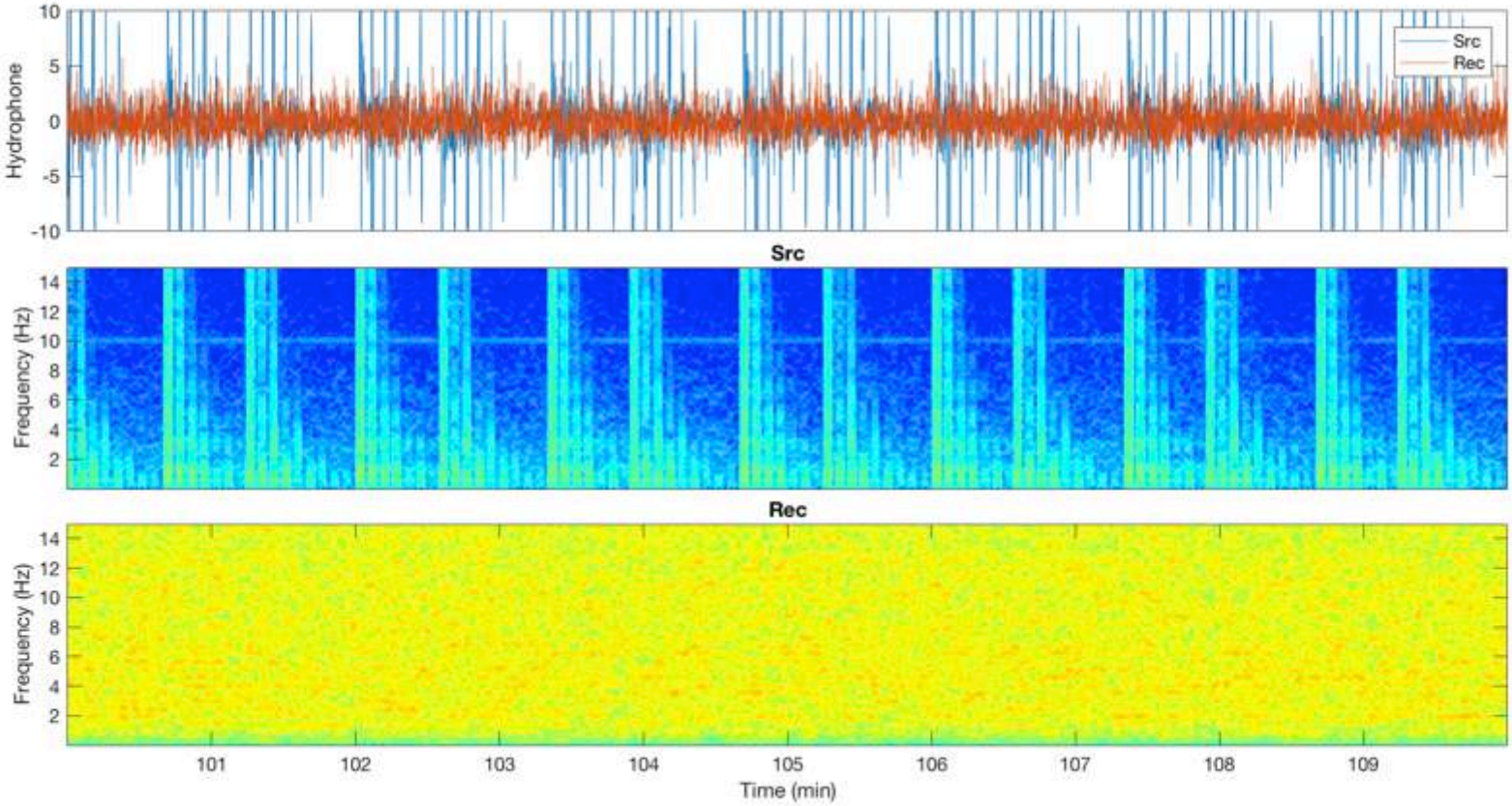
Hydrophone
10
5
0
-5
-10
Src
Rec
Src
Frequency (Hz)
14
12
10
8
6
4
2
Rec
Frequency (Hz)
14
12
10
8
6
4
2
101
102
103
104
105
106
107
108
109
Time (min)

Wells C -> D

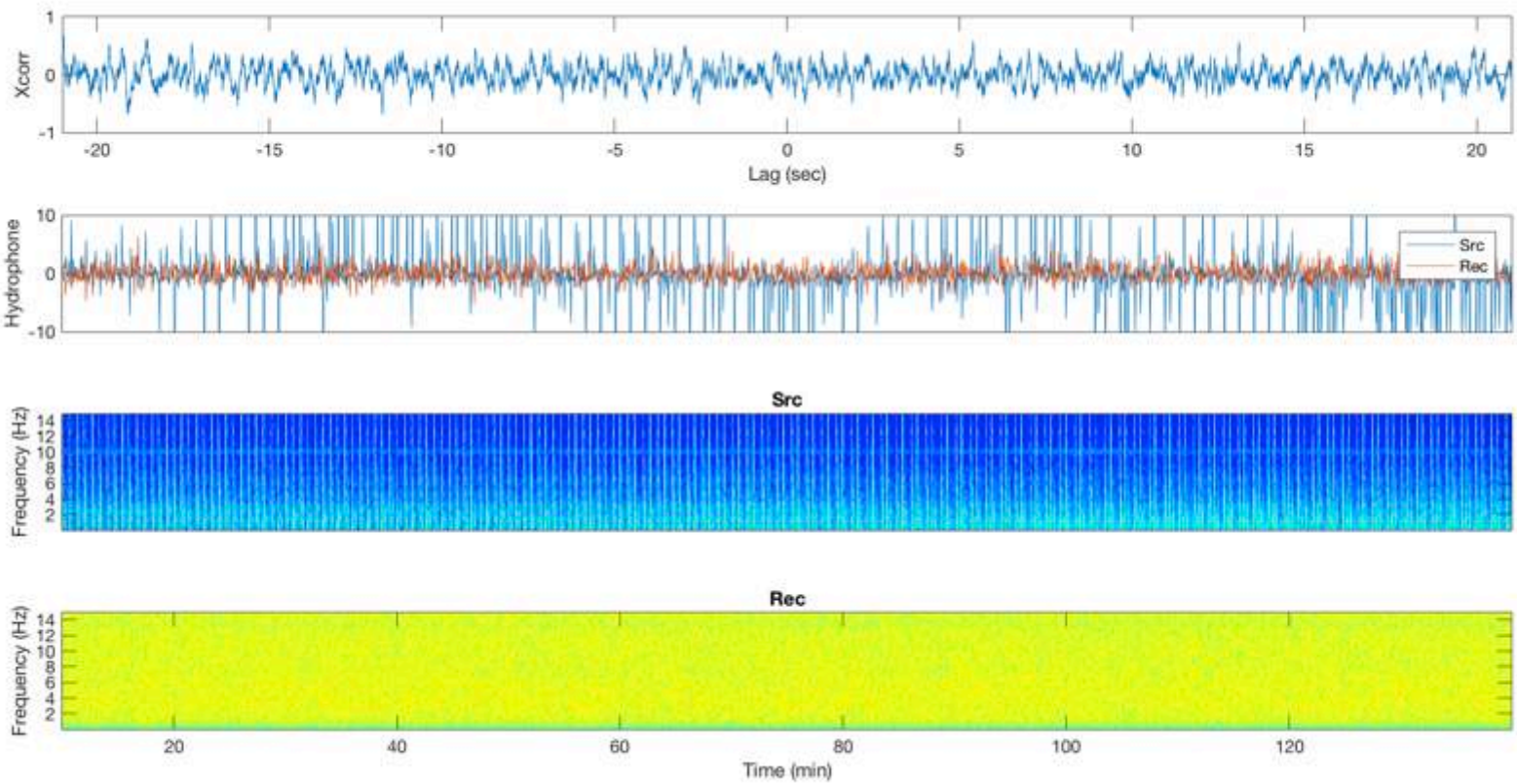
Xcorr
1
0
-1
-20
-15
-10
-5
0
5
10
15
20
Lag (sec)
Hydrophone
10
0
-10
Src
Rec
Src
Frequency (Hz)
14
12
10
8
6
4
2
Rec
Frequency (Hz)
14
12
10
8
6
4
2
20
40
60
80
100
120
Time (min)

Wells D -> A

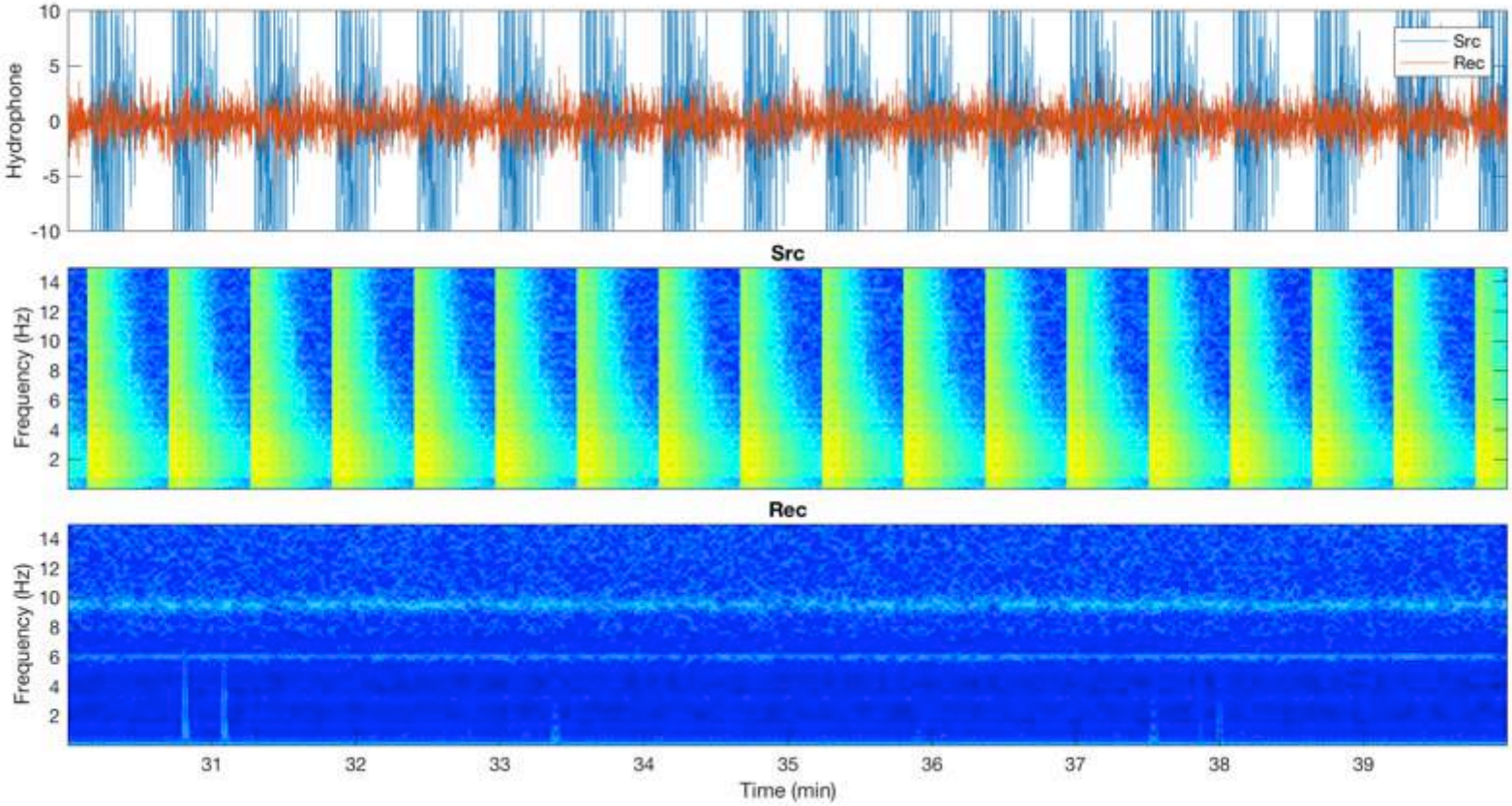
Hydrophone
10
5
0
-5
-10
Src
Rec
Src
Frequency (Hz)
14
12
10
8
6
4
2
Rec
Frequency (Hz)
14
12
10
8
6
4
2
31
32
33
34
35
36
37
38
39
Time (min)

Wells D -> B

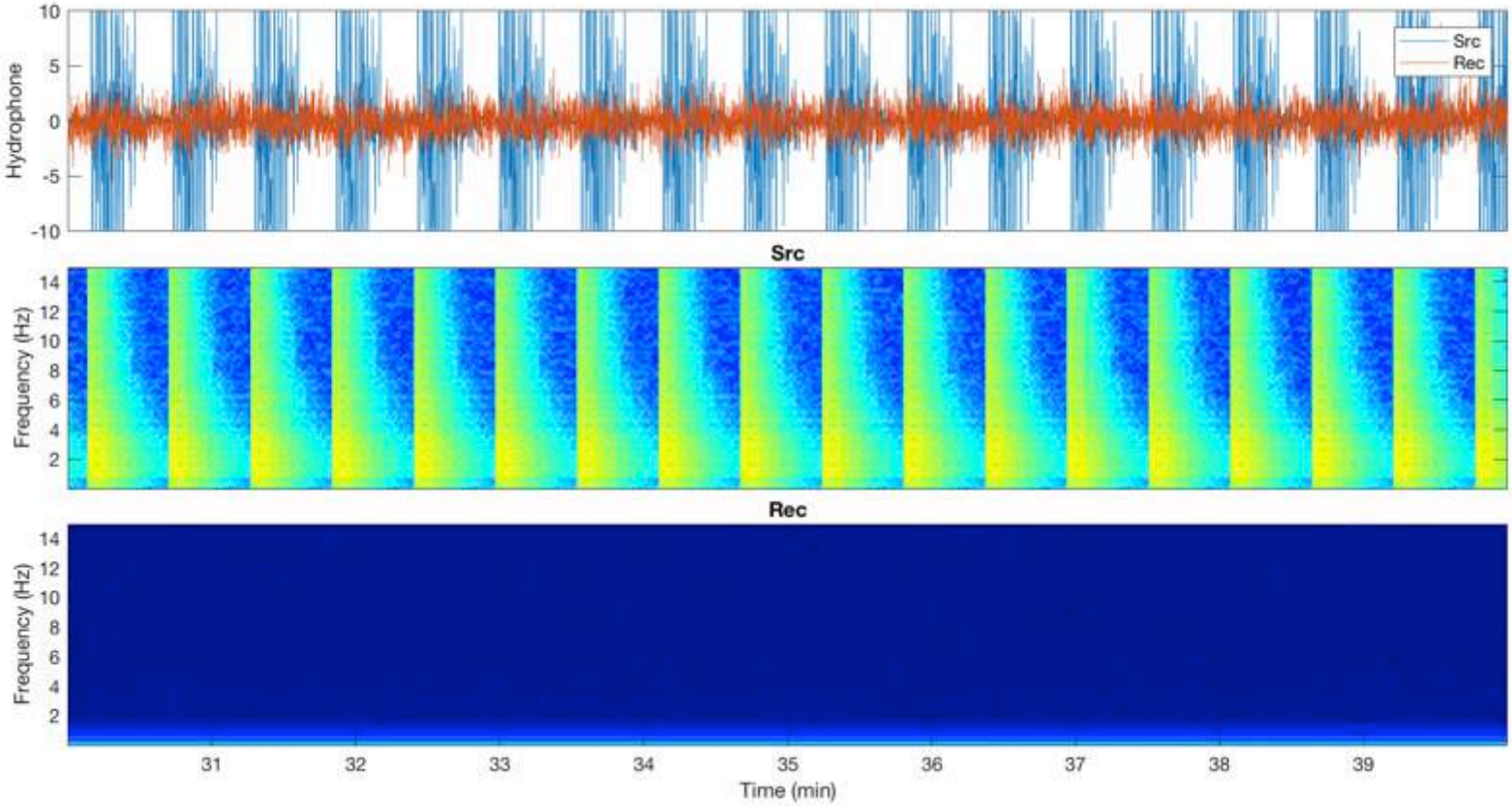
Hydrophone
10
5
0
-5
-10
Src
Rec
Src
Frequency (Hz)
14
12
10
8
6
4
2
Rec
Frequency (Hz)
14
12
10
8
6
4
2
31
32
33
34
35
36
37
38
39
Time (min)

Wells D -> C

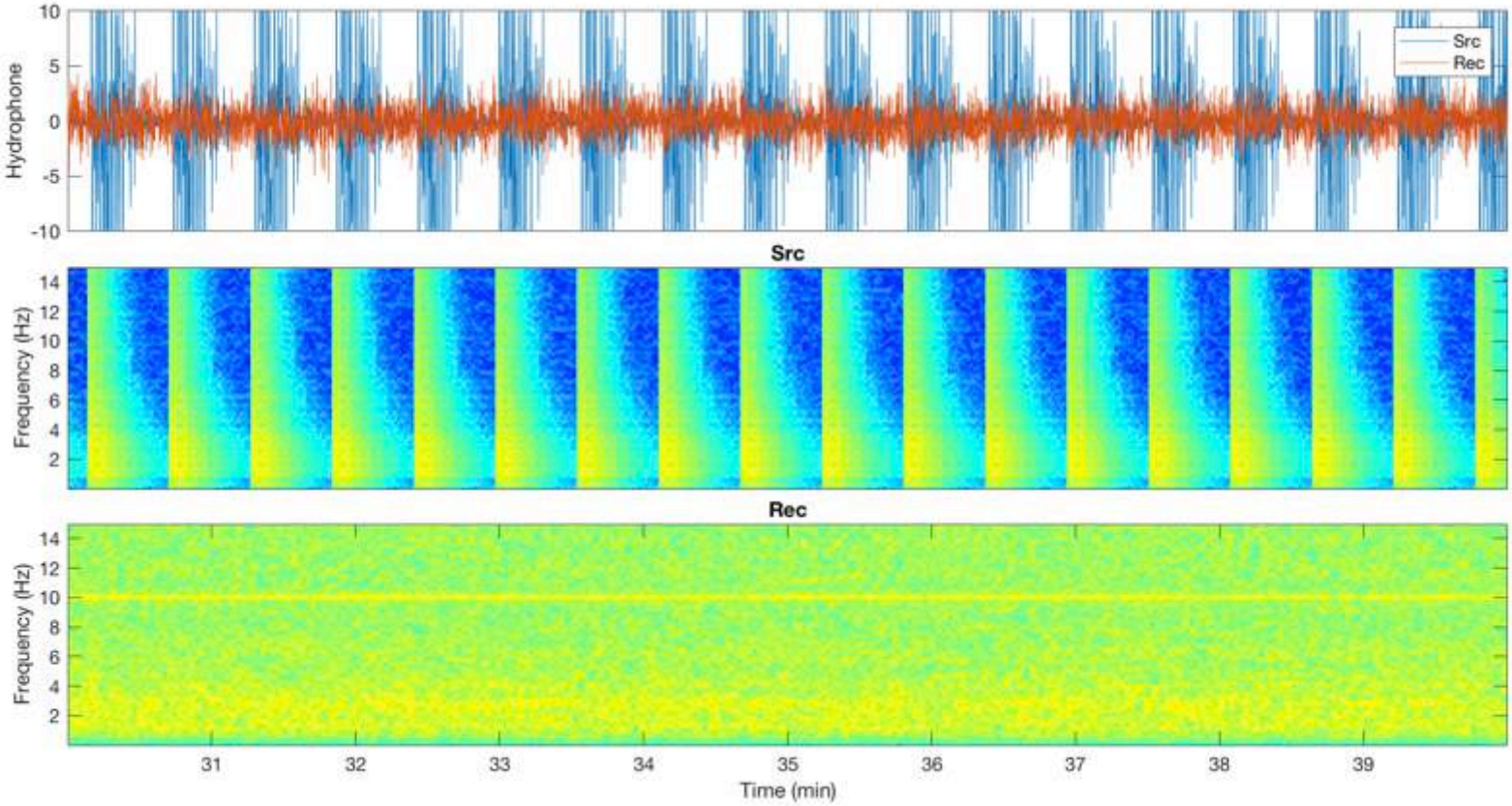
Hydrophone
10
5
0
-5
-10
Src
Rec
Src
Frequency (Hz)
14
12
10
8
6
4
2
Rec
Frequency (Hz)
14
12
10
8
6
4
2
31
32
33
34
35
36
37
38
39
Time (min)

Wells D -> C

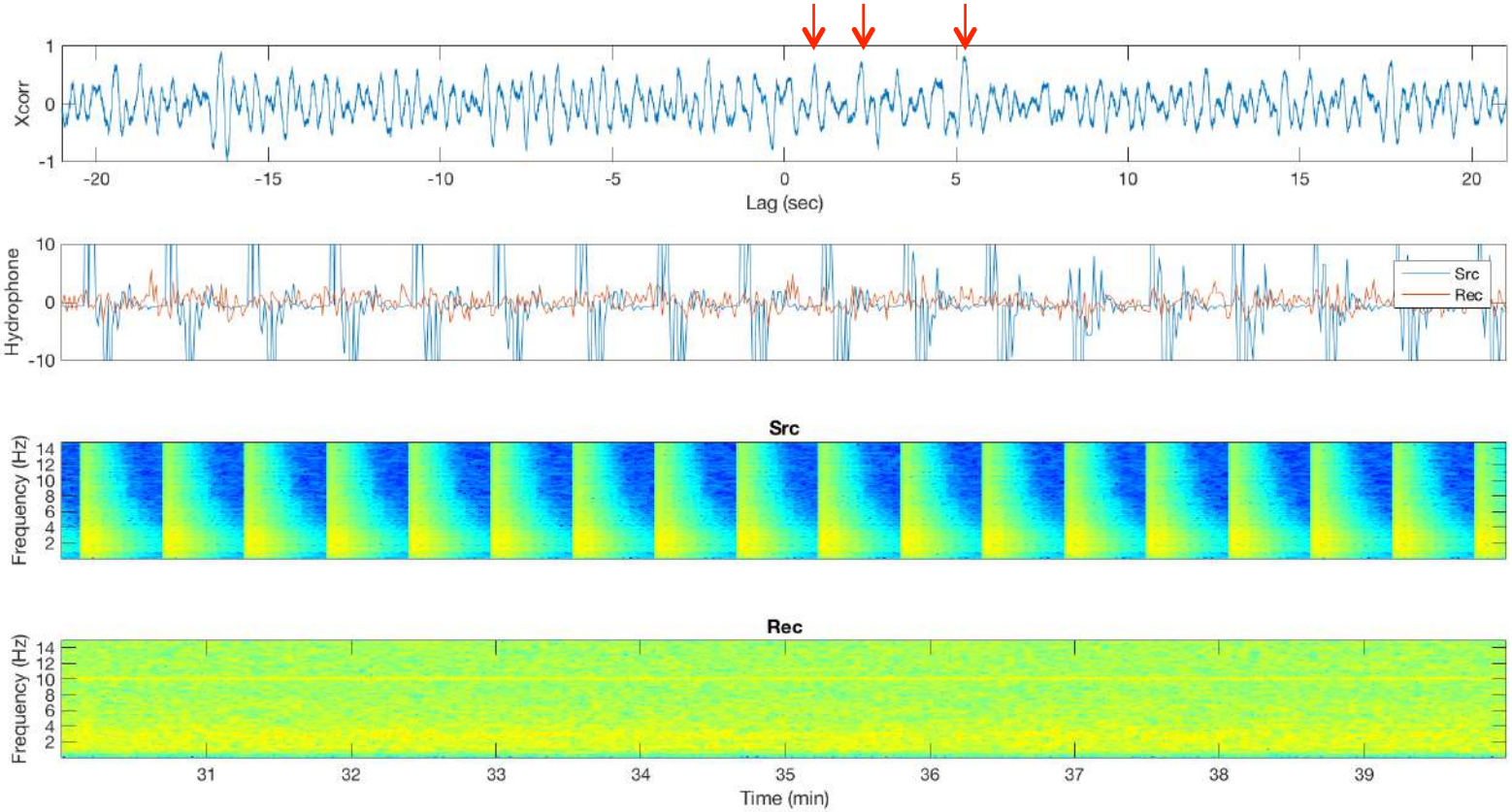
Xcorr
1
0
-1
-20
-15
-10
-5
0
5
10
15
20
Lag (sec)
Hydrophone
10
0
-10
Src
Rec
Src
Frequency (Hz)
14
12
10
8
6
4
2
Rec
Frequency (Hz)
14
12
10
8
6
4
2
31
32
33
34
35
36
37
38
39
Time (min)

Source Well A

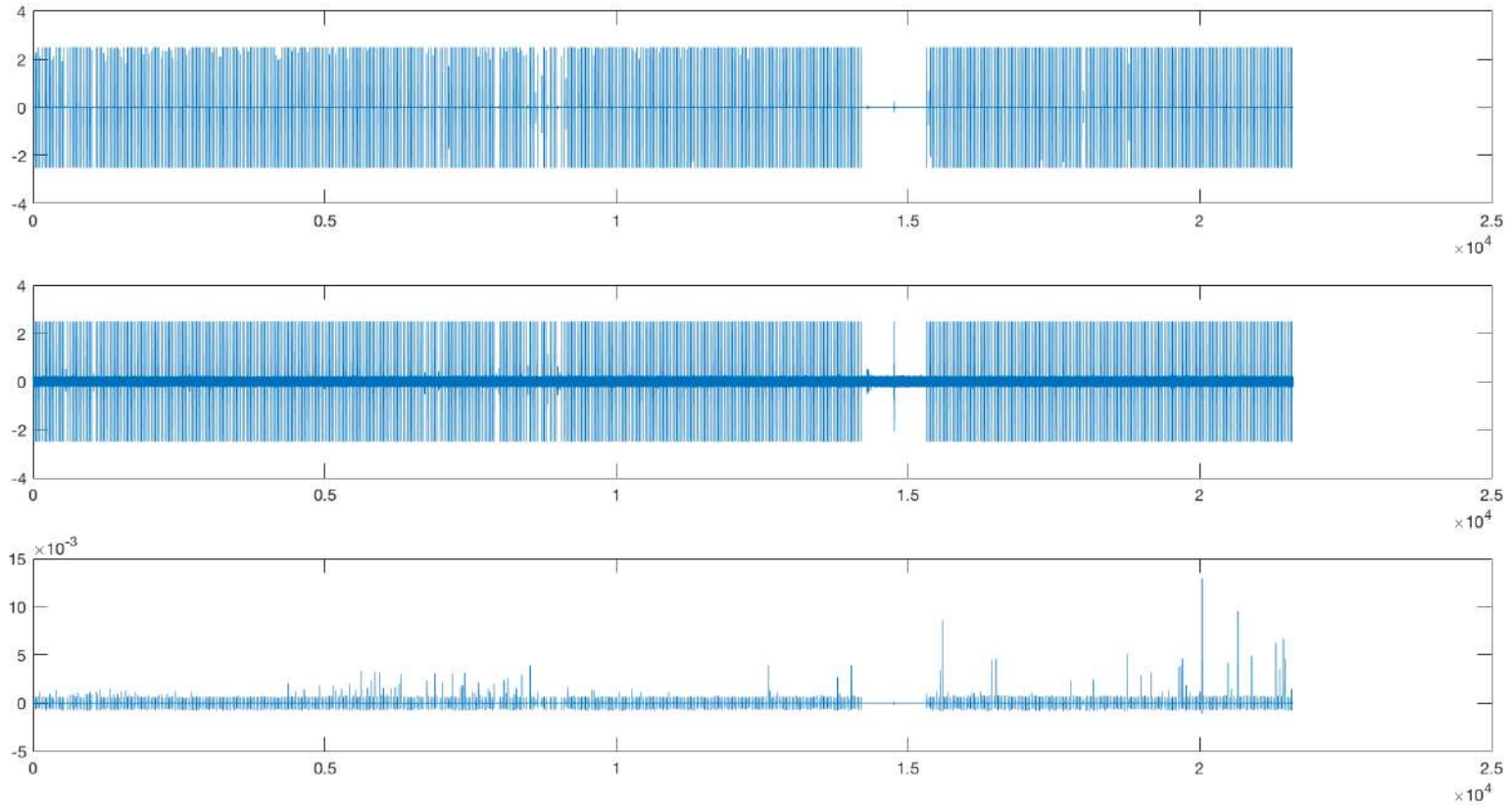

Wells A-B

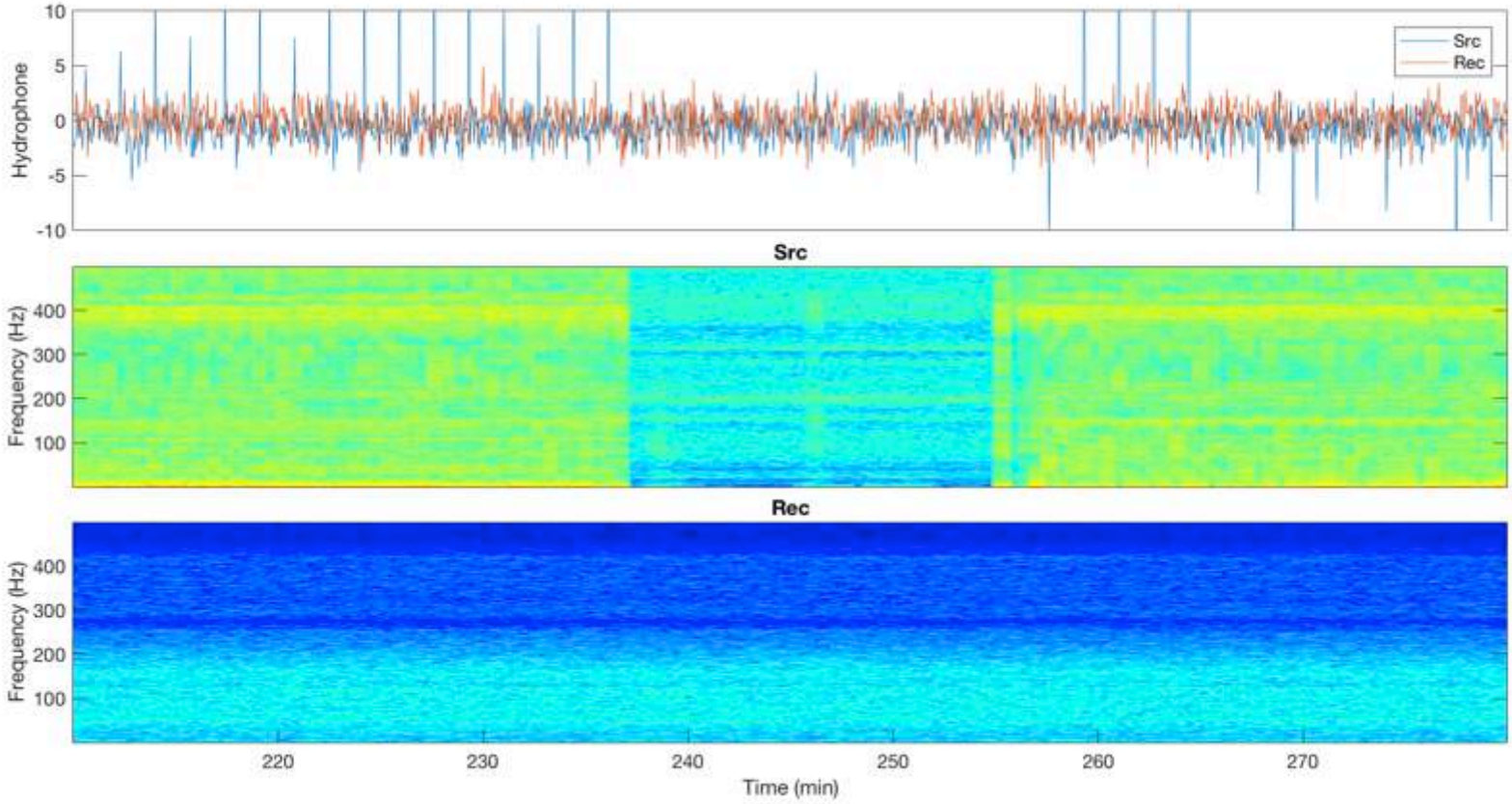
Hydrophone
10
5
0
-5
-10
Src
Rec
Src
Frequency (Hz)
400
300
200
100
Rec
Frequency (Hz)
400
300
200
100
220
230
240
250
260
270
Time (min)

Wells A-B

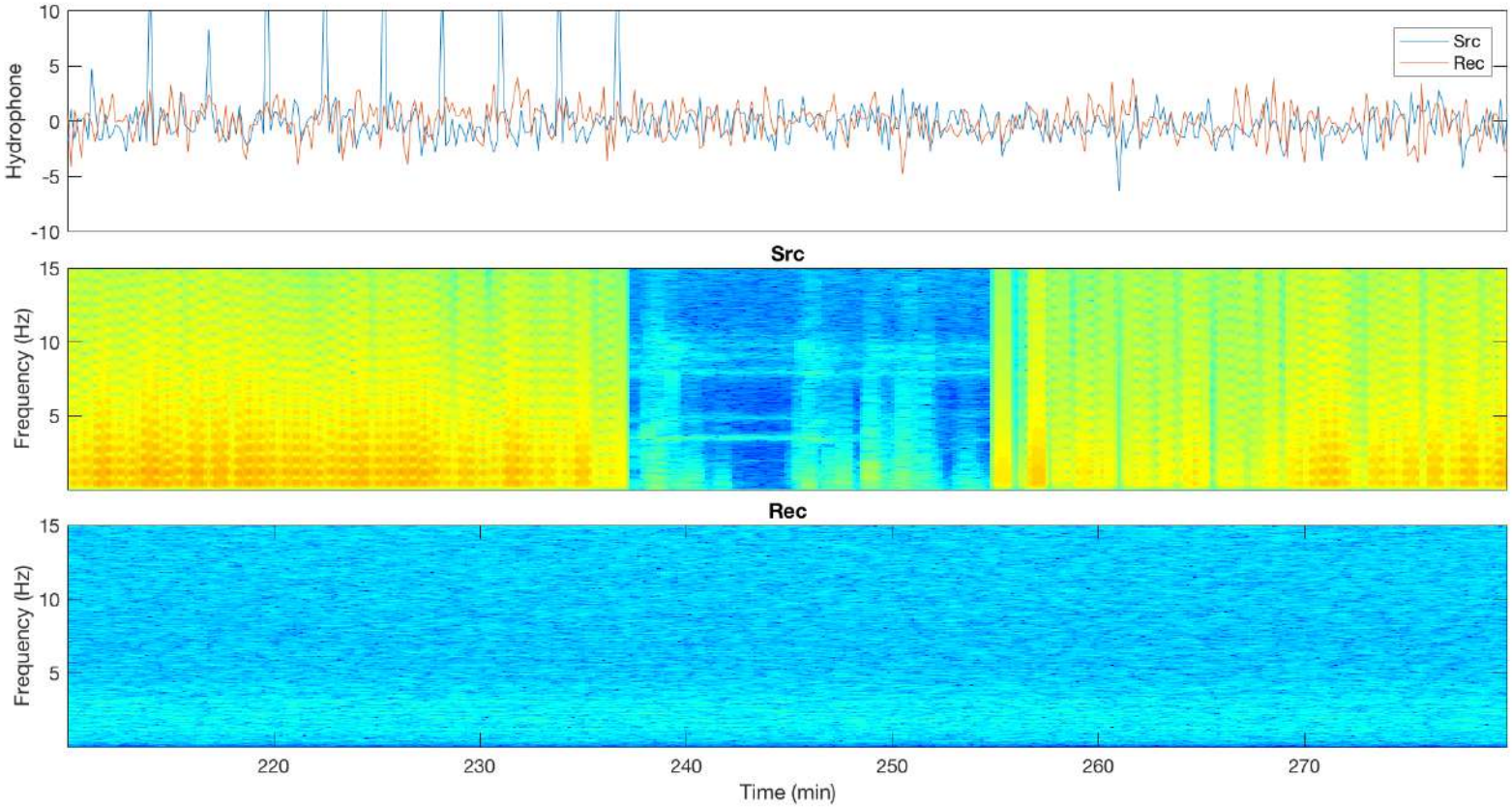
Hydrophone
10
5
0
-5
-10
Src
Rec
Src
Frequency (Hz)
15
10
5
Rec
Frequency (Hz)
15
10
5
220
230
240
250
260
270
Time (min)

Wells A-C

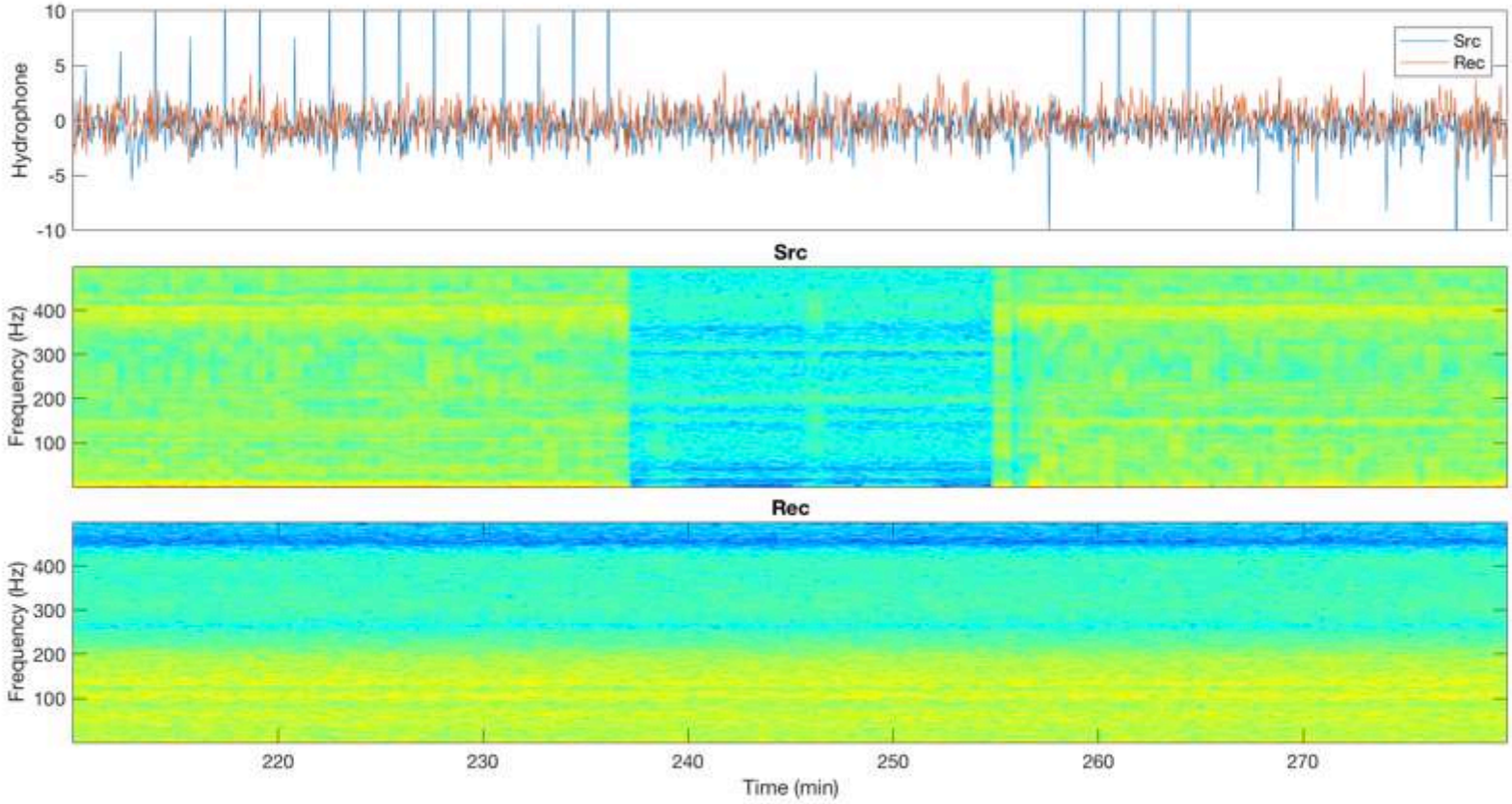
Hydrophone
10
5
0
-5
-10
Src
Rec
Src
Frequency (Hz)
400
300
200
100
Rec
Frequency (Hz)
400
300
200
100
220
230
240
250
260
270
Time (min)

Wells A-C

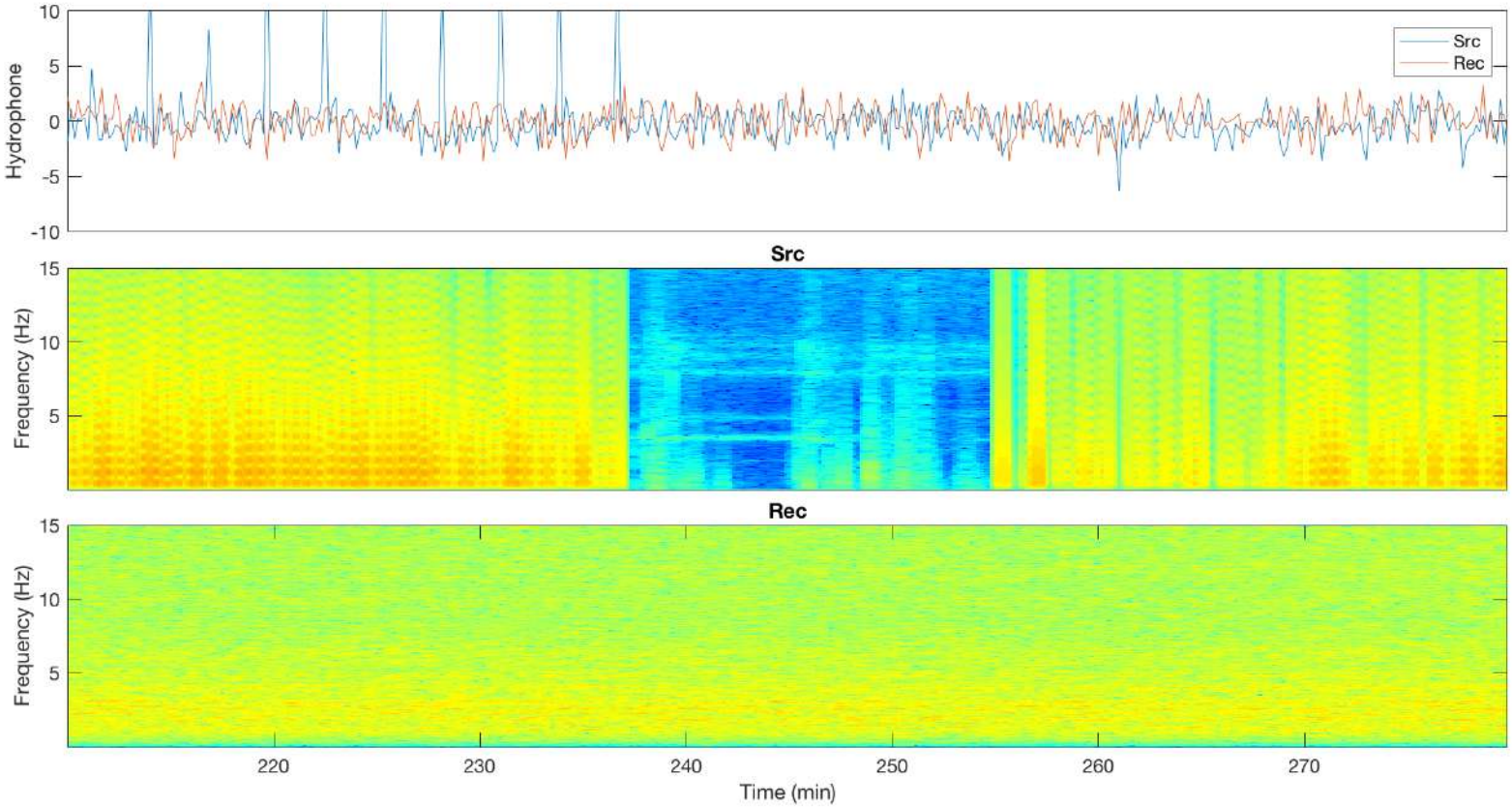
Hydrophone
10
5
0
-5
-10
Src
Rec
Src
Frequency (Hz)
15
10
5
Rec
Frequency (Hz)
15
10
5
220
230
240
250
260
270
Time (min)

Wells A-D

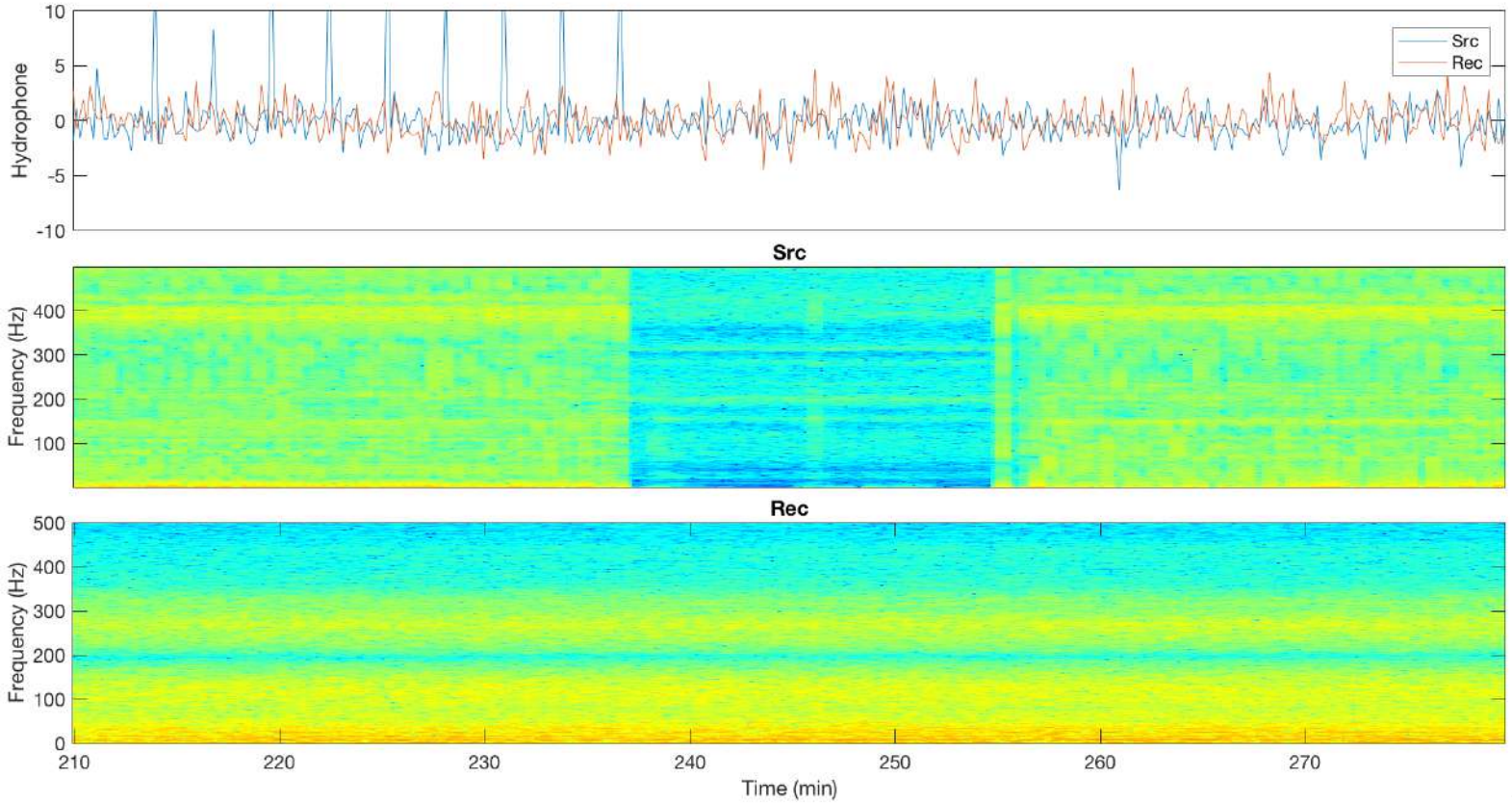
Hydrophone
10
5
0
-5
-10
Src
Rec
Src
Frequency (Hz)
400
300
200
100
Rec
Frequency (Hz)
500
400
300
200
100
0
210
220
230
240
250
260
270
Time (min)

Wells A-D

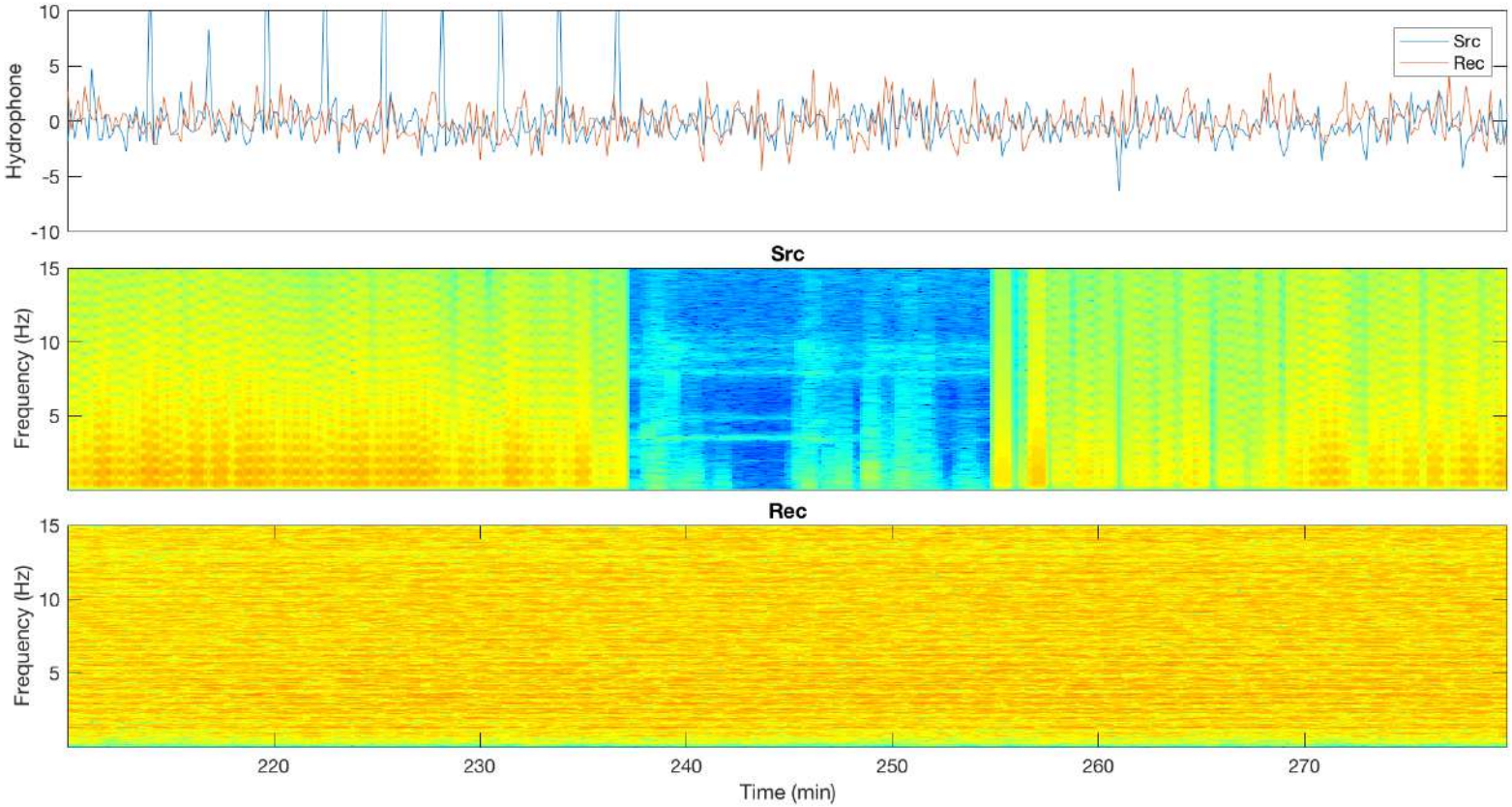
Hydrophone
10
5
0
-5
-10
Src
Rec
Src
Frequency (Hz)
15
10
5
Rec
Frequency (Hz)
15
10
5
220
230
240
250
260
270
Time (min)

Source Well B

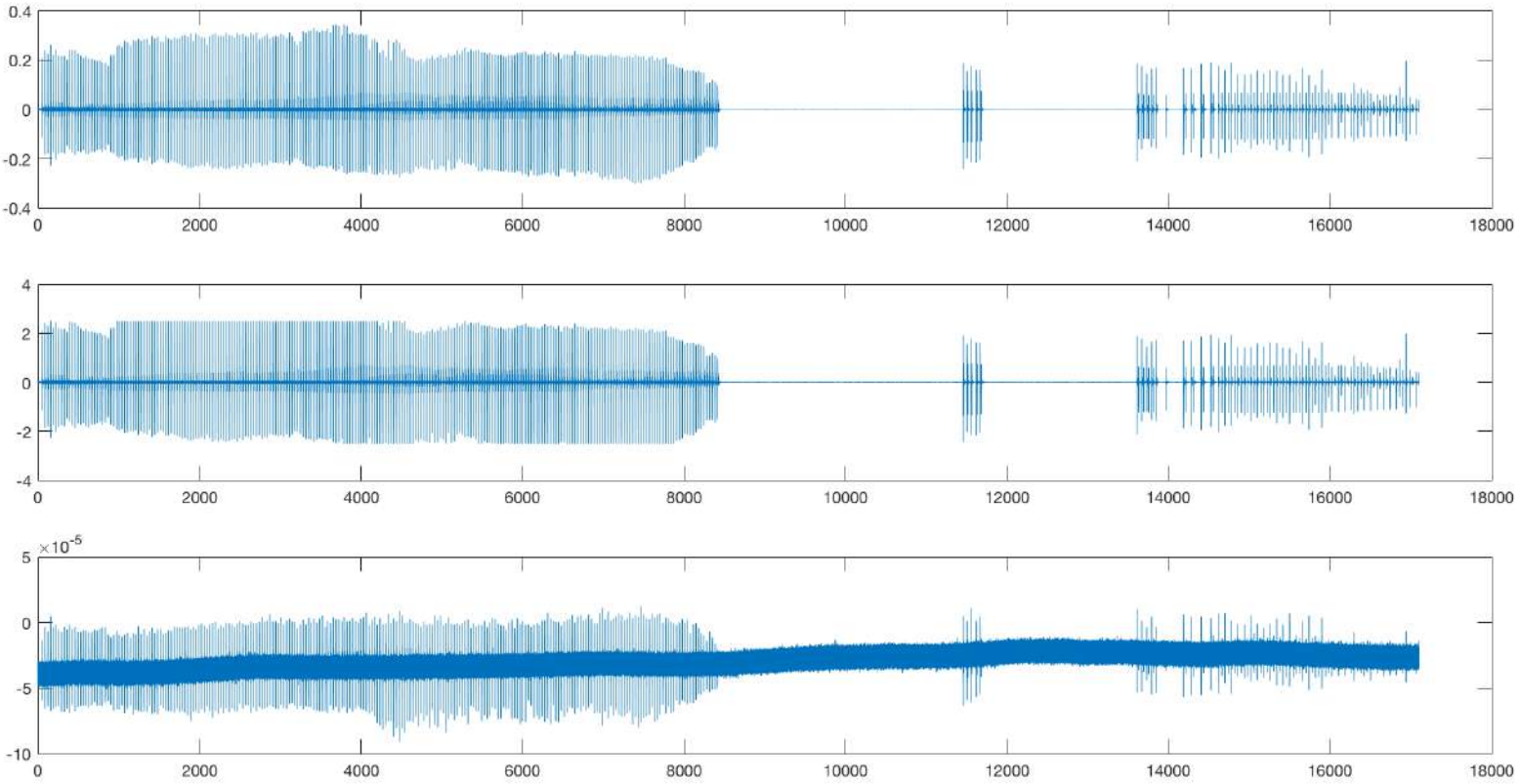

Wells B-A

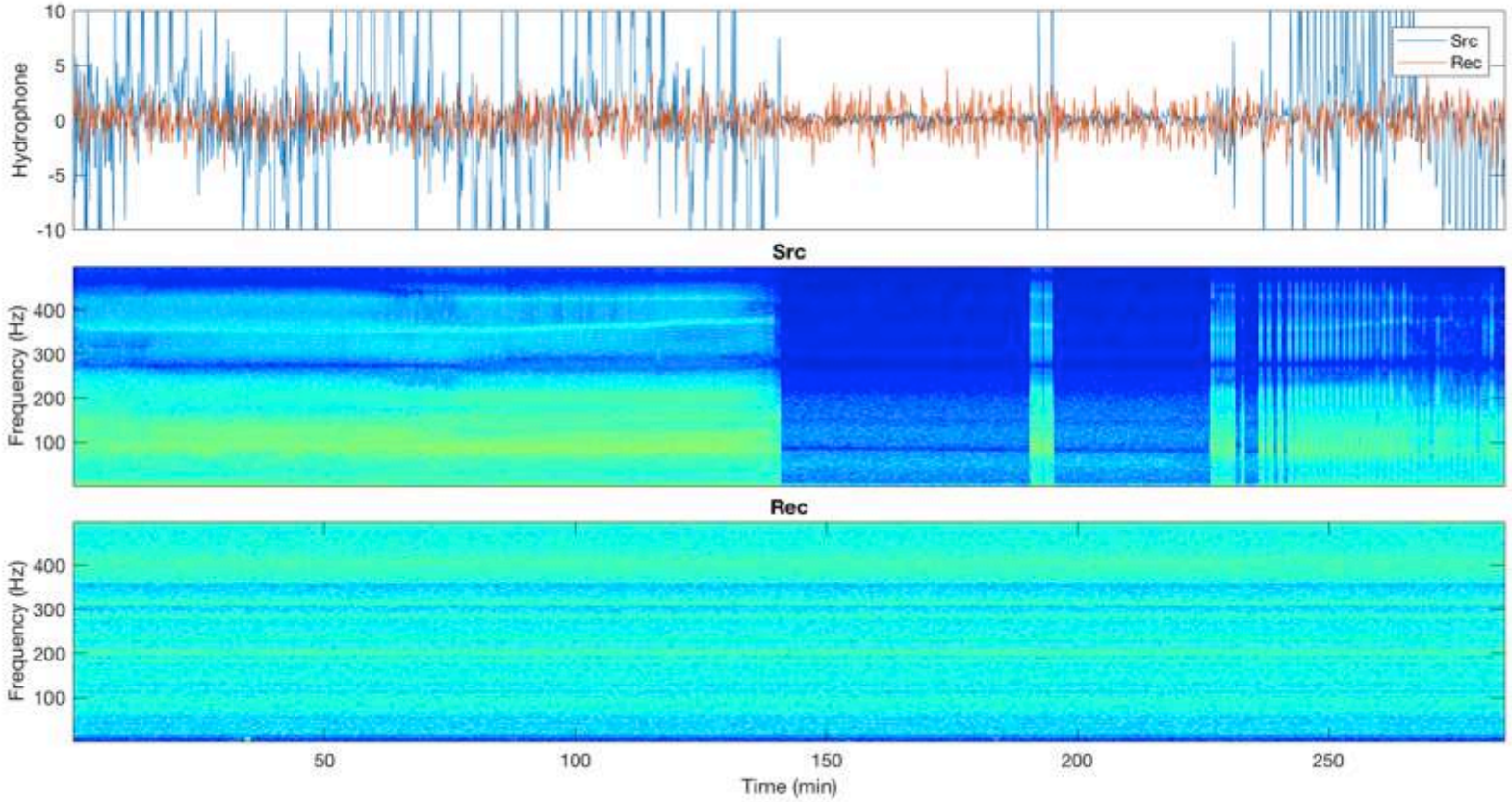
Hydrophone
10
5
0
-5
-10
Src
Rec
Src
Frequency (Hz)
400
300
200
100
Rec
Frequency (Hz)
400
300
200
100
50
100
150
200
250
Time (min)

Wells B-A

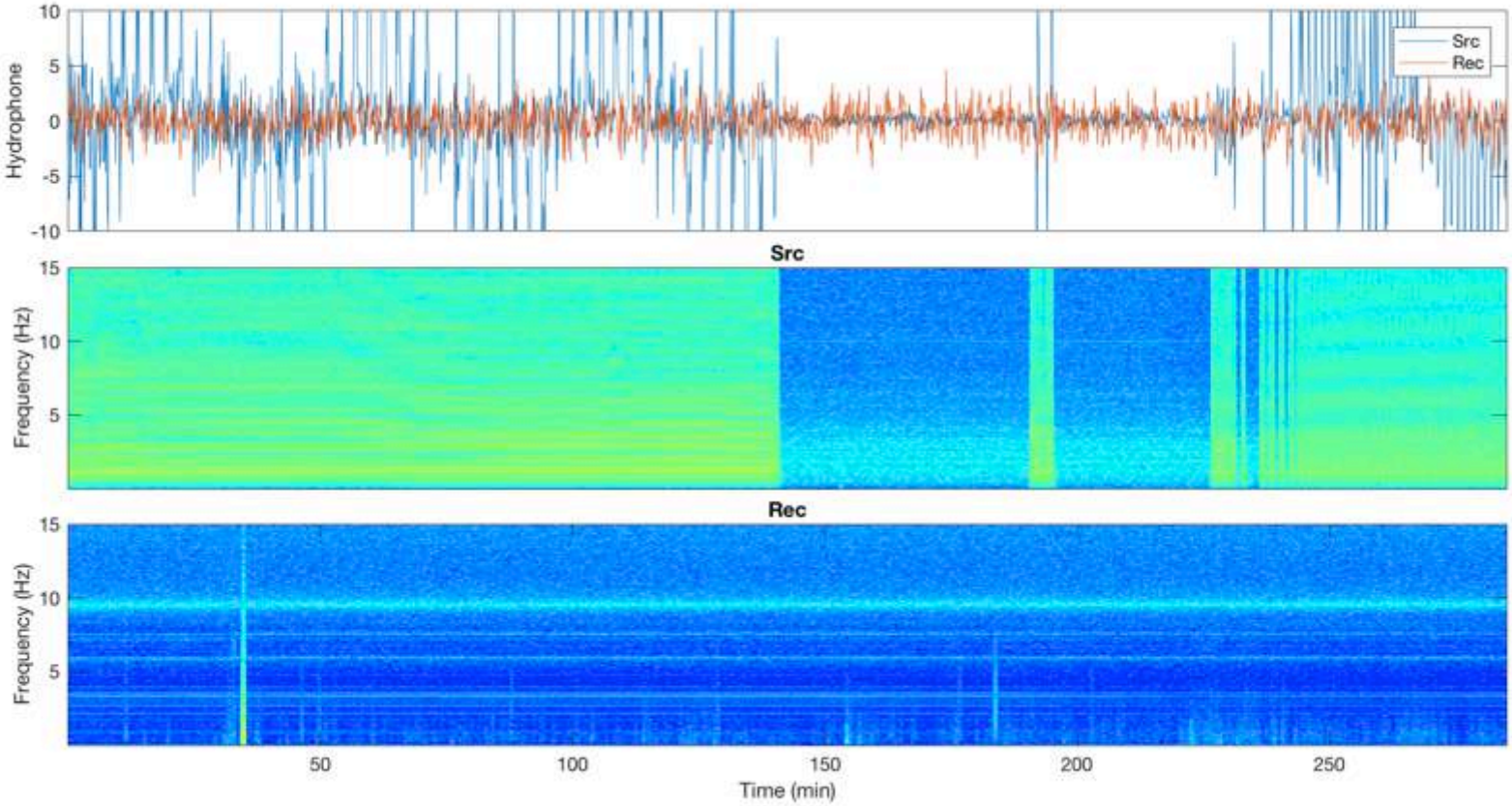
Hydrophone
10
5
0
-5
-10
Src
Rec
Src
Frequency (Hz)
15
10
5
Rec
Frequency (Hz)
15
10
5
50
100
150
200
250
Time (min)

Wells B-C

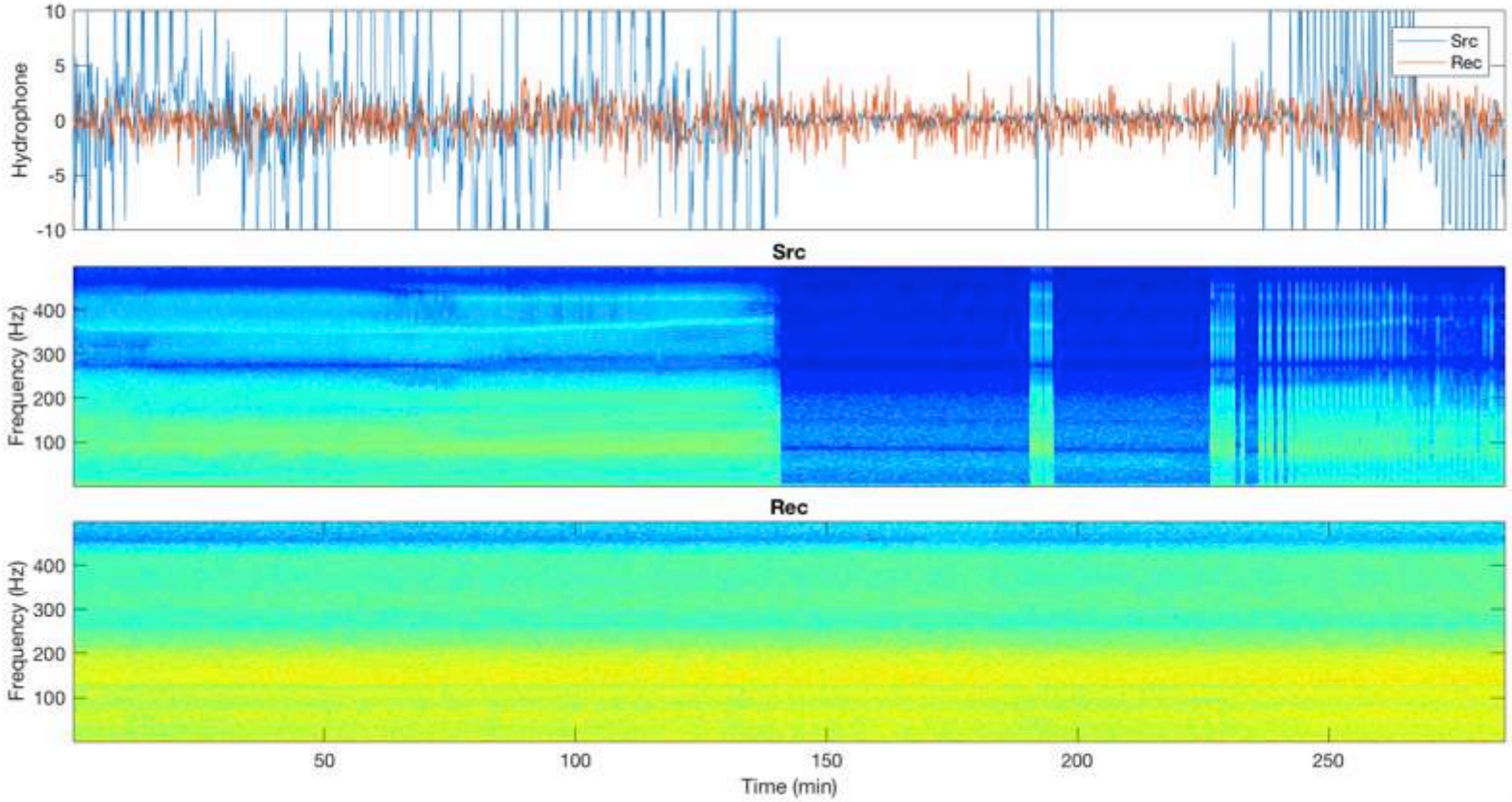
Hydrophone
10
5
0
-5
-10
Src
Rec
Src
Frequency (Hz)
400
300
200
100
Rec
Frequency (Hz)
400
300
200
100
50
100
150
200
250
Time (min)

Wells B-C

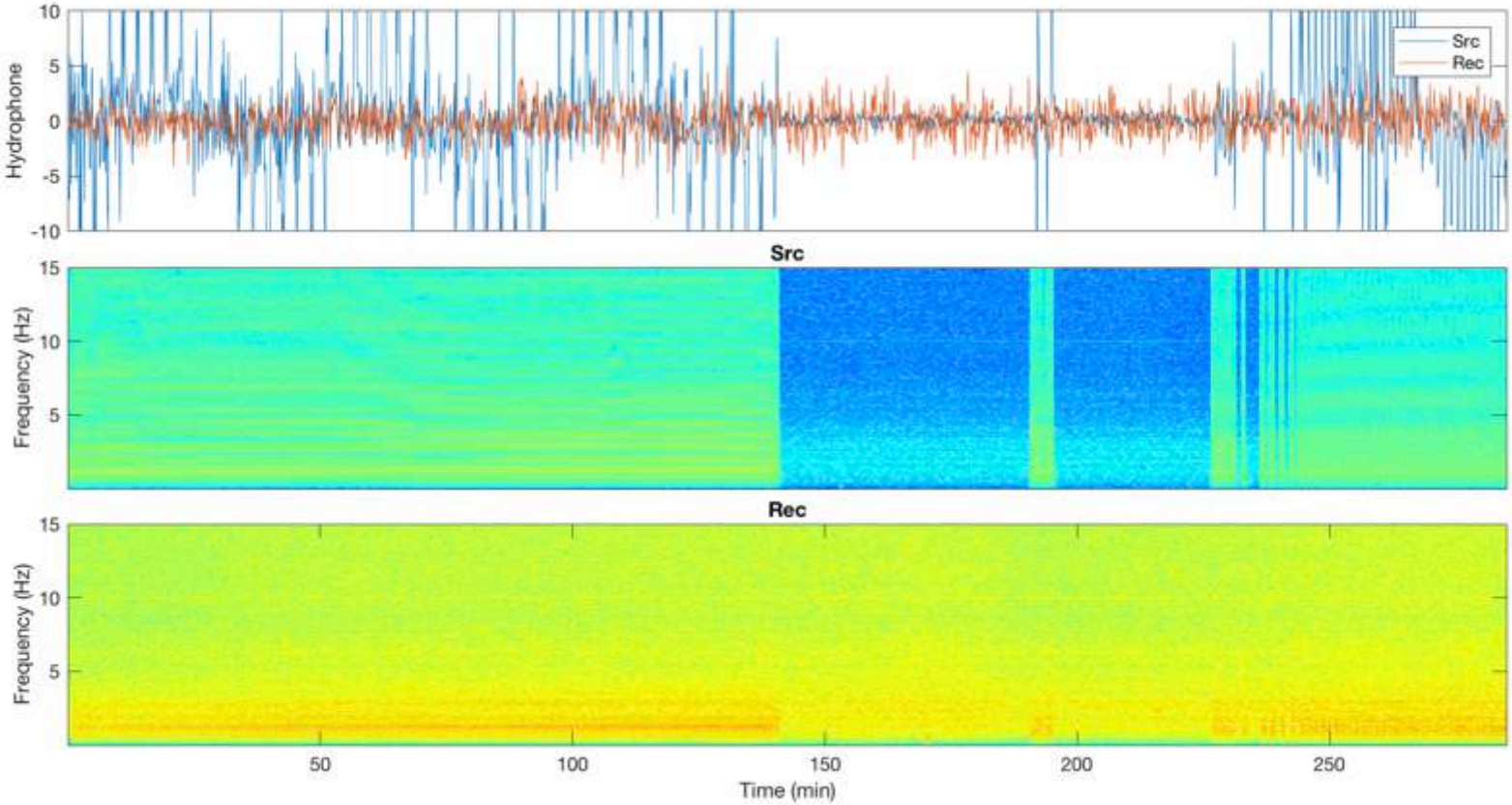
Hydrophone
10
5
0
-5
-10
Src
Rec
Src
Frequency (Hz)
15
10
5
Rec
Frequency (Hz)
15
10
5
50
100
150
200
250
Time (min)

Wells B-D

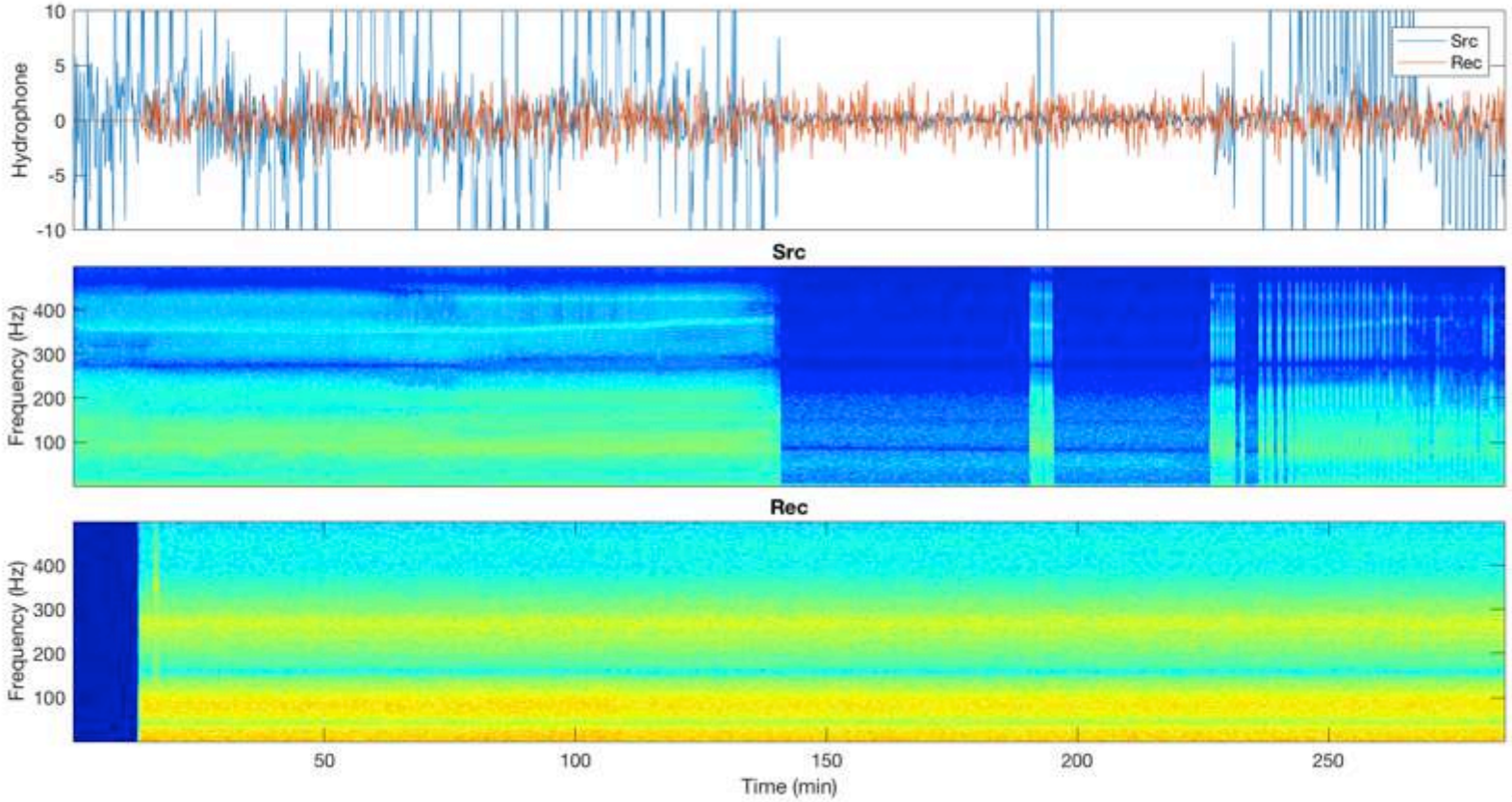
Hydrophone
10
5
0
-5
-10
Src
Rec
Src
Frequency (Hz)
400
300
200
100
Rec
Frequency (Hz)
400
300
200
100
50
100
150
200
250
Time (min)

Wells B-D

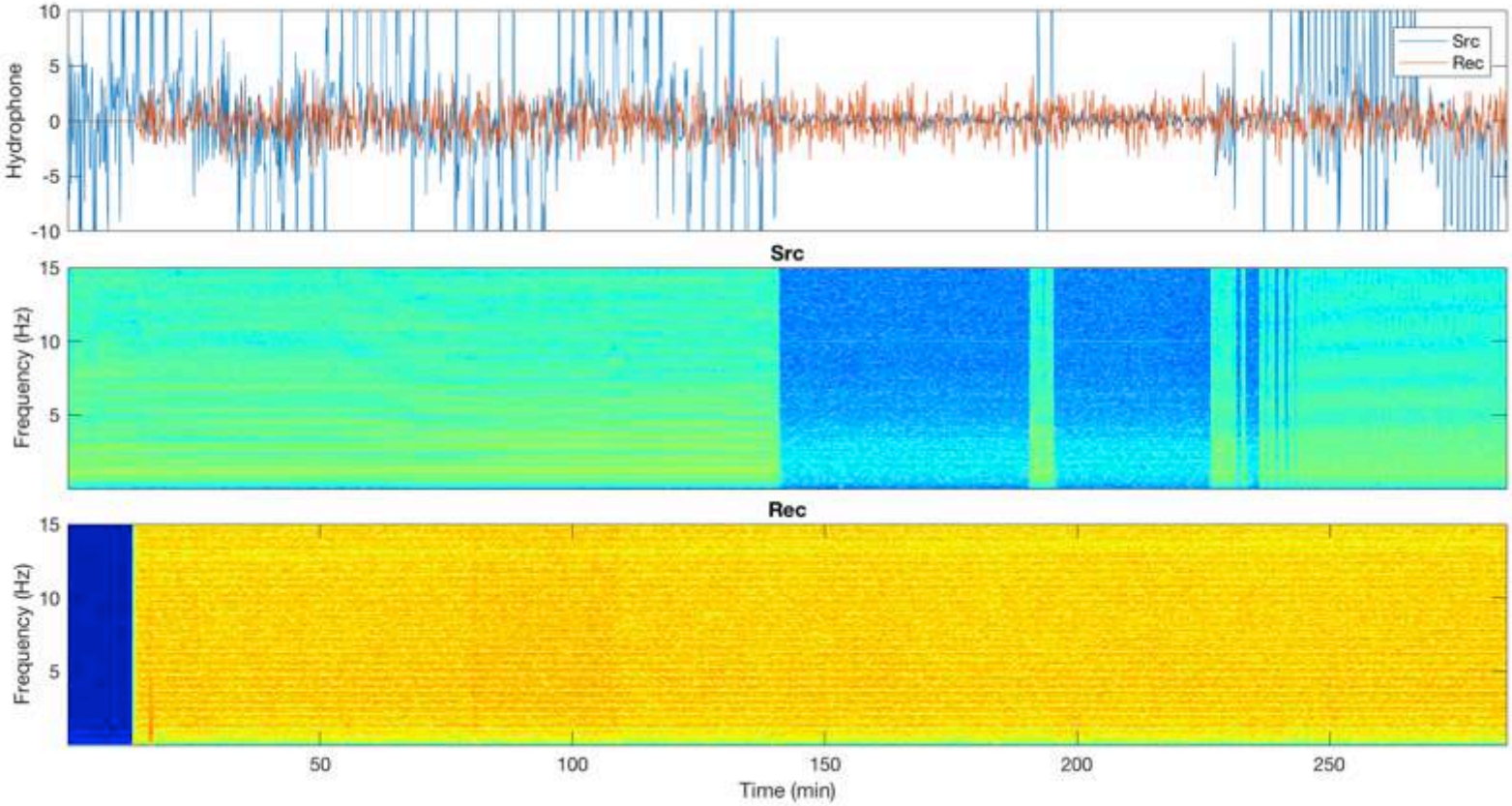
Hydrophone
10
5
0
-5
-10
Src
Rec
Src
Frequency (Hz)
15
10
5
Rec
Frequency (Hz)
15
10
5
50
100
150
200
250
Time (min)

Wells D-A

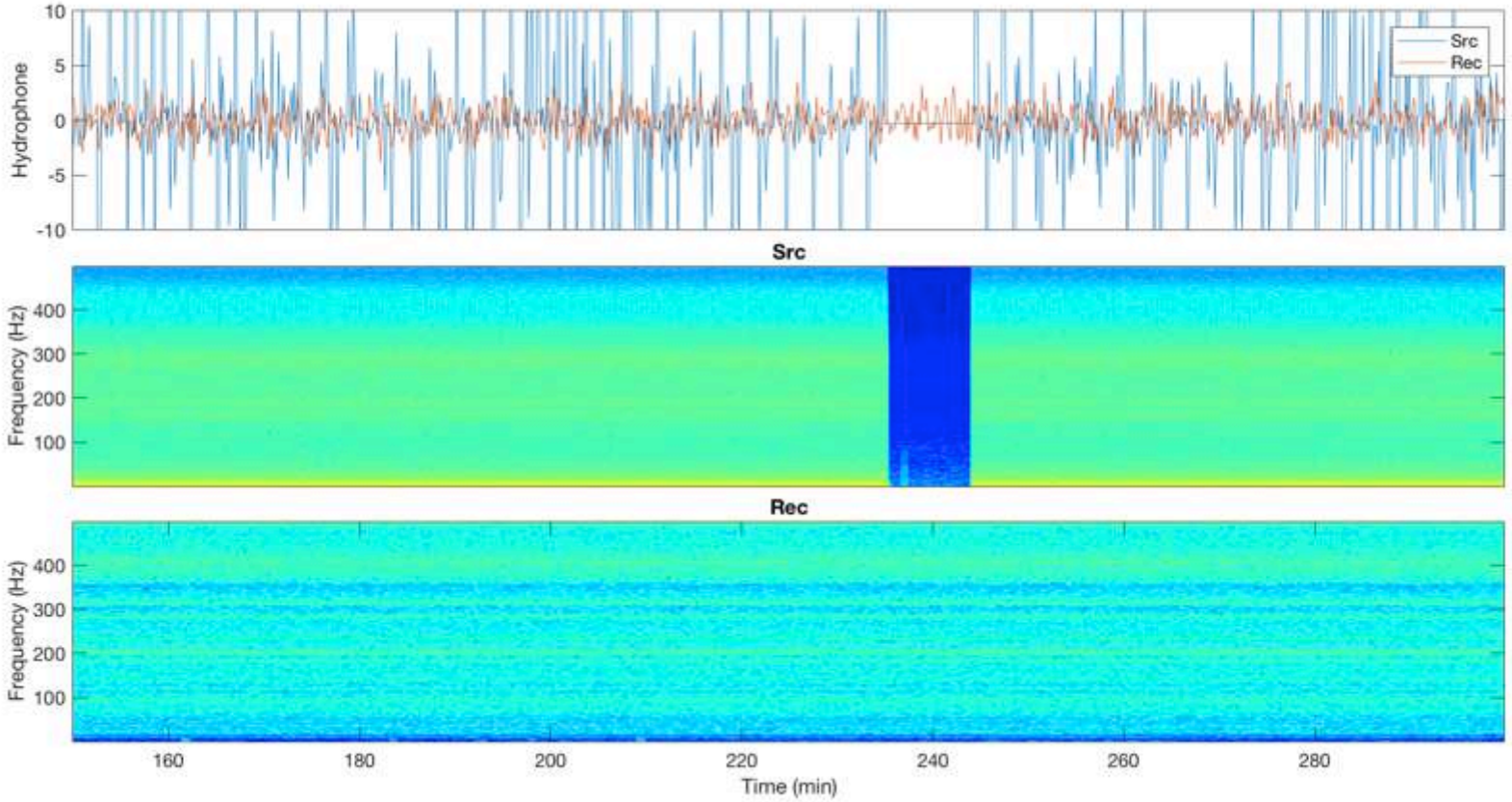
Hydrophone
10
5
0
-5
-10
Src
Rec
Src
Frequency (Hz)
400
300
200
100
Rec
Frequency (Hz)
400
300
200
100
160
180
200
220
240
260
280
Time (min)

Wells D-A

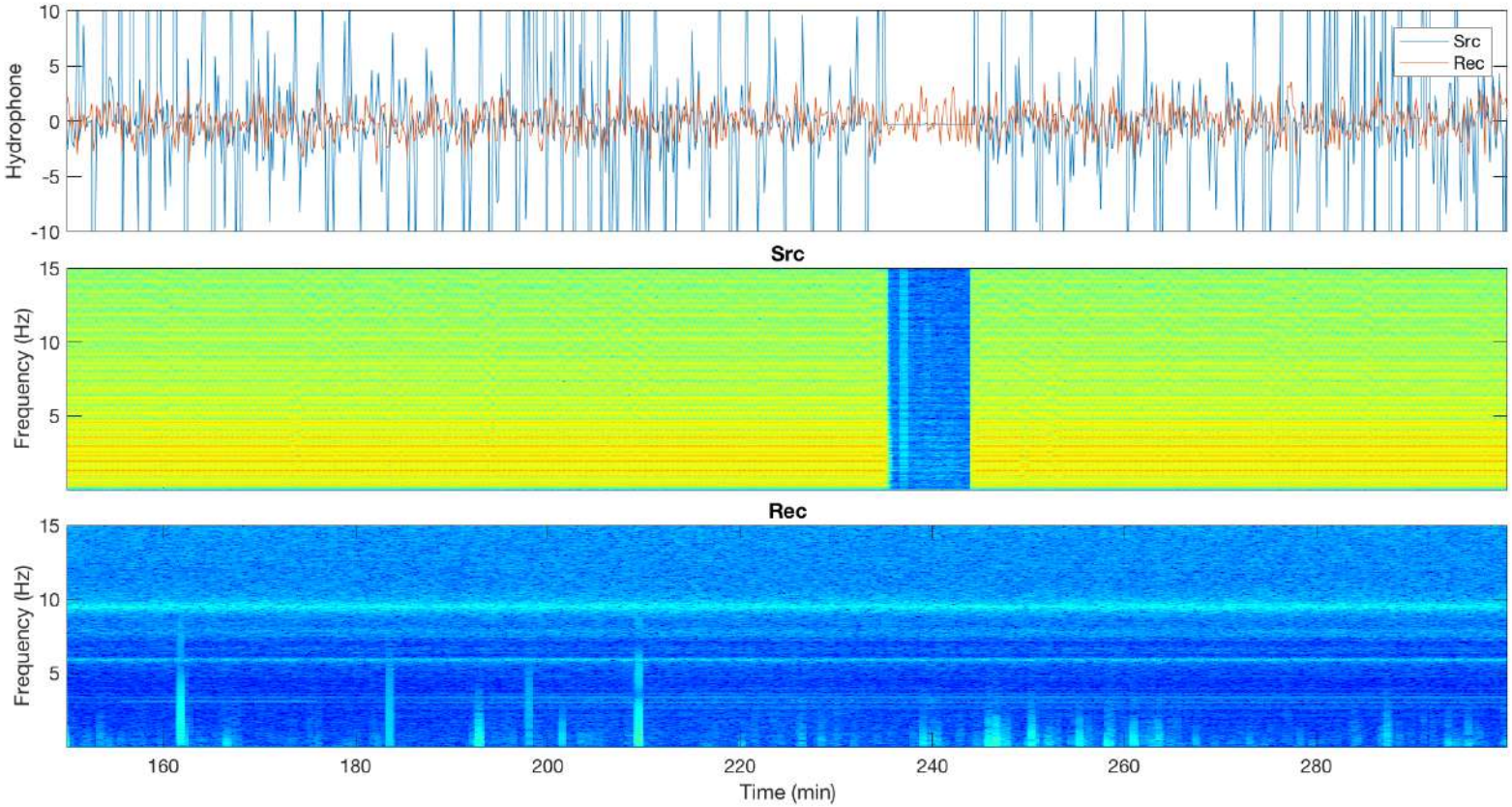
Hydrophone
10
5
0
-5
-10
Src
Rec
Src
Frequency (Hz)
15
10
5
Rec
Frequency (Hz)
15
10
5
160
180
200
220
240
260
280
Time (min)

APPENDIX E

RESERVOIR SIMULATION

RESERVOIR SIMULATION

A compositional simulation model was developed for the Phase 5 area of the Bell Creek oil field as shown in Figure E-1. The original project objective for the simulation results was to help validate the time-lapse K-wave results. The poststudy 3-D seismic survey was planned to validate the final K-wave monitoring results, whereas the simulation results would provide a means of incremental validation after each of the K-wave monitor surveys. Although simulation results were unable to be used for validation as part of this project, they provide great value to the site operator and other studies being done at the Bell Creek Field. The simulation results provided dynamic reservoir parameters such as pressure/fluid saturation distribution across the reservoir and well response, which enable the operator to conduct long-term technical and economic evaluations of CO_2 enhanced oil recovery (EOR) operations in the field. Since the model is history-matched, it can be used to predict future EOR performance in Phase 5 for the ongoing CO_2 flooding operations and assist the operator to determine the optimal flooding schedule. As the boundaries of Phase 5 are open to Phases 4 and 6, the simulation model is also helpful to estimate the fluid communication between these phases and help the operator to make a fit-to-purpose injection plan based on the available CO_2 supply.

The geologic structure of the simulation model was based on the geologic model described in Appendix A. The simulation model had 171 × 132 × 10 cells in the I, J, and K directions, respectively, resulting in 225,720 grid cells. 82 active wells were contained within the model, including 45 production wells, 20 water injection wells, and 17 WAG (water-alternating gas) injection wells. Figure E-2 shows the detailed well distribution in the model.

Since there was a considerable concentration of light hydrocarbon components in the original reservoir oil as illustrated in Figure E-3, a 9-component equation of state (EOS) model was used in simulation to calculate the pressure–volume–temperature (PVT) behavior of the fluids (Jin and others, 2018). The EOS model enables consideration of CO_2 and other light gas components individually in the field development process. The full length of production/injection history (from 1967 to 2018) of all 82 wells was integrated into the model, which covers the primary depletion, waterflooding, and the ongoing CO_2 flooding stages in the study area as shown in Figure E-4.

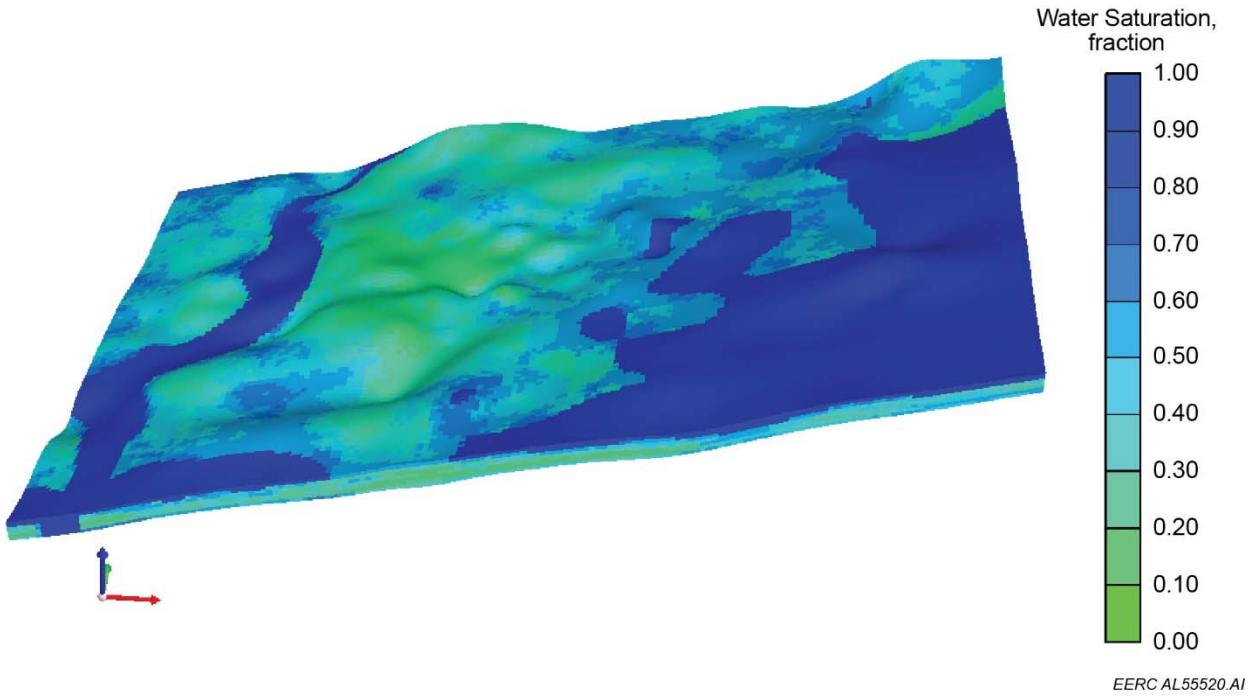

Figure E-1. Schematic of the Bell Creek Phase 5 model.

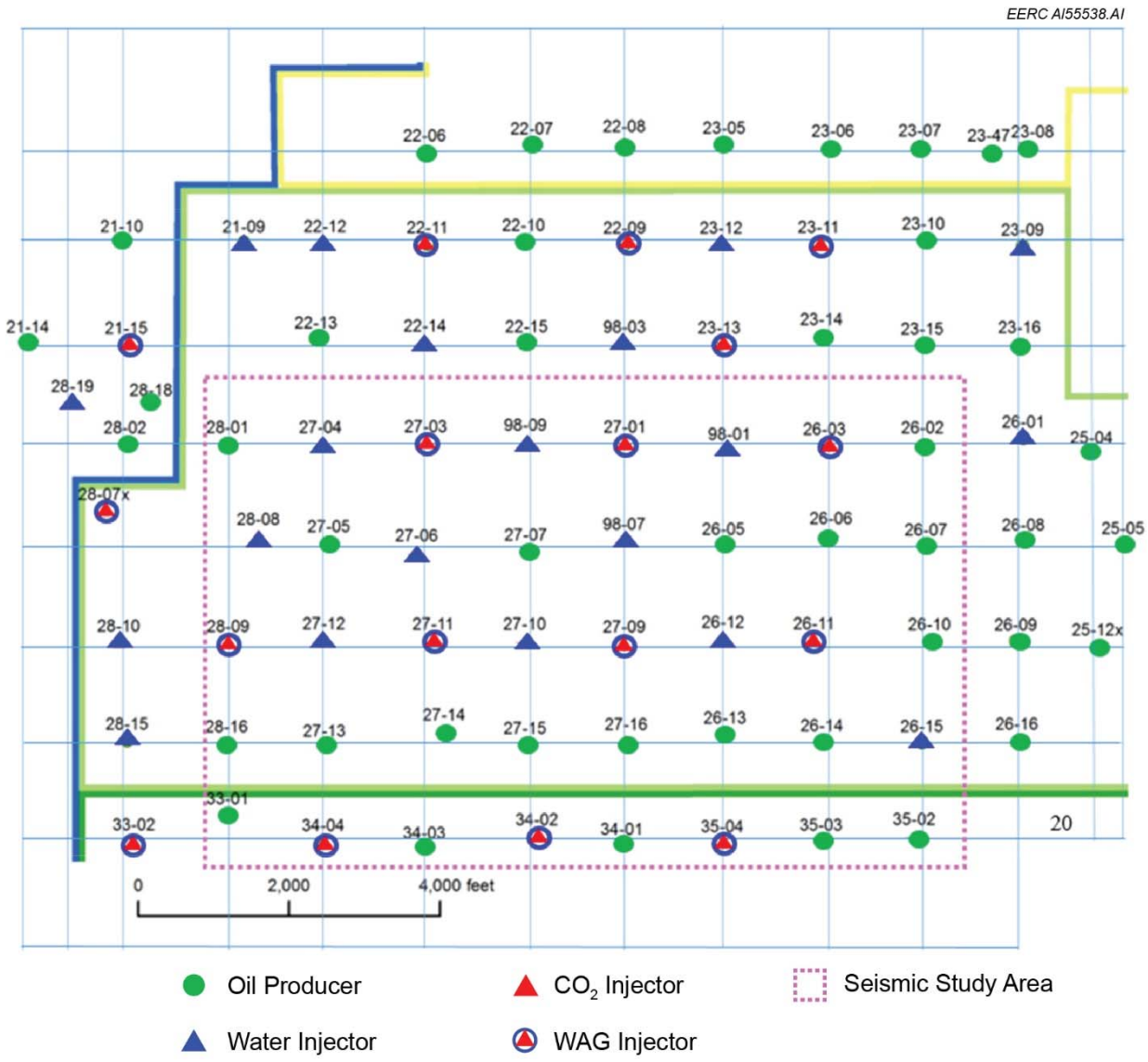

Figure E-2. Well distribution in the Bell Creek Phase 5 and surrounding area (as of October 2018).

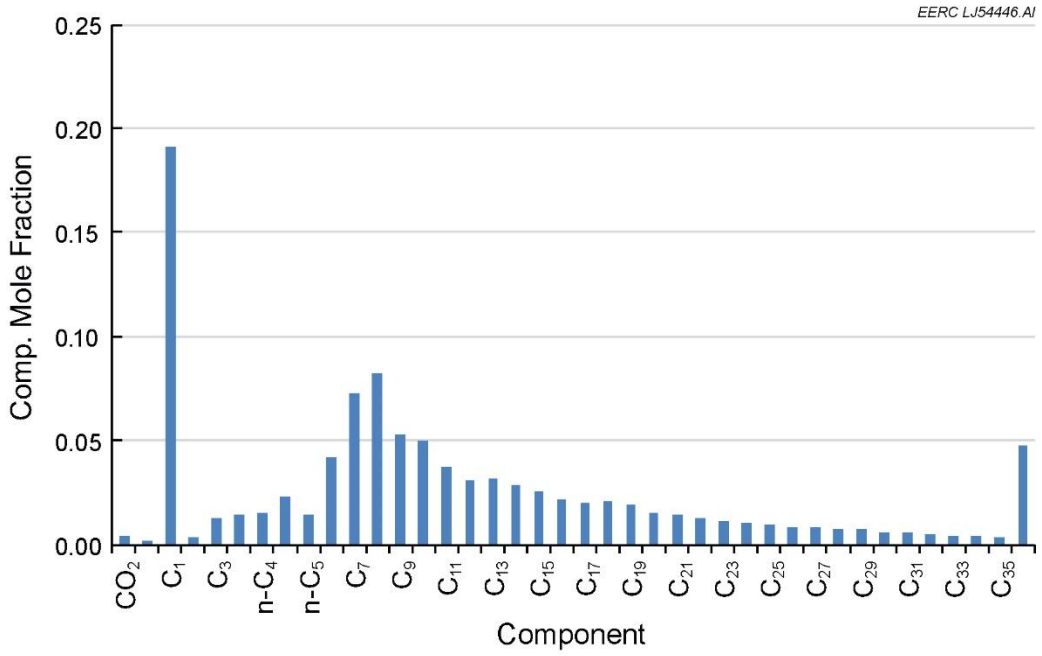

Figure E-3. High concentration of light components in the original reservoir oil.

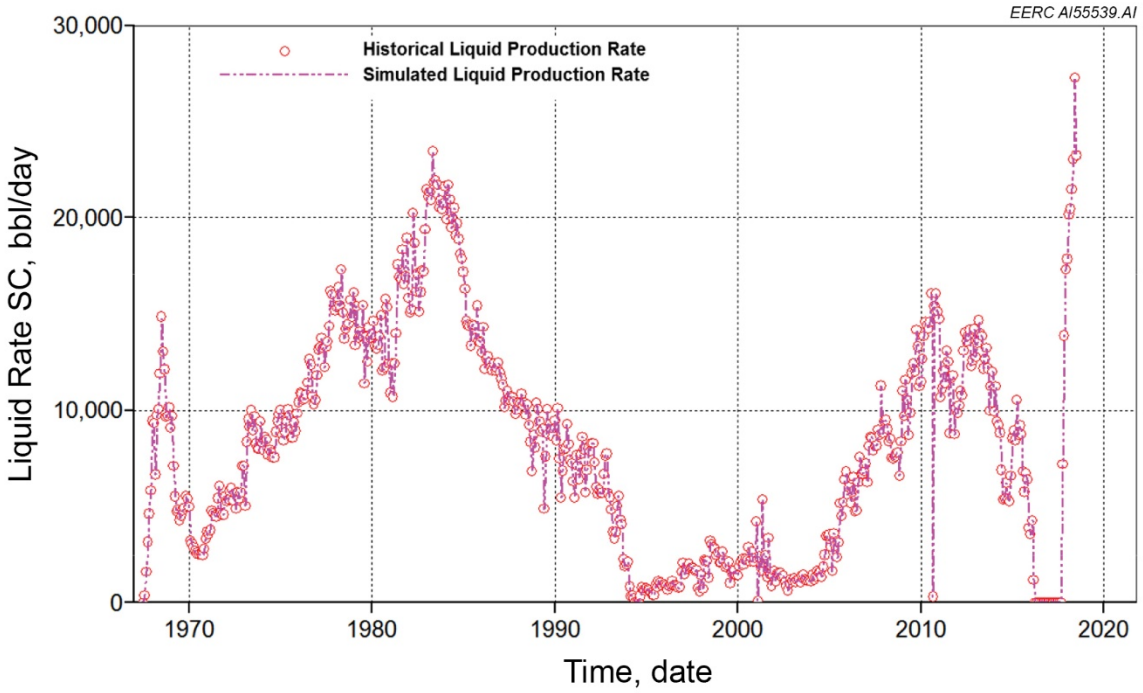

Figure E-4. Liquid production history of the Phase 5 area.

To ensure successful waterflood and CO_2 flood designs and operations in the field, detailed reservoir characterization and production performance analysis were conducted to analyze fluid flow between phase regions (Braunberger and others, 2013; Liu and others, 2014; Bosshart and others, 2015; Jin and others 2016, 2017). Results indicated that the reservoir was continuous from Phase 4 to Phase 7, which means there were no impermeable barriers to block fluid flow between Phase 5 and Phase 4. A systematic history-matching process was conducted to reproduce the production and injection data in Phase 5. Liquid production and injection rates were used as primary constraints. Recorded oil, water, and gas production rates were used in comparison to the simulated results. Because of the uncertainty of initial water saturation distribution in the reservoir, local water saturation was adjusted to match the water cut performance in the primary production stage. Since Phase 5 has open boundaries to Phases 4 and 6, out-of-boundary flow and petrophysical properties were adjusted to match the oil and water production rates in the water-flooding stage. Relative permeability curves and end point saturations were tuned to match gas production rate in the CO_2-flooding stage. A history match was achieved after careful tuning, and the results for oil/water/gas production rates, as well as water cut, are shown in Figures E-5–E-8. Using the history-matched model, dynamic simulations of Phase 5 injection activities through October 2017 show good correlation to 4-D seismic results (Figure E-9).

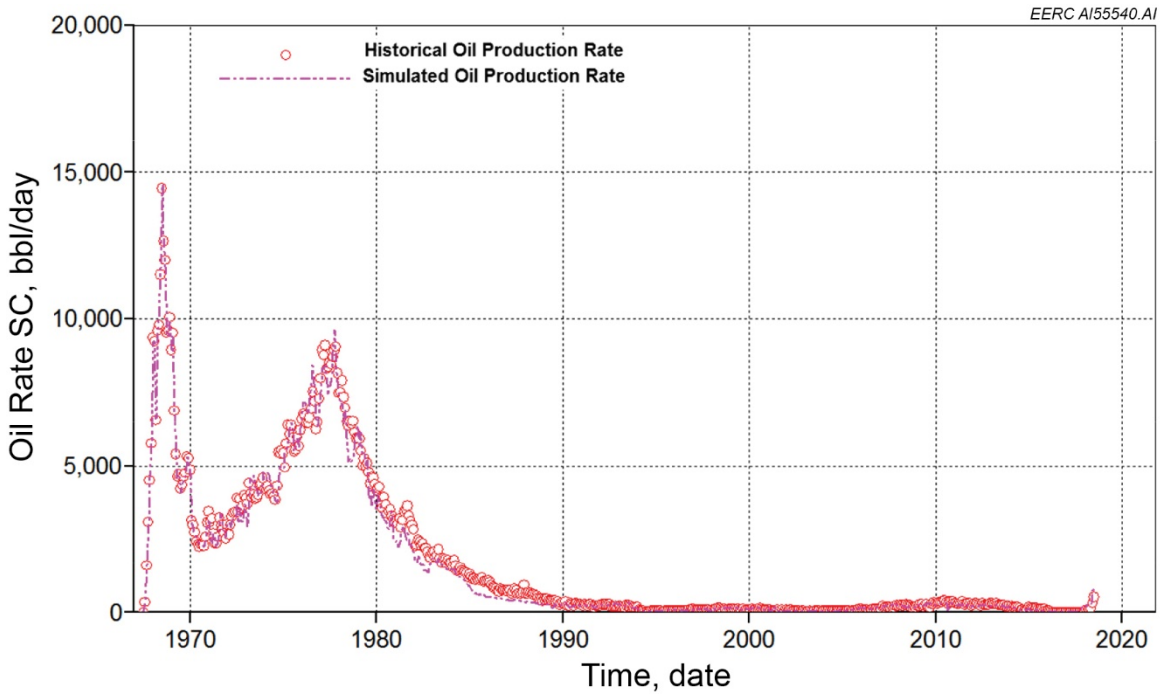

Figure E-5. Bell Creek Phase 5 oil production rate history match results.

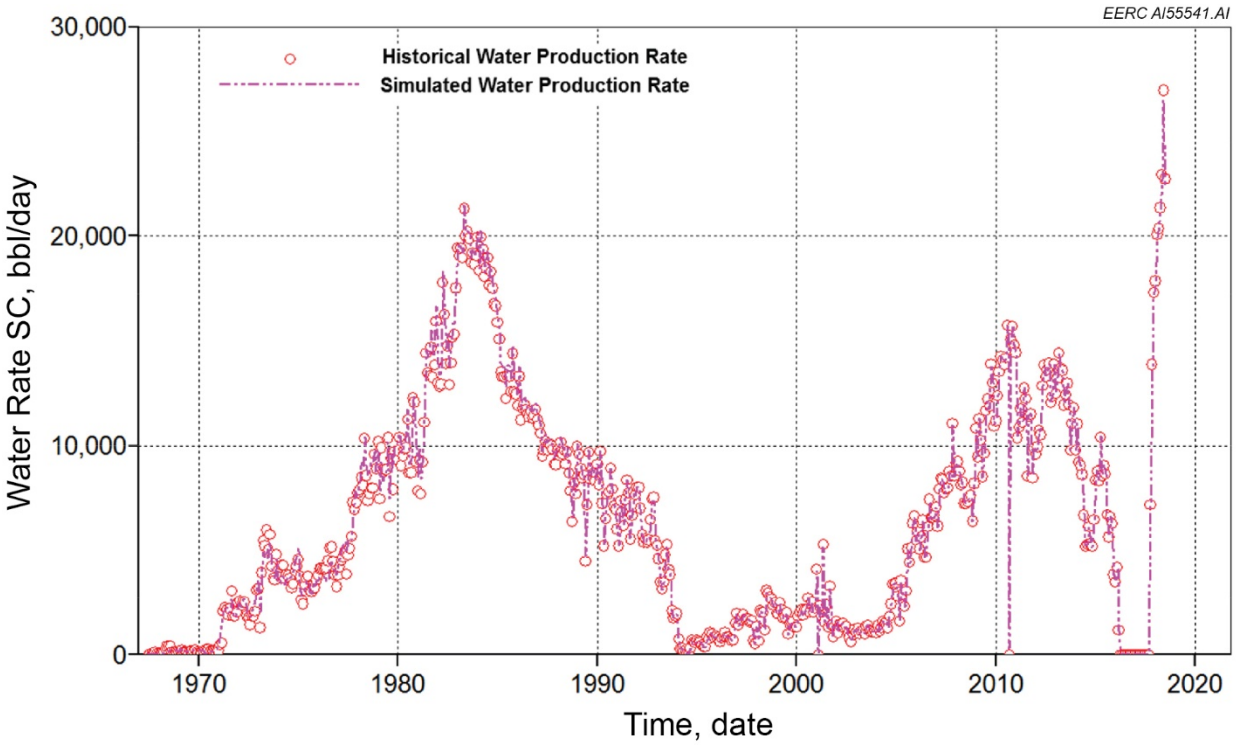

Figure E-6. Bell Creek Phase 5 water production rate history match results.

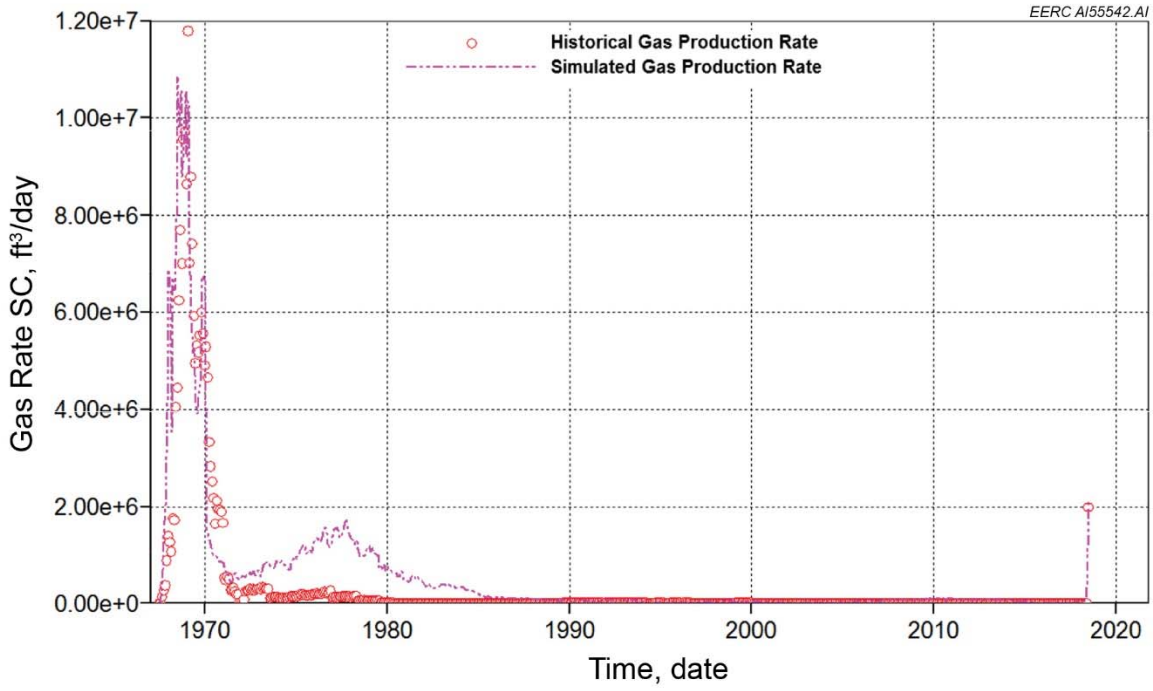

Figure E-7. Bell Creek Phase 5 gas production rate history match results.

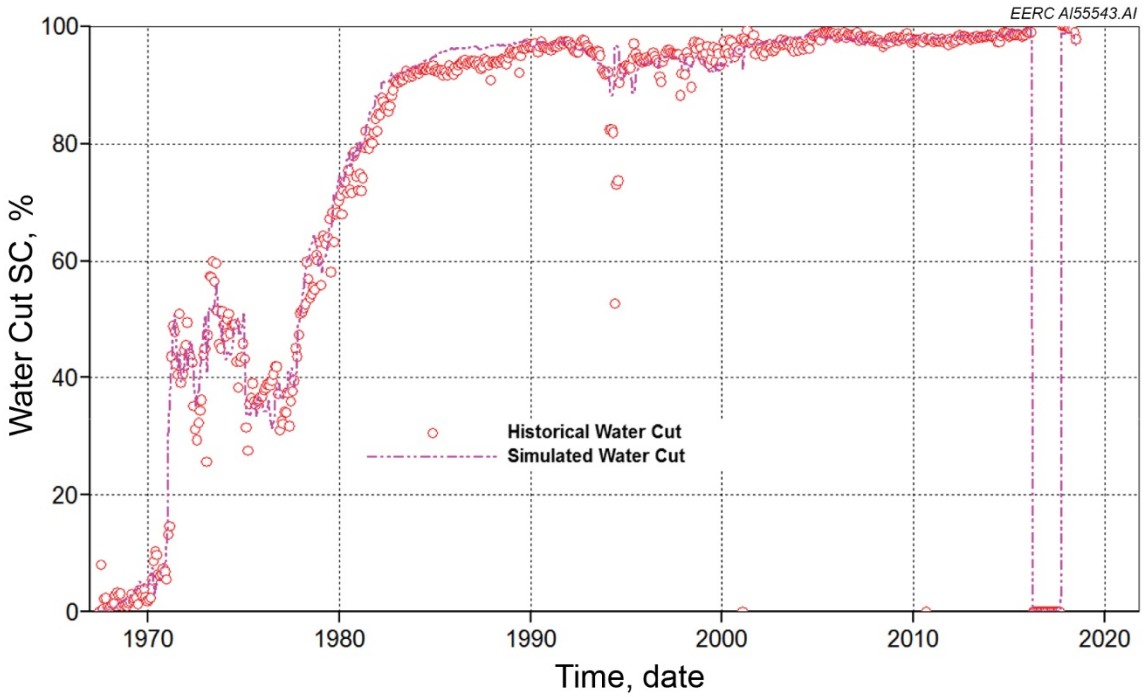

Figure E-8. Bell Creek Phase 5 water cut history match results.

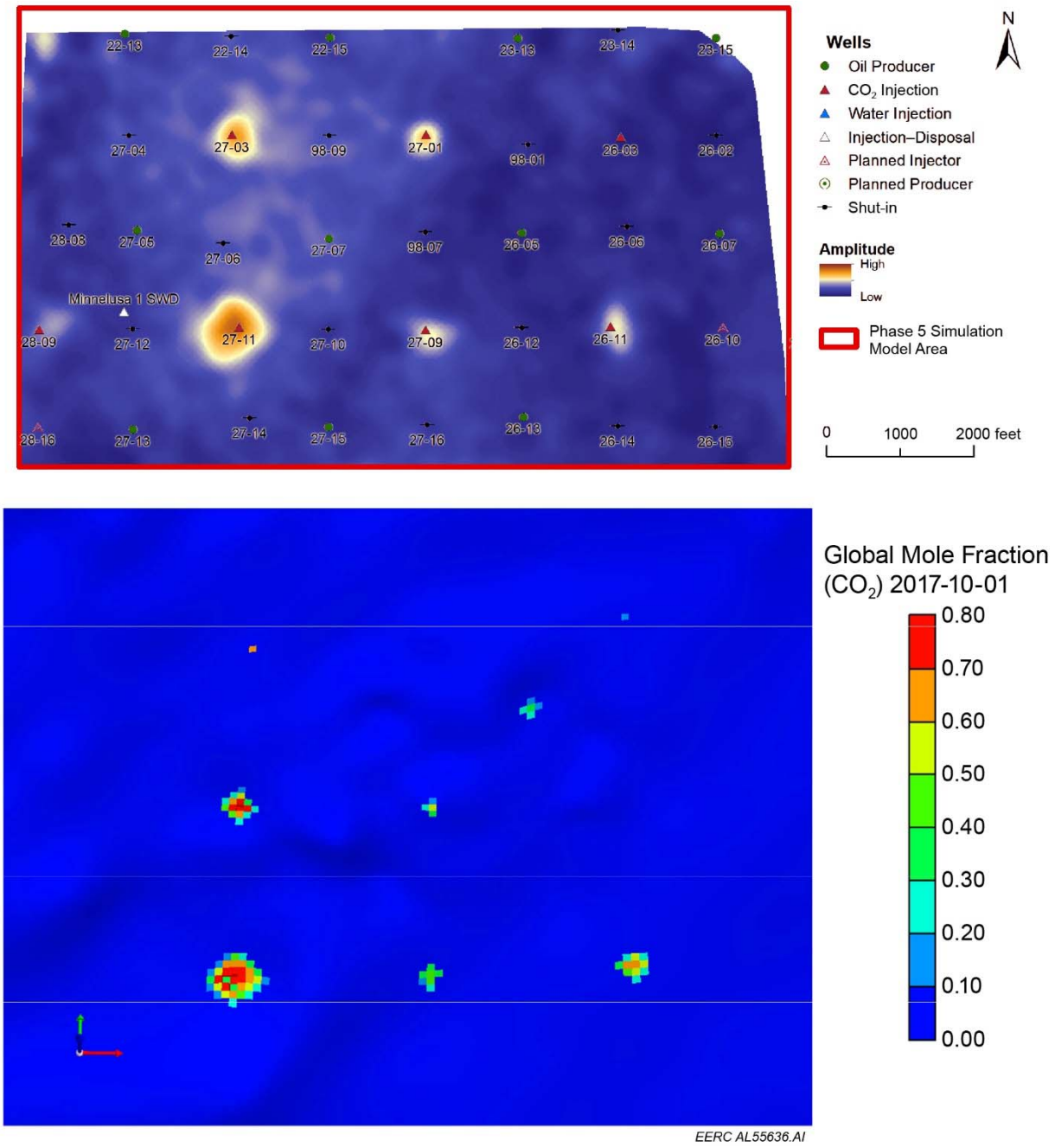

Figure E-9. Top: 2015–2017 amplitude difference map for the Phase 5 area with the simulation model extent outlined in red. Bottom: global mole fraction of CO_2 in the reservoir, computed after history matching.

REFERENCES

Bosshart, N.W., Jin, L., Dotzenrod, N.W., Burnison, S.A., Ge, J., He, J., Burton-Kelly, M.E., Ayash, S.C., Gorecki, C.D., Hamling, J.A., Steadman, E.N., and Harju, J.A., 2015, Bell Creek test site—simulation report: Plains CO_2 Reduction (PCOR) Partnership Phase III Task 9 Deliverable D66 (Update 4) for U.S. Department of Energy National Energy Technology Laboratory Cooperative Agreement No. DE-FC26-05NT42592, EERC Publication: EERC-10-09, Grand Forks, North Dakota, Energy & Environmental Research Center, August.

Braunberger, J.R., Pu, H., Gorecki, C.D., Bailey, T.P., Bremer, J.M., Peck, W.D., Gao, P., Ayash, S.C., Liu, G., Hamling, J.A., Steadman, E.N., and Harju, J.A., 2013, Bell Creek test site – simulation report: Plains CO_2 Reduction (PCOR) Partnership Phase III Task 9 Deliverable D66 Update 2 for U.S. Department of Energy National Energy Technology Laboratory Cooperative Agreement No. DE-FC26-05NT42592, August.

Jin, L., Bosshart, N.W., Oster, B.S., Hawthorne, S.B., Peterson, K.J., Burton-Kelly, M.E., Feole, I.K., Jiang, T., Pekot, L.J., Peck, W.D., Ayash, S.C., and Gorecki, C.D., 2016, Bell Creek test site – simulation report: Plains CO_2 Reduction (PCOR) Partnership Phase III draft Task 9 Deliverable D66 (Update 5) executive summary for U.S. Department of Energy National Energy Technology Laboratory Cooperative Agreement No. DE-FC26-05NT42592, Grand Forks, North Dakota, Energy & Environmental Research Center, August.

Jin, L., Peterson, K.J., Bosshart, N.W., Pekot, L.J., Salako, O., Burnison, S.A., Smith, S.A., Mibeck, B. A., Oster, B.S., He, J., Peck, W.D., Hamling, J.A., Ayash, S.C., Gorecki, C.D., 2017, Bell Creek test site – simulation report: Plains CO_2 Reduction (PCOR) Partnership Phase III draft Task 9 Deliverable D66 (Update 6) executive summary for U.S. Department of Energy National Energy Technology Laboratory Cooperative Agreement No. DE-FC26-05NT42592, Grand Forks, North Dakota, Energy & Environmental Research Center, August.

Jin, L., Pekot, L.J., Hawthorne, S.B., Salako, O., Peterson, K.J., Bosshart, N.W., Jiang,T., Hamling J.A., and Gorecki, C.D., 2018, Evaluation of recycle gas injection on CO_2 enhanced oil recovery, and associated storage performance: International Journal of Greenhouse Gas Control, August v. 31, no. 75, p. 151–61.

Liu, G., Braunberger, J.R., Pu, H., Gao, P., Gorecki, C.D., Ge, J., Klenner, R.C.L., Bailey, T.P., Dotzenrod, N.W., Bosshart, N.W., Ayash, S.C., Hamling, J.A., Steadman, E.N., and Harju, J.A., 2014, Bell Creek test site – simulation report: Plains CO_2 Reduction (PCOR) Partnership Phase III Task 9 Deliverable D66 Update 4 for U.S. Department of Energy National Energy Technology Laboratory Cooperative Agreement No. DE-FC26-05NT42592, August.